

Repeatability of Pre-Flashover Fire Patterns on
Gypsum Wallboard

A thesis
submitted in partial fulfilment
of the requirements for the Degree
of
Doctor of Philosophy
by
Daniel Madrzykowski



University of Canterbury
2015

To my wife and family

Abstract

Uncontrolled fires result in loss of life, property and can create an adverse economic impact on a community. The investigation of fires provides a means to identify the cause of the fire in order to develop a knowledge base that could enable the elimination of that cause and thus reduce the losses from fires. However, as the result of the review of several arson homicide cases and a review forensics by the U.S. National Academy of Sciences, questions about the lack of the use of science in the practice of fire investigation were raised. Specifically the National Academy of Sciences indicated that "... research is needed on the natural variability of burn patterns..." This study addresses that need in two ways:

1. Examining the repeatability of several small fire sources and the fire patterns that were generated by those fires
2. Examining the capability of using numerical models to simulate the fires and the resulting fire patterns based on input data collected from engineering reference sources, and bench scale and full scale fire experiments conducted in this study.

This paper highlights the many uncertainties involved in what appear to be simple fire experiments. A variety of uncertainties related to the composition of the fuels, measurement methods, and analysis techniques just to list a few of the areas considered. The objective of the research was to examine the repeatability of pre-flashover fire patterns generated from exposure to short duration (300 s maximum) well characterized fires. Three different fuels were used: natural gas, gasoline, and polyurethane foam. Each fuel had a similar top surface area. The heat release rate data showed that the variability was greater for more complex fuels. While the variation in peak heat release rate with the natural gas was similar to the expanded uncertainty of the measurement system, 11 %, the variation in the peak heat release rates of the gasoline and the polyurethane foam increased due to increased uncertainties in the burning behavior of the fuels. The patterns generated by the polyurethane foam fire, had more variability than the natural gas and the gasoline fire

patterns. This is likely due to the greater variability of the burning of the solid fuel and the lower heat release rate. The maximum fire pattern heights generated from the natural gas and gasoline fires were shown to have uncertainties of 18 % or less based on a Type A statistical analysis with 95 % confidence limits. The comparison of the fire pattern heights and the mean flame height demonstrated that the “steady state” natural gas fires exhibited the highest level of agreement and polyurethane foam fueled fire exhibited the least agreement, with the gasoline fueled fires in between.

This trend is the same as exhibited by the repeatability of the heat release rate measurements and the flame height measurements. *****Computational results here ****

Table of Contents

Abstract	iii
List of Figures	iv
List of Tables	viii
Acknowledgments	ix
Chapter 1: Introduction	1
1.1 Scope of Study	7
1.2 Technical Approach	8
1.2.1 Selection of Measurement Methods and Analytical Tools	8
1.2.2 Fire Pattern Experiments	10
1.2.3 Bench Scale Experiments	11
1.2.4 Numerical Fire Pattern Analysis	11
Chapter 2: Characterizing the Source Fires	13
2.1 Fuels	13
2.2 Experimental Arrangement	15
2.2.1 Instrumentation and Measurement Uncertainty	15
2.3 Results	17
2.3.1 HRR	17
2.3.2 Plume Temperatures	21
2.3.3 Total Heat Flux	21
2.3.4 Mass Loss	23
2.3.5 Flame Height	23
2.3.6 Summary	37
Chapter 3: Instrumented Non-combustible Wall Experiments	38
3.1 Experimental Arrangement	38

3.2	Results	39
3.2.1	Wall Temperatures	45
3.2.2	Heat Flux	48
3.3	Summary	49
Chapter 4:	Instrumented Gypsum Board Wall Experiments	57
4.1	Experimental Arrangement	57
4.2	Characterization of Gypsum WallBoard	58
4.3	Results	62
4.3.1	Wall Temperatures	62
4.3.2	Heat Flux	62
4.3.3	Fire Pattern	68
Chapter 5:	Bench Scale Experiments	80
5.1	Cone Calorimeter Experiments	80
5.2	Radiant Flooring Panel Experiments	82
5.3	Radiant Panel Experiments	85
5.4	Results	88
5.4.1	Ignition and Ignition Temperature	88
5.4.2	Heat Release Rate per Unit Area	91
5.4.3	Critical Heat Flux	91
Chapter 6:	Fire Pattern Compartment Experiments	96
6.1	Wall Position Experiments	97
6.1.1	Experimental Arrangement	98
6.1.2	Results	99
6.2	Corner Position Experiments	106
6.2.1	Experimental Arrangement	106
6.2.2	Results	106
Chapter 7:	Summary of Experimental Results	112
Chapter 8:	Comparison of Algebraic Fire Characterizations with Fire Pattern Results	113
8.1	Evidence of a Fire Pattern	113

8.2	Flame Height Correlation	113
8.2.1	Correlation Descriptions	114
8.3	Comparison of Results	114
Chapter 9:	Comparison of Field Model Simulations with Experimental Results	115
9.1	Fire Dynamics Simulator and Smokeview	115
9.1.1	Simulation of Fires	116
9.1.2	Input Data	116
9.2	Comparison of FDS with Source Fire Results	117
9.2.1	Grid Size Analysis	117
9.2.2	Plume Temperatures	117
9.2.3	Heat Flux	117
9.2.4	Flame Height	117
9.3	Comparison of FDS with Fire Pattern Results	117
Chapter 10:	Discussion	118
Chapter 11:	Future Research Needs	119
Chapter 12:	Conclusions	120
References		121

List of Figures

2.1	Diagram of the source fire flame and plume instrumentation apparatus	18
2.2	A photograph of the source fire flamer and plume instrumentation apparatus	19
2.3	Heat release rates for the natural gas and gasoline foam fires	20
2.4	Heat release rates for the polyurethane foam fires	21
2.5	Averaged centerline temperature for the natural gas, gasoline, and foam fires	22
2.6	Total heat flux versus time for natural gas, gasoline, and foam fires	24
2.7	Mass loss versus time for the gasoline and foam fueled fires	25
2.8	Photographs of the natural gas and polyurethane foam fires	26
2.9	Photographs of the gasoline fire	27
2.10	Example of sequential video frames sampled from a natural gas fueled experiment	29
2.11	Example of sequential video frames sampled from a gasoline fueled experiment	30
2.12	Example of sequential video frames sampled from a polyurethane foam fueled experiment	31
2.13	Comparison images of intensity fields derived from the video images of the natural gas fueled fire	33
2.14	Visibility fractions for the natural gas and gasoline fires	34
2.15	Visibility fractions for the polyurethane foam fire	35
3.1	Diagram of the instrumented non-combustible wall	40
3.2	Photograph of the front side of the instrumented non-combustible wall	41
3.3	Photograph of the rear side of the instrumented non-combustible wall	42

3.4	Photograph showing an example of the co-location of the heat flux gauges and the thermocouples on the front surface of the wall.	43
3.5	Photograph of an example of the co-location of the thermocouple on the rear surface of the wall relative to the thermocouple installed on the front surface of the wall	43
3.6	Plume temperatures along the centerline of the natural gas fueled burner	45
3.7	Wall Temperatures along the centerline of the natural gas fueled burner	46
3.8	Wall Temperatures along the edge of the natural gas fueled burner	47
3.9	Backside wall Temperatures along the centerline of the natural gas fueled burner	48
3.10	Heat flux at the wall along the centerline of the natural gas fueled burner	49
3.11	Heat flux at the wall along the edge of the natural gas fueled burner	50
3.12	Composite graph of the wall temperatures along the centerline of the burners	51
3.13	Composite graph of the wall temperatures along the edge of the burners	52
3.14	Composite graph of the backside wall temperatures along the center of the burners	53
3.15	Wall heat flux along the centerline of the burners	54
3.16	Wall heat flux along the edge of the burners	55
4.1	Diagram of the instrumented gypsum wallboard	59
4.2	Photograph of a thermocouple embedded in the gypsum wallboard	60
4.3	Plume temperatures for the natural gas fueled burner	63
4.4	Front surface wall temperatures for the natural gas fueled burner .	64
4.5	Backside wall temperatures for the natural gas fueled burner .	65

4.6	Wall heat flux along the centerline of the natural gas fueled burner	66
4.7	Wall heat flux along the edge of the natural gas fueled burner	67
4.8	Averaged peak temperatures on the backside of the gypsum board wall for the natural gas burner fires.	70
4.9	Averaged peak heat flux on the gypsum board wall for the natural gas burner fires.	71
4.10	Averaged centerline temperature for the natural gas, gasoline, and foam fires	72
4.11	Averaged burner centerline heat flux for the natural gas, gasoline, and foam fires	73
4.12	Averaged burner edge heat flux for the natural gas, gasoline, and foam fires	74
4.13	Photograph showing clear lines of demarcation	75
4.14	Photographs showing clear lines of demarcation with gasoline .	76
4.15	Photographs of the fire effects on the instrumented gypsum wallboard exposed to the natural gas burner fires	77
4.16	Photographs of the fire effects on the instrumented gypsum wallboard exposed to the gasoline burner fires	77
4.17	Photographs of the effect of soot removal on the instrumented gypsum wallboard exposed to the gasoline burner fires	78
4.18	Photographs of the fire effects on the instrumented gypsum wallboard exposed to the polyurethane foam fires	78
4.19	Photographs of the fire effects on the instrumented gypsum wallboard exposed to replicate polyurethane foam fires	79
5.1	Sketch of the cone calorimeter	81
5.2	Schematic of the radiant flooring panel apparatus	83
5.3	Incident heat flux profile in the radiant flooring panel test apparatus	84
5.4	Photographs of the radiant panel experimental arrangement .	85
5.5	Incident heat flux profile based on the distance between the sample face and the radiant panel	87

5.6	Photograph of the flame front burning on the gypsum wallboard sample in the flooring radiant panel	90
5.7	Photographs of the fire effects on the instrumented gypsum wallboard exposed to radiant heat from a natural gas fired panel.	92
5.8	Time vs. temperature curves for the gypsum wallboard samples exposed to radiant heat from a natural gas fired panel . .	93
5.9	Photographs of the radiant flooring panel experiments	94
6.1	Photograph of the wall fire pattern experiments compartment arrangement	98
6.2	Photographs of the fire patterns from ten replicate natural gas burner against open wall construction	102
6.3	Photographs of the fire patterns from ten replicate natural gas burner against closed wall construction	103
6.4	Photographs of the fire patterns from ten replicate natural gas burner against insulated wall construction	104
6.5	Photographs of the fire patterns from ten replicate gasoline burner against open wall construction	107
6.6	Photographs of the fire patterns from ten replicate gasoline burner against closed wall construction	108
6.7	Photographs of the fire patterns from ten replicate gasoline burner against insulated wall construction	109
6.8	Photographs of the fire patterns from ten replicate polyurethane foam burner against open wall construction	110

List of Tables

2.1	Mean visible flame height and averaged minimums and maximums	28
2.2	Average flame heights for three fuels	37
3.1	Thermal properties for Marinite I	39
4.1	Thermal properties for 12.7 mm gypsum wallboard	61
4.2	Matrix of instrumented gypsum wallboard experiments	62
5.1	Painted gypsum wallboard time to ignition results	88
5.2	Painted gypsum wallboard ignition temperature results	89
5.3	Flooring radiant panel experiment flame spread results	91
5.4	Painted gypsum wallboard time heat release rate per unit area results	93
6.1	Comparison of fire pattern dimensions as a function of wall construction type	111

Acknowledgments

I would like to thank Prof. Fleishmann, my senior advisor with the University of Canterbury, as well as, Dr. Kevin McGrattan, and Dr. Craig Weinschenk from the National Institute of Standards and Technology for their guidance, assistance, and support throughout this study.

The full-scale and bench-scale experiments were conducted over a period of several years whenever funding and laboratory availability coincided. These experiments were conducted with the support of several engineering technicians from the NIST Fire Research Division, especially Roy McLane, Jay McElroy, Laurean DeLauter, and Anthony Chakalis. Their assistance was essential. Their patience and attention to detail during this study is greatly appreciated

This work was partially funded by the National Institute of Justice (NIJ) through an inter-agency agreement with the NIST Office of Law Enforcement Standards (OLES). I would like to thank Susan Ballou of OLES for her support of this project. This work was also partially supported by the U.S. Fire Administration.

I would also like to thank Roger Nokes for his development and continued assistance with Streams and to the New Zealand Fire Commission for their financial support to the University of Canterbury

Last but not least, I thank my wife, Liz, for her patience and support of my pursuit of higher education throughout our 37 years of marriage. I would also like to thank my children; Catherine, Stephanie, Michael, Christina, and Veronica for "buying me time" to work on my studies.

Chapter I

Introduction

Uncontrolled fires result in loss of life, property and can create an adverse economic impact on a community. Findings from an archaeological site in South Africa, published in 2012, indicate that mankind has productively used fire for approximately 1 million years [1]. This is 300 thousand years earlier than previously thought. Despite mankinds extensive history with fire, according to the World Health Organization, an estimated 265,000 people die each year as a result of burn injuries [2]. Based on an estimated global population of 7.3 billion people, the death rate due to burns from all sources would be 3.6 per 100,000 populations. The World Fire Statistics Center collects data from European, North American and a few Asia-Oceania countries. Within this group of countries the fire deaths per 100,000 population range from 0.02 (Singapore) to 2.03 (Finland) [3]. There are a significant number of factors that determine the variability of fire death rates between nations, socio-economic conditions being a leading factor [2].

In the United States, the loss of life due to unwanted fire has been decreasing steadily since the 1970s. This trend does not include loss of life as a result of the terrorist attack on September 11, 2001. The estimated number of fire deaths in the U.S. in 1975 was 8,100 or 3.75 deaths per 100,000 population [4]. In 2013, there were 3,240 civilian fire fatalities or 1.02 deaths per 100,000 population [5]. During this same period, the number of fires in the United States has decreased from 2.5 million fires to 1.24 million fires. There are many reasons that led to this decrease in loss of life due to fire in the United States. An example would be research and data that enabled the development of product safety standards, improved building codes, improved fire safety systems, and fire prevention programs to name just a few. None of this happened without the constant effort of agencies at the Federal, state,

and, local levels working with professional fire organizations to deliver the five Es of fire prevention; Engineering, Education, Enforcement, Economic Incentive, and Emergency Response [6].

Fire investigation is a key element in the fire prevention system that generates data to enable the reduction of fire losses. The investigation of fires provides a means to identify the cause of the fire in order to develop a knowledge base that could enable the elimination of that cause and thus further reduce the losses from fires. Data such as the room of fire origin, the first item ignited and ultimately the cause of the fire is information that is critical to understanding and reducing the number of fires. For example, the identification of products that are involved in ignitions due to a design flaw, in many cases result in the U.S. Consumer Product Safety Commission or a manufacturer issuing a product recall.

In some cases, the fire investigation determines that the fire was intentional. An intentional fire as defined in the National Fire Incident Reporting System (NFIRS) are those fires that are deliberately set and include fires that result from deliberate misuse of a heat source, fires of an incendiary nature (arson), as well as controlled burn fires, such as crop clearing, that required fire service intervention [7]. An incendiary fire, as defined by the National Fire Protection Association (NFPA) Guide for Fire & Explosion Investigations, commonly referred to as NFPA 921, is “a fire that is deliberately set with the intent to cause a fire to occur in an area where the fire should not be” [8].

According to the NFPA, there were approximately 282,600 intentionally set fires each year during the period of 2007 through 2011 in the United States. The average annual loss totals for that period were approximately 420 civilian deaths and 1,360 civilian injuries. More than \$1.3 billion dollars (U.S.) was lost per year due to direct property damage. Fires involving structures account for more than 84 % of the civilian deaths, injuries and property loss from all intentional fires. Approximately two-thirds of the structure fires occurred in residential occupancies. 95 % of the civilian deaths and 86 % of the civilian injuries also occurred in the intentional fires in residential occupancies [7].

A subset of the intentional fires are considered arson. Arson as defined

by the U.S. Federal Bureau of Investigation (FBI) Uniform Crime Reporting (UCR) Program defines arson as any willful or malicious burning or attempting to burn, with or without intent to defraud, a dwelling house, public building, motor vehicle or aircraft, personal property of another, etc. [9].

The national rate of arson fire cases cleared by arrest or exceptional means is less than 20 %. Of those cases approximately 46 % of the suspects were prosecuted [7]. Arson is a challenging crime to solve because typically there are no witnesses present at the time of the crime.

The values cited above are believed to be the best available in the United States and perhaps one of the better fire incident databases in the world. However an investigative report by Icove and Hargrove, indicates that arson fires are underreported to the National Fire Incident Reporting System (NFIRS). The investigation provided examples from several major cities, such as New York City, where in 2011, 11 arson fires in buildings were reported to NFIRS, while the Fire Department of the City of New York's Bureau of Fire Investigation had recorded 1,347 arson fires in buildings that year. Similar discrepancies were found in eight other large U.S. cities. On average, three-fourths of the arsons uncovered by city fire investigators went unreported to NFIRS [10].

Fires are investigated in order to determine the “origin and cause” of the fire and in cases of arson there is an effort to determine who was responsible for setting the fire. This investigation process must follow the scientific method as documented in NFPA 921 [8]. There are numerous textbooks on the subject of conducting a fire investigation [11, 12, 13, 14, 15, 16]. The NFPA guide and the texts provide information to a fire investigator collecting data from the scene, analyzing the data, and developing a hypothesis about the fire.

Patterns produced by the fire are in many cases a significant portion of the data collected and are analyzed at the scene to determine the area of origin. One of the basic methods of documenting the fire scene is to photograph fire patterns. As noted by Icove, DeHaan, and Haynes “the ability to document and interpret fire patterns accurately is essential to investigators reconstructing fire scenes” [14]. A fire pattern is defined in NFPA 921 as, “the visible or measurable physical change, or identifiable shapes, formed by

a fire effect or group of fire effects” [8].

DeHaan [13] categorizes the fire effects that form patterns as follows:

1. Surface deposits - no irreversible effect on surface
2. Surface thermal effects - physical change such a discoloration or melting
3. Charring - evidence of surface burning
4. Penetration - charring below the surface
5. Consumption - loss of surface material, charring throughout

Lentini points out that most fire patterns are generated and later observed on two-dimensional surfaces at the place where those surfaces intersect with the three-dimensional fire. Various types of fire patterns, such as; “V-shaped”, “hour-glass”, and “inverted cone”, have come from common observation at actual fire scenes [15]. As a result, the observations are typically qualitative in nature.

Previous fire pattern research by the National Institute of Justice (NIJ), the National Institute of Standards and Technology (NIST), and the United States Fire Administration (USFA) has shown that fire patterns provide data useful for the determination of fire origin. The reports noted the impact of ventilation on the development of the burn patterns [17, 18]. A large number of other factors affect the formation of these patterns: burn time, heat release rate of the fire source, fire exposure, target fuel composition, adjacent fuel(s) and compartmentalization, to name a few. Given the limited number of experiments in the literature and the large number of variables, it has been difficult to fully understand a cause and effect relationship between the fire scenarios and the resulting patterns.

Fire models are another tool that may be used by a fire investigation team to gain insight into the growth and development of a fire and to test the investigators hypothesis on origin and cause [19]. Many theoretical and empirical correlations and computational fire models have been developed for use in fire protection design, fire hazard analysis, and fire investigation. A collection of the widely used correlations can be found in the U.S. Nuclear

Regulatory Commissions (NRC) Fire Dynamics Tools (FDTs). These spread sheets incorporate references to the source documents and experimental work upon which the correlations are based. In addition, NRC tasked NIST with conducting a verification and validation study of the correlations. Overholt developed the NIST verification and validation study [20]. Not all of the correlations in the FDTs were included in the study because an insufficient amount of reliable data is available to conduct validation. Two correlations that could not be validated were for flame height and time to ignition.

In 2003, a list of zone and computational fluid dynamics (CFD) fire models was compiled by Olenick and Carpenter [21]. A similar survey was conducted in 1992, and Olenick has updated the list in 2014. There are 53 zone models listed, but only three are actively supported or maintained. The survey also includes 22 field models of which 10 are listed as being actively supported. All of the correlations and models have been to some extent been validated or checked against experimental data for a limited set of scenarios [22].

Of the active field models, FDS version 6 has one of the most rigorous and publicly accessible verification and validation programs [23]. More than 45 experimental data sets are used to quantify the prediction capabilities of the model. Results are presented in terms of model bias and variation to inform users of whether particular quantities (temperature, heat flux, pressure, etc.) are over or under predicted compared to experimental data.

However for fire models to be demonstrated as reliable and suitable for use in court, studies such as the one conducted here need to be conducted to provide the scientific basis for the use of fire models for re-construction. The research results may enable fire investigation teams to have a better understanding of the fire scene and enable improved support of their hypothesis on the area of origin based on fire patterns. This idea was discussed when the Fire Protection Research Foundation convened a Research Advisory Council on Post-fire Analysis in 2002. Recommendations for research and development in their white paper included, “advance the capabilities of computational fluid dynamics fire modeling, particularly as applied to fire ignition scenarios and fire pattern development and interpretation” [24].

Given that fire pattern interpretation and analysis is a critical step in most

fire investigations, it is surprising to find the limited amount of research and analysis tools directly related to this practice. Gorbett recently conducted a review of fire pattern research that has been conducted over the last 80 years. The review points out many gaps, especially with how fire patterns are used to determine the area of origin. A key limitation is the assumption by many of the researchers, or text authors, that investigators are able to visibly assess varying degrees of fire damage and then determine the area of origin [25]. Studies have shown that investigators have not been able to use only the location of the fire patterns as means of reliably determining the area of origin, some amount of analysis and fire dynamics knowledge is required [26], [27].

The fire investigation community recognized a need to improve the science and practice of fire investigation. One of the manifestations of the efforts to improve the practice was the development of NFPA 921, *Guide for Fire and Explosion Investigations* [8]. The first edition of NFPA 921 was issued in 1992. As provided by the document scope, it “is designed to assist individuals who are charged with the responsibility of investigating and analyzing fire and explosion incidents and rendering opinions as to the origin, cause, responsibility, or prevention of such incidents, and the damage and injuries which arise from such incidents.” The documents purpose includes the goal to be “a model for the advancement and practice of fire and explosion investigation, fire science, and methodology.” However, NFPA 921 can only incorporate the fire science and research results that have been produced. Although NFPA 921 is a “guide” as opposed to a “standard,” it is considered the standard of care for the fire investigation community in countries that recognize and use NFPA standards and guides.

As the result of the review of several arson cases, most notably the cases of Ernest Ray Willis and Cameron Todd Willingham, the practice of fire investigation as a forensic science was called into question. Beyler conducted a review of both cases for the Texas Forensic Science Commission. Both fires occurred prior to the release of NFPA 921 in 1992. The Beyler analysis, issued in August of 2009, concluded that the investigations of both cases “did not comport with either the modern standard of care expressed by NFPA 921, or the standard of care expressed by fire investigation texts and papers in

the period 1980–1992.” The fire investigators had a poor understanding of science and their findings of arson could not be sustained [28].

Another landmark document regarding the state of forensic science in the United States was published in 2009. The 328 page report, entitled *Strengthening Forensic Science in the United States: A Path Forward*, by the U.S. National Academy of Sciences, reviewed 13 different forensic science disciplines including biological evidence, friction ridge patterns, tool mark and firearms identification, and analysis of explosives evidence and fire debris. The review of the analysis of explosives evidence and fire debris is covered in three pages of the report. The summary assessment of analysis of explosives evidence is positive, “the scientific foundations exist to support the analysis of explosions, because such analysis is based primarily on well-established chemistry” [29]. The complete summary assessment for fire debris analysis is included here: “By contrast, much more research is needed on the natural variability of burn patterns and damage characteristics and how they are affected by the presence of various accelerants. Despite the paucity of research, some arson investigators continue to make determinations about whether or not a particular fire was set. However, according to testimony presented to the committee, many of the rules of thumb, that were typically assumed to indicate that an accelerant was used (e.g. “alligatoring” of wood, specific char patterns) have been shown not to be true. Experiments should be designed to put arson investigations on a more solid scientific footing.” This study is in response to the assessment above, specifically regarding the natural variability of fire patterns.

1.1 Scope of Study

Given that the majority of intentional fires in structures occurred in residential occupancies, this study will focus on fire patterns on painted gypsum wallboard, which is 2.4 m in height. Given the upper bound of 2.4 m, the experiments will use small fires with mean flame heights of approximately 1.2 m. The resulting patterns on the gypsum board wall would be representative of a pre-flashover fire pattern.

In order to understand the variability or repeatability of fire patterns, the

repeatability of the fire generating the fire pattern must be quantified. The fires were characterized in terms of heat release rate, mass loss rate (when appropriate), plume temperature, heat flux, and visible flame height.

Replicate experiments exposing gypsum wallboard to the fires were conducted in order to examine the repeatability of the fire patterns. Correlations between the fire characteristics and the fire patterns will be examined.

The last component of this study examines the capability of using numerical models to simulate the fires and the resulting fire patterns based on input data collected from engineering reference sources, as well as bench scale and full scale fire experiments conducted in this study.

1.2 Technical Approach

This study includes several series of real-scale, replicate fire experiments to examine the repeatability of pre-flashover fire patterns, and ultimately examine the ability of simple correlations and the Fire Dynamic Simulator to recreate characteristics of the fire patterns.

1.2.1 Selection of Measurement Methods and Analytical Tools

Well-documented and characterized technologies such as thermocouples and heat flux gauges were used to assess the fire and the thermal exposure of the target material. Oxygen consumption calorimetry and mass loss measurements were used for the determining the heat release rate of the fires.

The most important measurements for the field investigator are the visual measurements that can be made at the scene or determined from scene photographs. Several methods of imaging were used for these experiments: still photography, digital video, and infrared video. Computer based imaging techniques, such as those contained in the Image Stream program suite, were examined and adapted to analyze the flame height of the source fires [30].

Statistical methods were used to guide the wall fire and corner fire experiments. The analysis ensured that the appropriate number of replicate experiments were conducted to provide an assessment of burn pattern repeatability within a given level of uncertainty. Given that the coefficient of variation (COV) may be different for a given type of experiment, the number

of replicates required would be larger for experiments with a larger COV in order obtain a valid assessment of repeatability.

The series of experiments listed below are ordered in such a manner to optimize the total number of experiments required.

Characterization of Source Fires

The fires were characterized in terms of heat release rate, mass loss rate, fire plume temperatures and emitted heat flux. Videos were recorded for each experiment. This “field” data from the videos was used to determine the flame heights. Experiments were conducted with three different fuel types: a gas fueled mass flow controlled burner, a liquid fueled burner, and a solid fuel.

Instrumented Calibration Target Wall

A free standing, steel frame with non-combustible, calcium silicate faced wall was instrumented to measure the thermal exposure of the wall from the fire in terms of temperature and heat flux. The fires were initially placed at predetermined, fixed positions away from the wall. The burner was moved toward the wall until the burner was against the wall.

Instrumented Gypsum Wallboard Target Wall

A free standing, steel frame with a panel of gypsum wallboard attached to the surface was instrumented to measure the thermal exposure of the wall from the fire in terms of temperature and heat flux. The fires were initially placed at predetermined, fixed positions away from the wall. The burner was moved toward the wall until the burner was against the wall. If the results indicated that no burn pattern would result from a given combination of fuel and position, then that fuel and position combination were eliminated from the remainder of the test matrix.

1.2.2 Fire Pattern Experiments

Impact of Construction

Comparative experiments were conducted to examine the impact of the method of construction and support of the walls and corner sections on the development of the burn patterns. Three cases were examined: (1) 12.7 mm thick, regular core, painted gypsum wallboard on the front of a wall frame (open back); (2) 12.7 mm thick, regular core, painted gypsum wallboard on the front and back of a wall frame (interior wall); and 3) 12.7 mm thick, regular core, painted gypsum wallboard on the front and back of a wall frame, with fiberglass batting insulation in the voids of the wood frame (exterior wall). The main consideration was to identify any differences in the height, width, shape, and area of the fire patterns. The results of these experiments determined the construction of the walls and corners used in subsequent phases of this study.

Wall Fires

Each of the test compartments consisted of three 3.6 m long by 2.4 m high wood framed walls. A partial ceiling was installed over the wall. The interior of the wall sections and ceilings were covered with painted gypsum wallboard. These experiments were conducted without instrumentation in the walls. Based on the outcome of the instrumented calibration target wall results, burner positions were chosen. After each burn, the fire patterns were measured, photographed and analyzed for repeatability. The fire damaged wallboard was subsequently removed and replaced with new sections of painted gypsum wallboard. The number of experiments for each case was dependent on the repeatability and similarity of the pattern development.

Corner Fires

These experiments used the same test compartment as the wall fire pattern experiments. In these cases the fire was located against both walls in a corner of the compartment. The experimental process was the same as the wall fire pattern experiments.

1.2.3 Bench Scale Experiments

Several types of bench scale experiments were conducted to generate data. This data could be used to assist in the analysis of the fire patterns and potentially be used as input for the FDS models.

Critical Heat Flux

A series of experiments were conducted with samples of painted gypsum wallboard to determine the repeatability of a “critical heat flux” that results in a clear line of demarcation, a “burn/no burn” line. The flooring radiant panel, ASTM E648, and a modified radiant panel apparatus based on ASTM E162 were used to examine this value [31], [32].

Cone Calorimeter

Cone calorimeter, ASTM E1354, experiments were conducted to estimate the ignition temperature, the time to ignition and the heat release rate from samples of painted gypsum wallboard under thermal flux conditions ranging from 25 kW/m² to 75 kW/m² [33].

1.2.4 Numerical Fire Pattern Analysis

The ability to recreate or simulate a fire pattern or certain characteristics of a fire pattern was examined with a variety of tools. The first characteristic examined was the ability to determine, based on the calculated heat flux to the wall, if a “visible or measurable physical change” would occur to the painted paper surface of the gypsum wallboard. The next characteristic of the fire pattern that was examined was the height. The height of the fire pattern was then compared to the predictive results from flame height correlations. Heskstad developed an empirical method for calculating the mean visible flame height for fuels which do not have substantial in-depth combustion [34, 35]. This correlation was compared with the flame height results of the source fires and the instrumented wall experiments.

FDS [23] and Smokeview [36] were used to examine the ability to numerically reproduce the source fires and the instrumented wall experiments.

These simulation tools provide results in the form of visual field data, in other words they provide results in the same format that the investigator would see or document the fire pattern. Comparison between the experiments and the model may provide valuable validation data for the model.

Data Analysis

Point measurements were reduced and compared with values from the literature on fire plumes and their interaction with vertical surfaces. The heat release rates, heat flux measurements, flame and surface temperatures were used as input for heat transfer analysis to develop empirical coefficients for the specific experimental arrangements which would be useful in the model recreations. The key measurements for repeatability of the fire patterns on the gypsum wallboard are height, maximum width, shape, and area. The two significant outcomes will be the repeatability of the fire patterns themselves and the ability to numerically recreate key measures of the pattern.

Chapter II

Characterizing the Source Fires

A series of experiments were conducted to characterize a limited set of residential scale, pre-flashover or incipient fires. A fixed fire source footprint, 30.5 cm square, was chosen for this study and a range of common fuels was selected. The fires were positioned under an oxygen consumption calorimetry hood to determine the heat release rate. Heat release rate, flame/plume gas temperatures, and total heat flux from the flames were measured and flame movement and height were recorded with photographs and videos. Given the focus on residential fires, small source fires were selected so that the burn pattern would be limited to less than 2.4 m in height. Replicate experiments were conducted with each of the fuels, in order to examine the repeatability of the fires and to quantify the variability in the flames.

2.1 Fuels

Three different fuels were used in this study. Experiments were conducted with a natural gas fueled burner, a liquid fueled pan fire, and a solid fuel. Natural gas was chosen as a fuel because it is used for calibrating the oxygen depletion calorimeters in NISTs Large Fire Laboratory. Therefore the heat content of the gas was monitored and mass flow controlled to provide a heat release rate based on fuel mass flow for comparison with the heat release rate values measured with the calorimeter. The gas burner arrangement provides the most idealized fire, in that it can be ignited and brought up to a near steady state heat release rate within a few seconds and then be shut down just as quickly. This provided an approximate ‘square wave’ exposure to the gypsum wallboard. This is important for determining the potential amount of energy transferred to the exposed surface.

The natural gas burner was 30.5 cm on a side and the top surface of the burner was 7.5 cm above the floor. The shell of the burner was made from steel and filled with “pea sized” gravel with an average diameter of 6 mm. A steady state heat release rate of approximately 80 kW was used for the experiments.

Gasoline was the fuel of choice for the liquid fueled pan fire. Gasoline is not an ideal fuel to use in experiments because it is a mixture of components and additives that are specific to manufacturers. In addition the mixtures change from season to season, and vary based on requirements or restrictions of the locality. However, fire incident data shows that gasoline was the first item ignited in the majority of intentional fires where flammable or combustible liquids were used [37]. In addition, data from forensic laboratories, collected by Babrauskas and others, indicates that gasoline is the most prevalent accelerant found as part of the analysis of fire debris samples [38, 39].

The gasoline pan fire used 500 mL of unleaded, 87 octane gasoline. The pan was constructed from 6 mm thick steel. The inner dimension of the pan was 30.5 cm on a side and 1.9 cm high. The pan was elevated in order to bring the pan lip height up to 7.5 cm above the floor to be the same height as the natural gas burner. The 500 mL of gasoline had a fuel depth of 5.5 mm and provided a burn time of approximately 300 s.

Polyurethane foam was chosen as the solid fuel. According to the Polyurethane Foam Association, flexible polyurethane foam is the most widely used cushioning material in upholstered furnishing and mattresses. More than 1.2 billion pounds are produced in the U.S. every year [40, 41]. In studies by Ahrens and Evarts of the NFPA, upholstered furniture and mattresses and bedding were the first items ignited in 33 % of the fatal fires in the U.S. based on averaged data from 2005 through 2009 [42, 43].

The flexible polyurethane foam had a density of approximately 23 kg/m³. Each block of foam was 30.5 cm on a side and was 7.5 cm thick. The bottom and sides of the foam block were wrapped in aluminum foil to prevent the fuel from flowing or spreading as it burned to ensure that the fuel area remained with the same fixed area as the gasoline and natural gas.

2.2 Experimental Arrangement

The source fire characterization experiments were conducted in the NIST Large Fire Research Laboratory's 3 m by 3 m hood oxygen consumption calorimeter. This apparatus follows the methodology of ASTM E 2067-08, *Standard Practice for Full-Scale Oxygen Consumption Calorimetry Fire Tests* [44]. The fires were centered under the hood of the calorimeter and positioned in an open steel frame which provided support for the thermocouples and heat flux sensors. A load cell was positioned as a support for the fuels. All of the data was recorded at intervals of 1 s on a computer based data acquisition system.

2.2.1 Instrumentation and Measurement Uncertainty

Heat Release Rate

The NIST Large Fire Research Laboratory's 3 m by 3 m oxygen depletion calorimeter has an estimated peak heat release rate capacity of approximately 700 kW. Details on the operation and uncertainty in measurements associated with NISTs 6 m by 6 m oxygen consumption calorimeter were documented by Bryant et al. [45]. Many of the same instruments are shared between the two calorimeters and calibration burns were conducted during each experimental series. As a result, the expanded uncertainty of this device has been estimated as 11 % on the measured heat release rate.

Flame/Plume Gas Temperatures

Gas temperatures were measured with exposed-bead, Chromel-Alumel (type K) thermocouples, with a 1.0 mm nominal diameter. Starting from the exposed bead, the thermocouple wire was sheathed in a 3.2 mm diameter inconel shield, 0.76 m in length. The standard uncertainty in temperature of the thermocouple wire itself is 2.2 °C at 277 °C and increases to 9.5 °C at 871 °C as determined by the wire manufacturer [46]. The variation of the temperature in the environment surrounding the thermocouple is known to be much greater than that of the wire uncertainty [47, 48]. Small diameter thermocouples were used to limit the impact of radiative heating and cool-

ing. The estimated combined expanded uncertainty for temperature in these experiments is 15 %.

Heat Flux

The heat flux was measured with water cooled, Schmidt-Boelter total heat flux gauges. The sensing surface of the heat flux gauges were located 0.95 m horizontally from the center of the burner/fuel and 0.50 m above the top of the burner/pan lip/fuel surface. The manufacturer reports a 3 % calibration expanded uncertainty for these devices [49]. Results from an international study on total heat flux gauge calibration and response demonstrated that the uncertainty of a Schmidt-Boelter gauge is typically 8 % [50]. The gauges were mounted to uprights of the steel instrumentation support frame on opposite sides of the fire.

Mass Loss

The fires were centered under the hood of the calorimeter on a non-combustible platform measuring 0.91 m x 1.2 m x 12 mm thick supported by the load cell. The load cell had a resolution of 1.0 g [51]. The expanded uncertainty is estimated to be 5 %. The load cell was checked between experiments with calibrated weights during the zero and span checks of the calorimeter.

Video and Photographs

A 35 mm single lens reflex camera was used to record digital still photographs of the fires. The camera had an 8 megapixel resolution. A mini DV camcorder with 0.7 megapixel resolution was used to capture the video. A firefighting type thermal imager with 0.08 megapixel resolution was used to capture infrared images in the 8 to 14 micron range. Each camera was positioned on a tripod with a distance of 4.5 m between the centerline of burner to camera lens 4.5 m. The height of each camera was adjusted so that the center of camera lens was positioned 0.5 m above top of the burner.

A schematic drawing of the instrumentation arrangement is shown in Fig. 2.1. The thermocouples were mounted on a steel frame. The frame enabled the thermocouples to be installed at 10 cm intervals from 10 cm to

120 cm above the burner/pan lip/fuel surface. At each 10 cm interval, there were five thermocouples: one centered above the burner/fuel surface and one centered above each edge of the burner/fuel surface, for a total of 70 thermocouples. A plumb bob and steel tape measure, with a resolution of ± 0.5 mm, were used to position and align the thermocouples. The expanded uncertainty for the location of each thermocouple tip is estimated to be $\pm 2.5\%$. The same applies to the location of the heat flux sensor surfaces.

2.3 Results

2.3.1 HRR

Figures 2.3-2.4 show the measured heat release rates for the natural gas, gasoline and polyurethane foam fueled fires. In each graph, the replicate heat release time histories are overlaid to give a sense of the experimental repeatability for each fuel.

On each fuels averaged heat release rate curve, the filled area surrounding the average represents the 95 % confidence level (2σ), based on Type A evaluation of the uncertainty is provided [52]. A Type A evaluation of the uncertainty is any statistical analysis of the data from a series of observations. In this case the evaluation assumed a normal distribution of the data such that doubling the calculated standard deviation (2σ) would yield a confidence level of approximately 95 %.

The natural gas burner provided the most repeatable results, with an average steady state heat release rate of $80 \text{ kW} \pm 9 \text{ kW}$ with an average total heat release of $23.3 \text{ MJ} \pm 1.6 \text{ MJ}$ or 11 % over a 100 s period. It should be noted that 11 % is also the (2σ) uncertainty estimate of the calorimeter. The gasoline, based on the average over a 30 s interval bounding the peak heat release rate of each of the 18 experiments, provided an average peak heat release rate of $80 \text{ kW} \pm 24 \text{ kW}$ or 20 %. The total heat release of the gasoline over the 300 s period after ignition was $13.6 \text{ MJ} \pm 0.6 \text{ MJ}$. The polyurethane foam demonstrated the largest variability of the three fuels in terms of peak heat release rate and time to peak heat release. Averaging over a 15 s interval bounding the peak heat release rate from each of the ten experiments yielded an average peak heat release rate of $45 \text{ kW} \pm 21 \text{ kW}$ or 34 %. The total heat

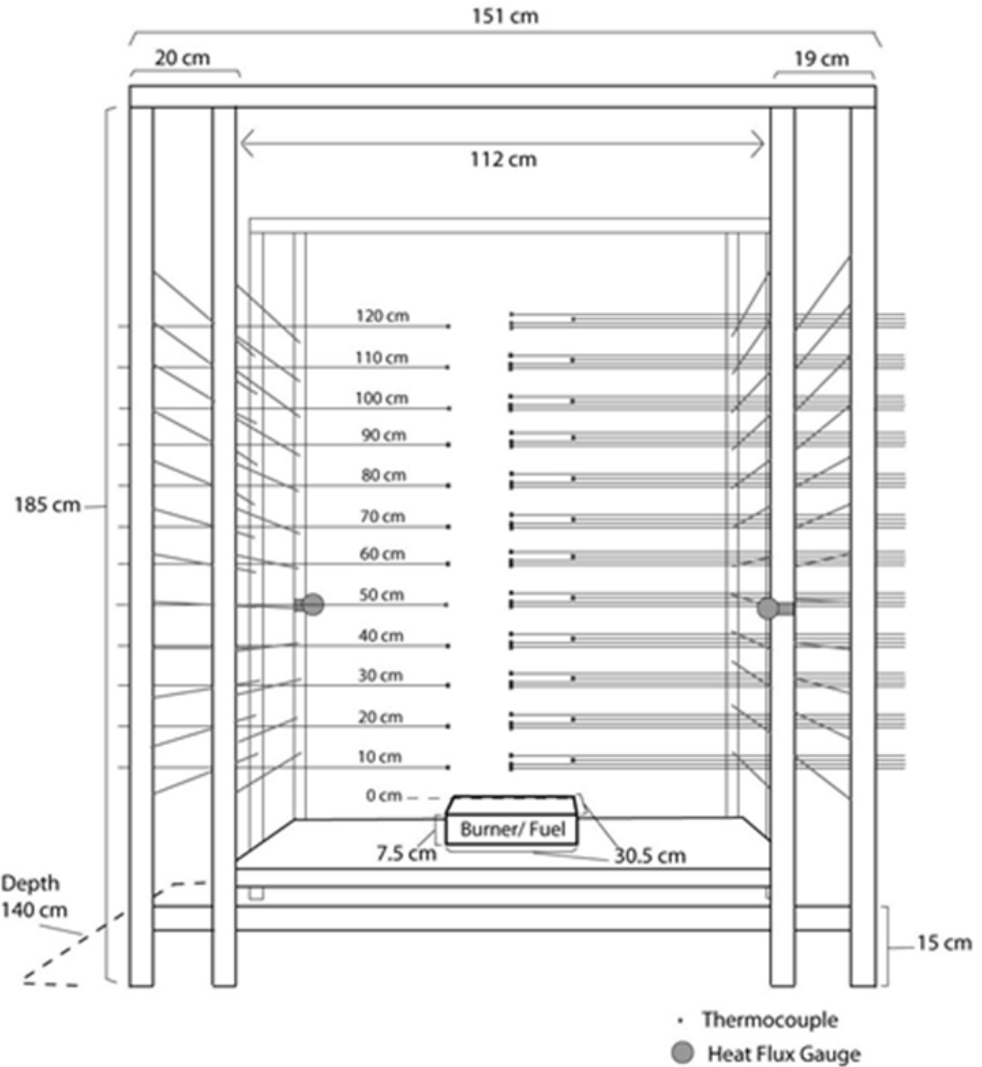


Figure 2.1: Diagram of the source fire flame and plume instrumentation apparatus which was centered under the 3 m by 3 m oxygen consumption calorimeter. The heat flux gauges were facing toward the center of the burner/fuel area.



Figure 2.2: A photograph of the source fire flamer and plume instrumentation apparatus which was centered under the 3 m by 3 m hood of the oxygen consumption calorimeter. In the foreground, from left to right, are the video, 35 mm SLR and thermal imaging camera.

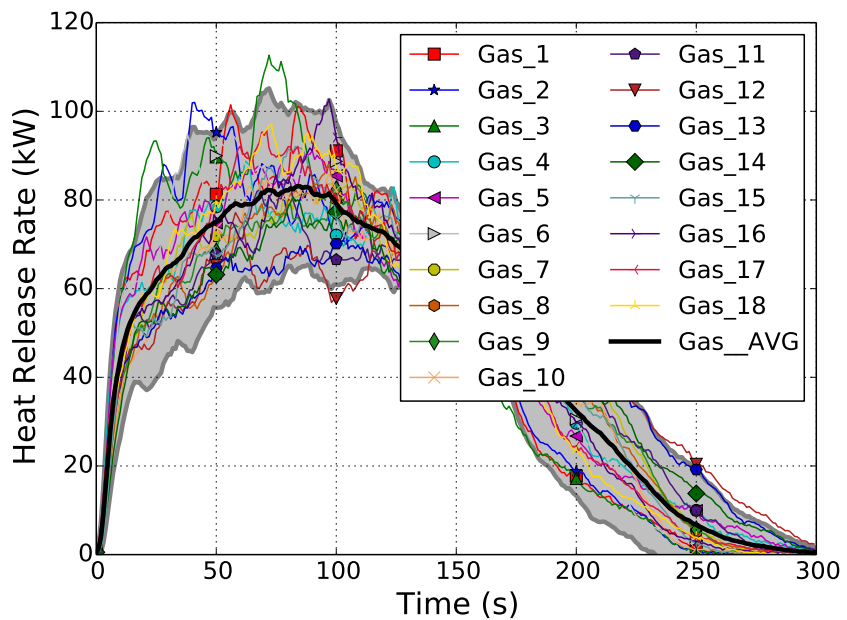
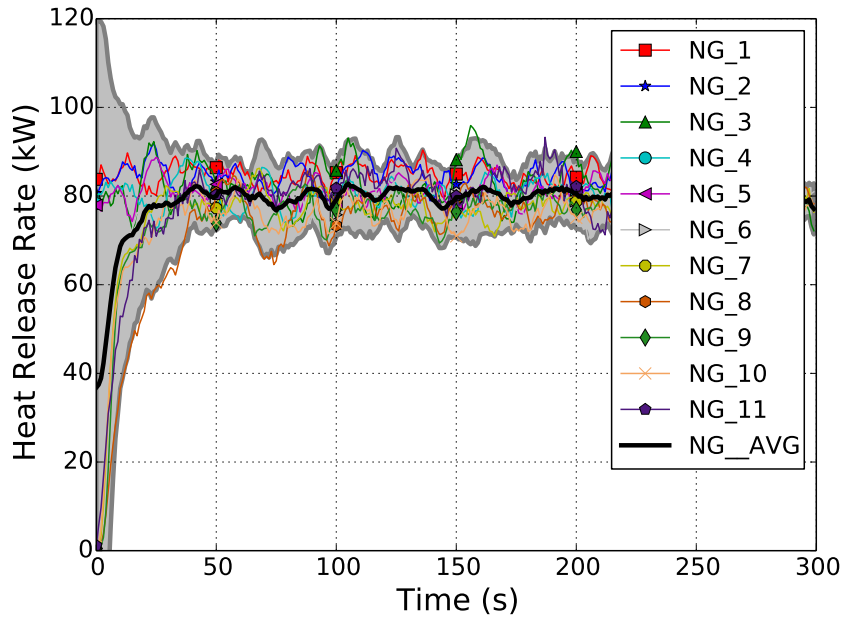


Figure 2.3: Heat release rates for the natural gas and gasoline fires.

release over the 300 s period after ignition was $4.1 \text{ MJ} \pm 0.2 \text{ MJ}$

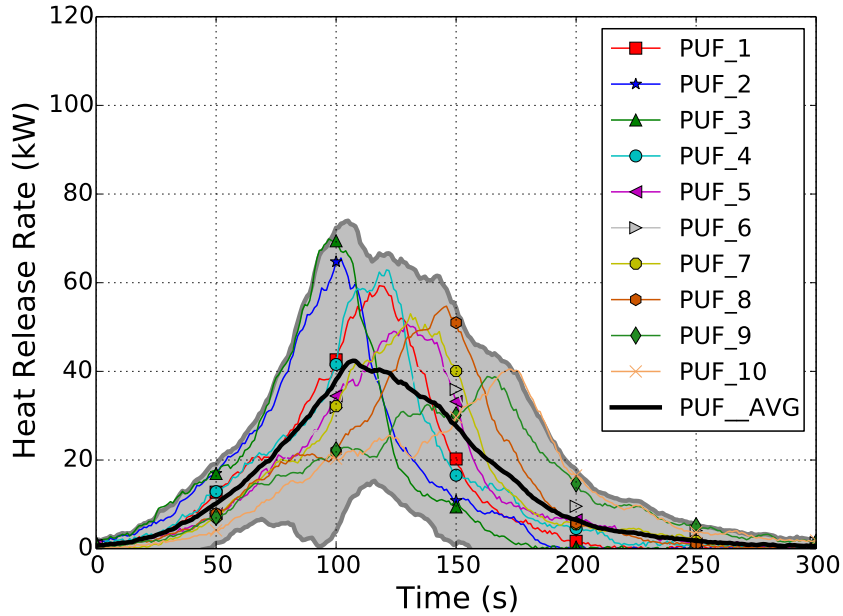


Figure 2.4: Heat release rates for the polyurethane foam fires.

2.3.2 Plume Temperatures

Plots of the centerline temperatures averaged over the replicate experiments for each of the fuels are presented in Fig. 2.5. The natural gas temperatures were averaged over a “steady-state” burning period. The temperature differences between the vertical thermocouple locations, for locations greater than 20 cm above the fire location, begin to decrease as the distances from the top of the burner increase. This trend is similar for both the gasoline fires and the polyurethane foam fires as well. The most notable difference between the natural gas and the other fuels is the growth and decay of the fire during the test period.

2.3.3 Total Heat Flux

Plots of the total heat flux for each of the fuels are presented in Fig. 2.6. The repeatability of the total heat flux values varied in a manner similar to the heat release rates, in that the natural gas fires provided a steady state value while the gasoline and the polyurethane foam fires generated a

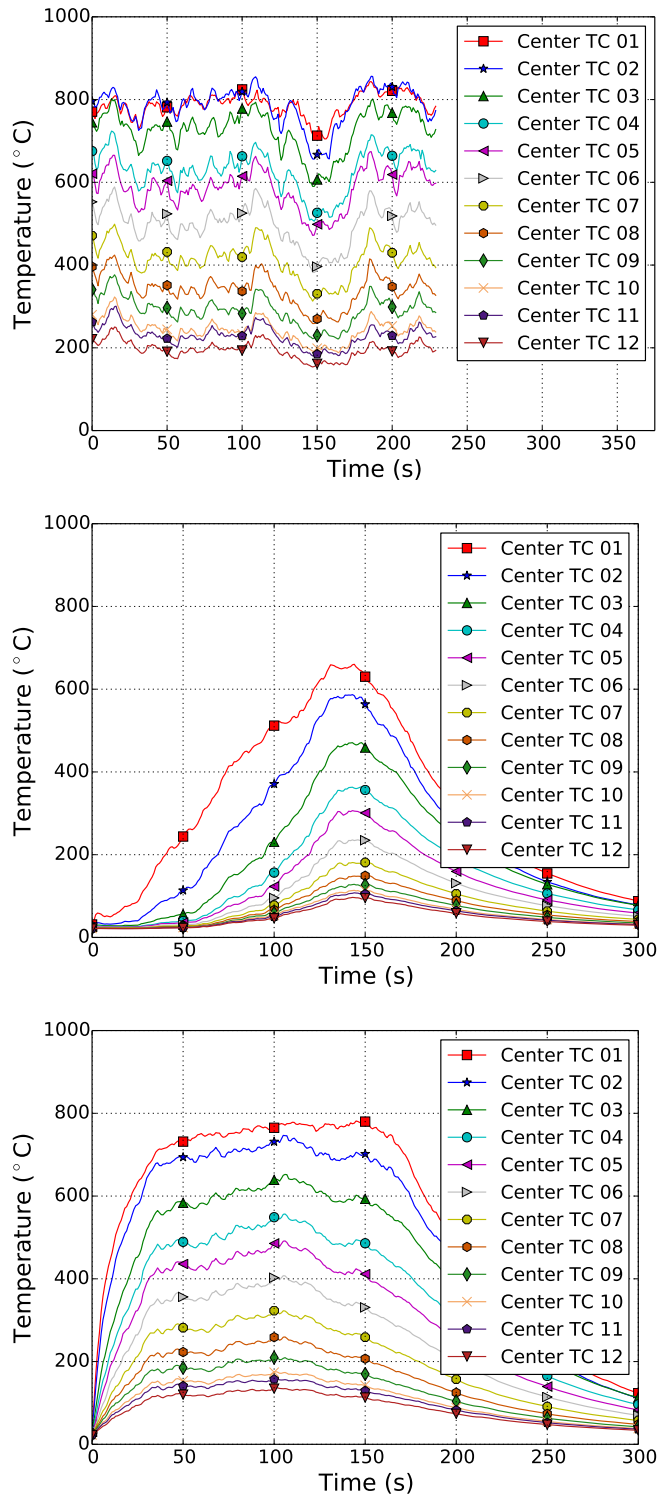


Figure 2.5: Averaged centerline temperature for the natural gas, gasoline, and foam fires. The number following the TC represents the height of thermocouple in decimeters above the surface of the burner.

fire curve that has periods of growth and decay. The sensing surface of the heat flux gauges were located 0.95 m horizontally from the center of the burner/fuel and 0.50 m above the top of the burner/pan lip/fuel surface. The average peak total heat flux for the natural gas fires were approximately 2.0 kW/m^2 . The average peak values for the gasoline and polyurethane foam were approximately 3.5 kW/m^2 and 2.5 kW/m^2 respectively. The values are only presented for the experiments which had two heat flux gauges installed as described in the instrumentation section above.

2.3.4 Mass Loss

Mass loss measurements were not possible for the natural gas burner experiments. The mass loss versus time curves for the gasoline and the polyurethane experiments are shown in Fig. 2.7. The gasoline exhibits a linear mass loss rate for the initial 150 s of approximately 2 g/s. The polyurethane foam was ignited with a small flame in the center of the top surface of the foam block. As the flame spread across the surface it also began to burn down into the foam sample. As a result the exposed surface of the foam began to take the shape of a bowl as the burning rate became linear at approximately 2 g/s.

2.3.5 Flame Height

Each of the experiments was photographed with a digital single lens reflex (SLR) camera, fixed on a tripod, with a capability of capturing at least five images per second. Located adjacent to the camera was a video camera recording images at approximately thirty 30 frames per second (fps). The experiments were also recorded with a thermal imager, however the videos were not used for analysis as it was difficult to determine the differences between the visible flame and the thermal plume from the black and white images.

In engineering terms, the “flame height” is typically discussed as the median flame height. A position above the top of the fuel surface where the flame is observed to be present at least 50 % of the time. As a starting point, the mean flame height for each fuel was estimated from a measurement of the uppermost continuous flame tip from the still photographic images.

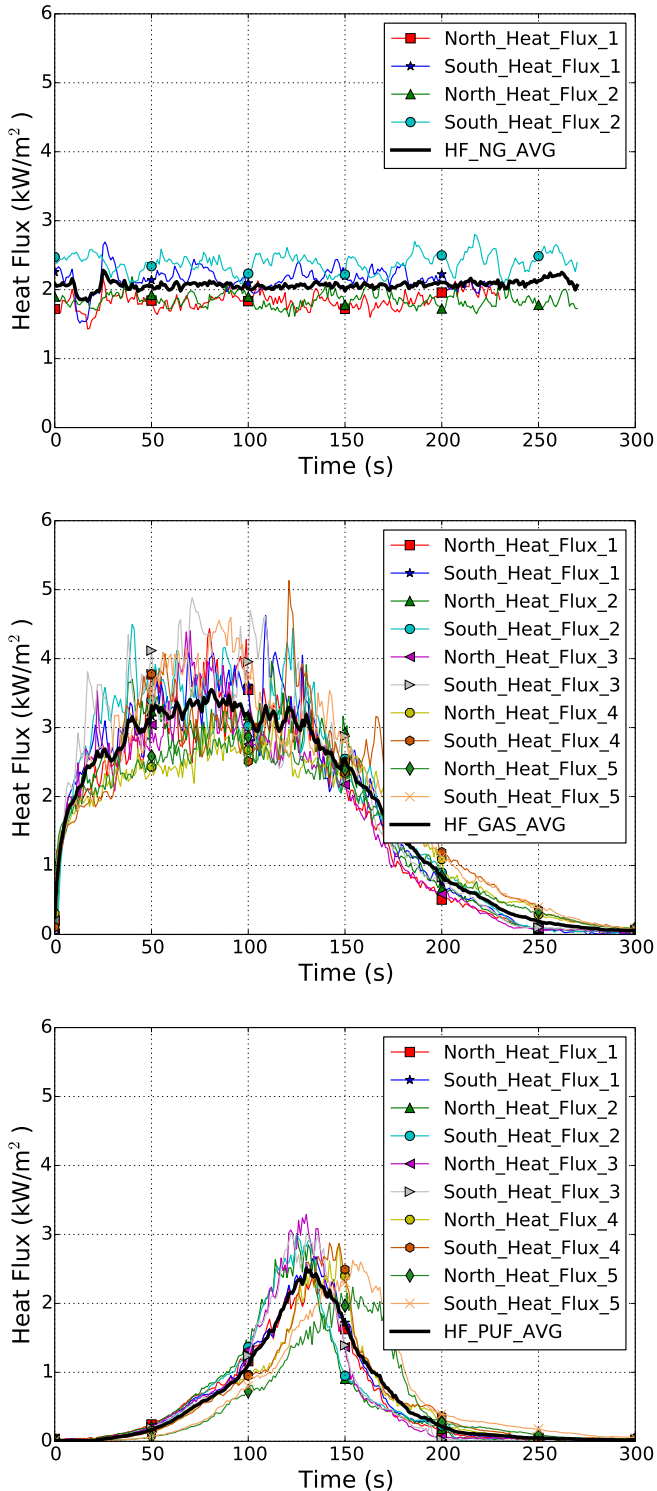


Figure 2.6: Total heat flux versus time for natural gas, gasoline, and foam fires.

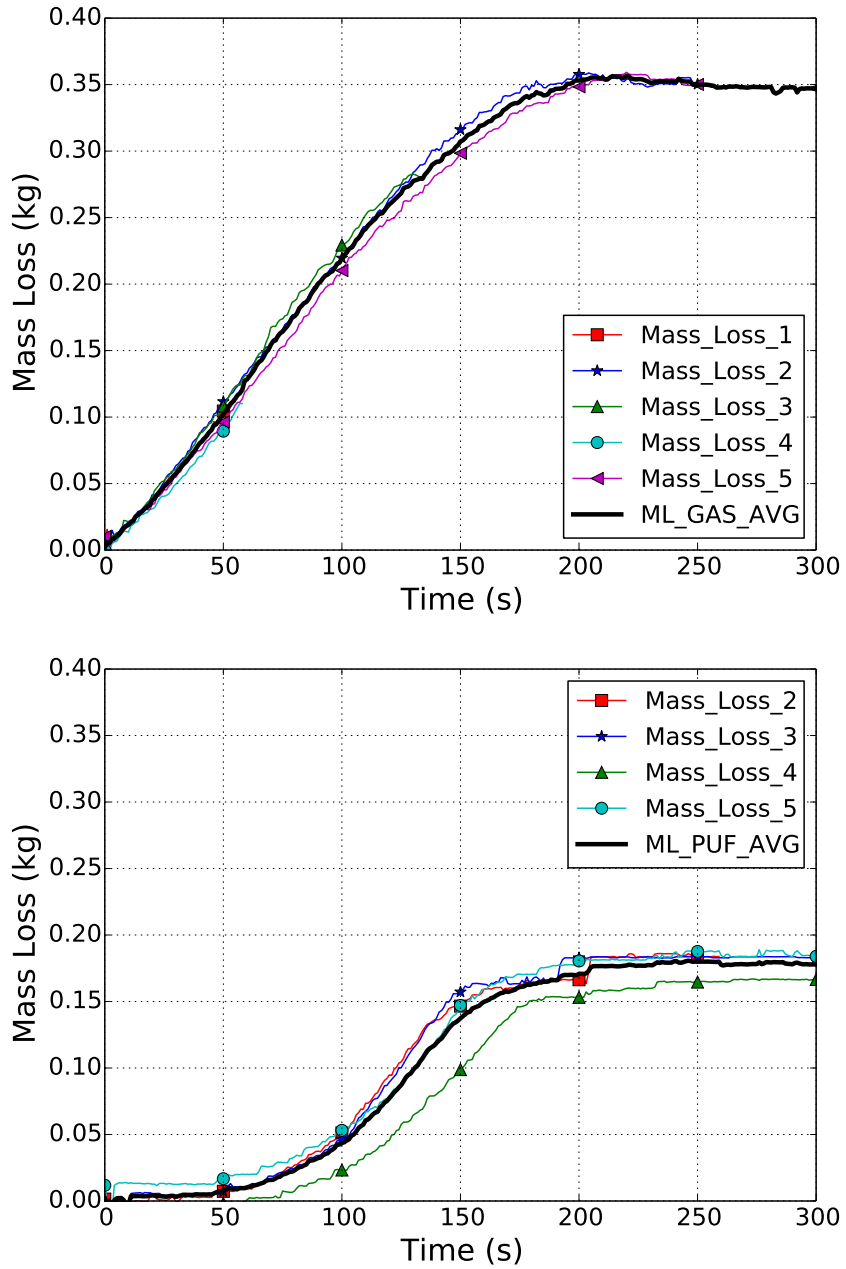


Figure 2.7: Mass loss versus time for the gasoline and foam fueled fires.

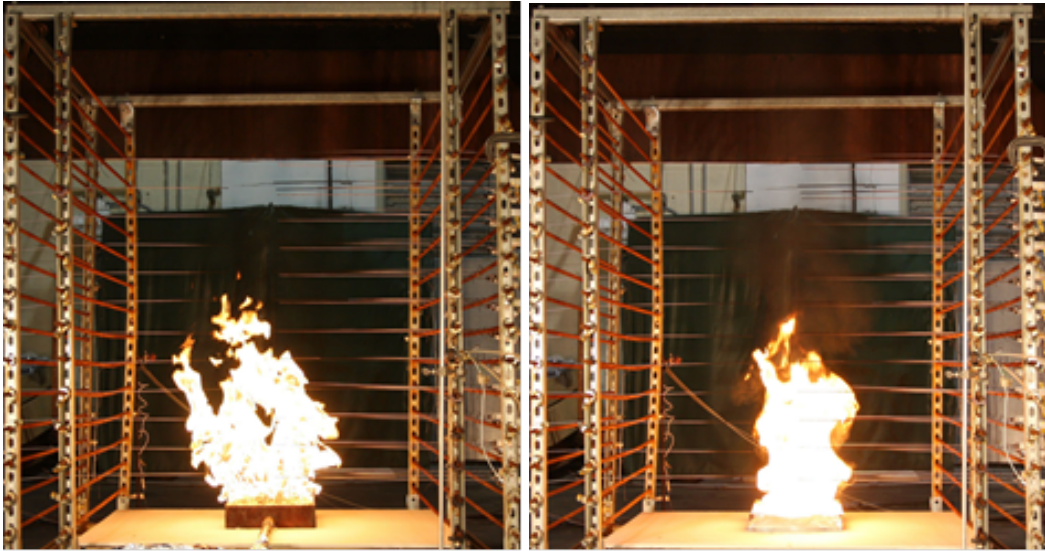


Figure 2.8: Photographs showing a natural gas fire (left) and a polyurethane foam fire (right) under the oxygen consumption calorimeter.

Examples of the photographic images are presented in Figs. 2.8 and 2.9. Figure 2.8 is a photograph of the natural gas flame taken during a period of “steady state” burning at approximately 80 kW and a photograph of the polyurethane foam fire taken near its peak heat release rate of approximately 60 kW. Figure 2.9 presents two photographs of the same gasoline fueled fire when it was burning near its peak heat release rate of 100 kW. The two photographs, taken 0.2 s apart, represent the range of the observed flame heights from one of the gasoline experiments from 0.65 m and 1.0 m, respectively.

Table 2.1 provides the mean visible flame height, as well as the range of flame heights for each fuel, based on analysis of the photographs for three replicate experiments. In each case, the photographs were chosen for analysis while the fire was generating its peak heat release rate. The range of flame heights for each fuel is approximately twice the minimum flame height or the continuous flame height. Analyzing the photographs in this manner was very time consuming and was based on making measurements on each photograph with a scale. The limit of 5 frames per second also introduces additional uncertainty in determining the flame height. These values will serve as a

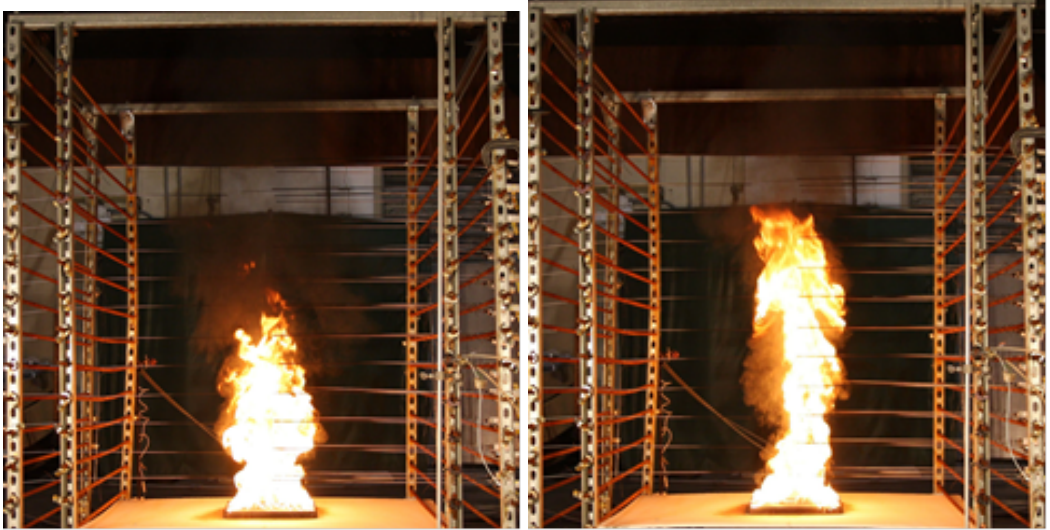


Figure 2.9: Photograph showing a gasoline fueled experiment with a flame height of 0.65 m (left) and a photograph taken approximately 0.2 s later with a flame height of 1.0 m (right).

basis for comparing with mean flame height values determined with video analysis.

As noted by Beyler in his review of fire plume correlations, video tape analysis seems to provide the best estimates of flame height [34]. Each experiment was recorded with a digital video camera at a refresh rate frequency of 29.97 fps which is the National Television Standards Committee (NTSC) standard. The resulting image in each frame was 720 pixels wide by 480 pixels high. Segments of the video which corresponded to the peak heat release of each experiment were captured with a video editing program.

For the natural gas experiments, approximately 30 s of “steady state” video were captured. In the cases of the gasoline and polyurethane fueled experiments, the video capture period bounded the peak heat release rate. In the case of the gasoline fueled fires, the peaks occurred over a long period of time, so a 30 s video capture could be made which was representative of the peak burning rate. The peak duration for the polyurethane foam fires was shorter so, only a 15 s video capture was used.

Each frame from the video clip was saved as a full color Tagged Image

Fuel	Mean (m)	Range (m)
Natural Gas	0.70	0.50 to 0.98
Gasoline	0.84	0.52 to 1.10
Polyurethane Foam	0.46	0.30 to 0.78

Table 2.1: Mean visible flame height and averaged minimums and maximums (Range) of visible flame heights for each of the fuels during peak heat release rate.

File Format (TIFF) file and the pixel aspect ratio was changed from 0.9 to 1, so that each pixel had the same dimension in both the horizontal and vertical directions. Once these images were rendered by the video editing program, each image was scaled and cropped to provide input for Streams, a suite of image processing programs developed by Nokes for analyzing fluid flow visualization experiments [30]. The images were scaled so that one pixel equals 5 mm in height and width.

Examples of a set of TIFF images for each fuel are shown in Figures 2.10 through 2.12. Each figure has 56 sequential images from the video segment. The images total almost 2 s of actual burn time. Notice how the flame height cycles up and down in each of the sequences. These images provide additional information and continuity of the motion of the flame so that the analysis is less likely to miss an extreme (minimum or maximum) position when compared to the still photographs.

From each of the peak heat release rate video clips, the edited TIFF files were loaded into Streams [30]. For the natural gas and gasoline fueled fires, approximately 900 images were used in each image sequence. The polyurethane foam experiments had approximately 450 images in each sequence for each experiment. Once the image sequence was created, a series of filters and amplifiers are applied to the images to eliminate all colors but red, based on a method developed by Goble [53]. Once all of the images were converted to a pure red “flame” which represented the area of visible fire, on a black background, the images were processed within Streams to develop an intensity field based on all of the images being “overlaid” on each other. The end result is a contour plot of the intermittency of the flame ranging from zero to one.

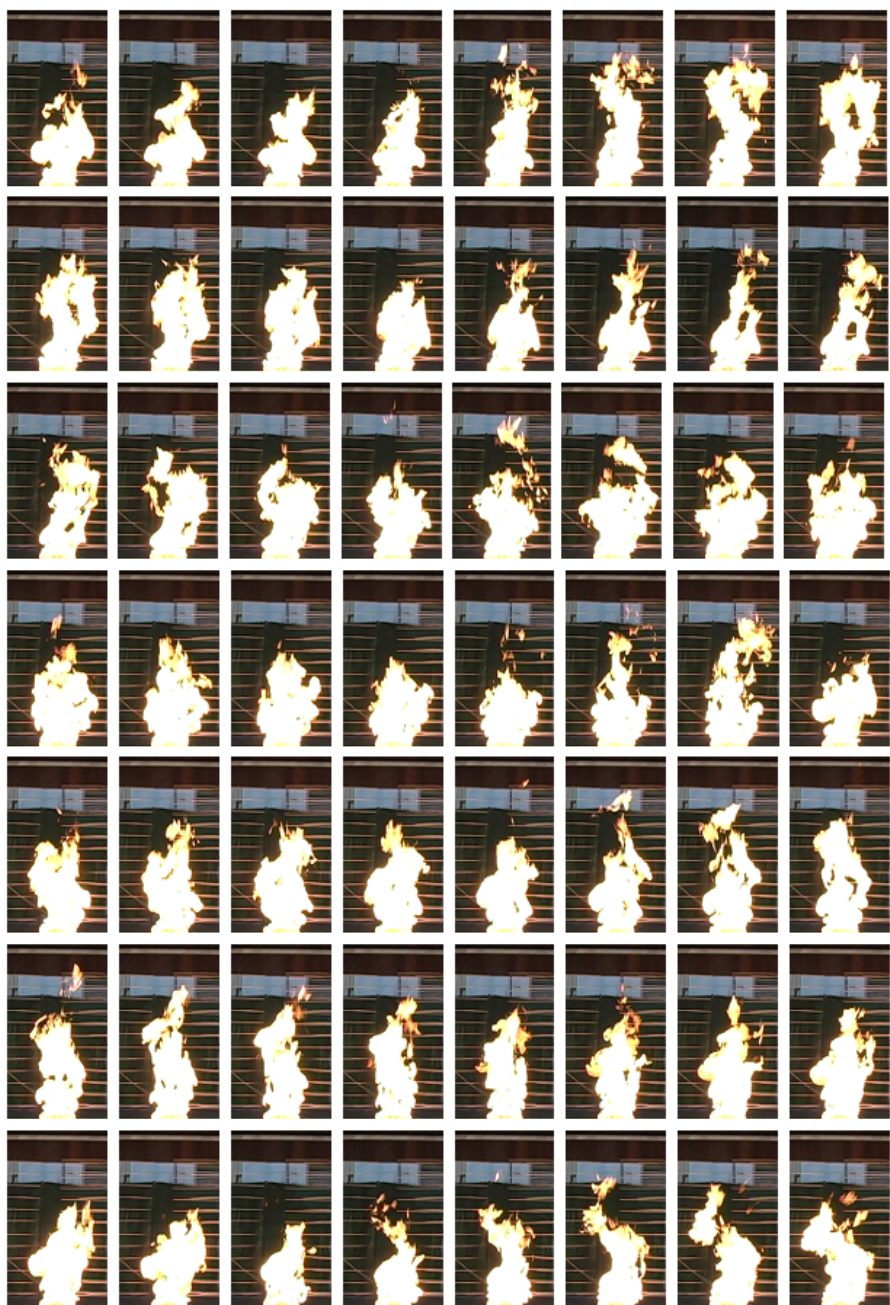


Figure 2.10: Example of sequential video frames sampled from a natural gas fueled experiment. In this set of images, which spans almost two seconds, the visual continuous flame height fluctuates from approximately 0.6 m to 1.1 m.

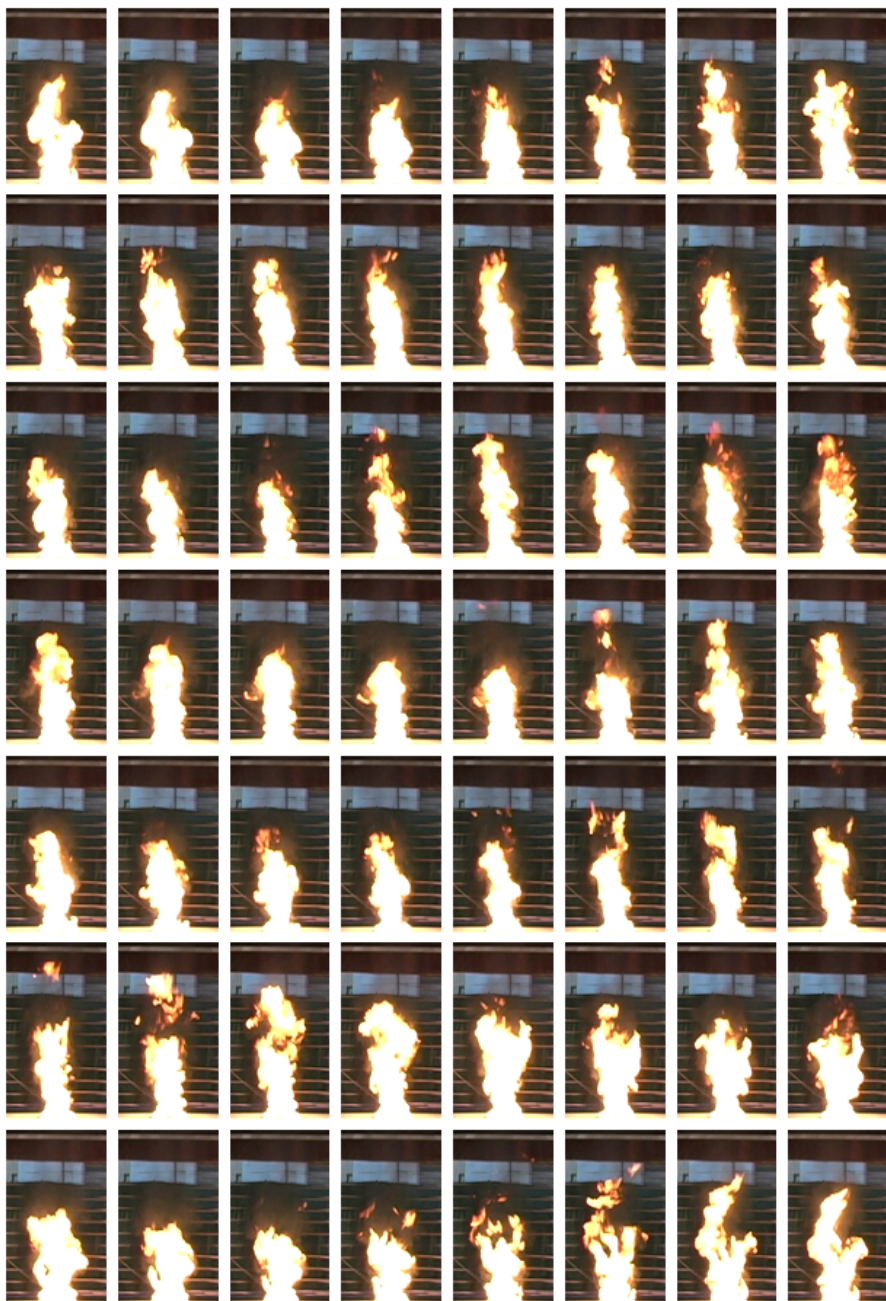


Figure 2.11: Example of sequential video frames sampled from a gasoline fueled experiment. In this set of images which spans almost two seconds the visual continuous flame height fluctuates from approximately 0.6 m to 1.1 m.

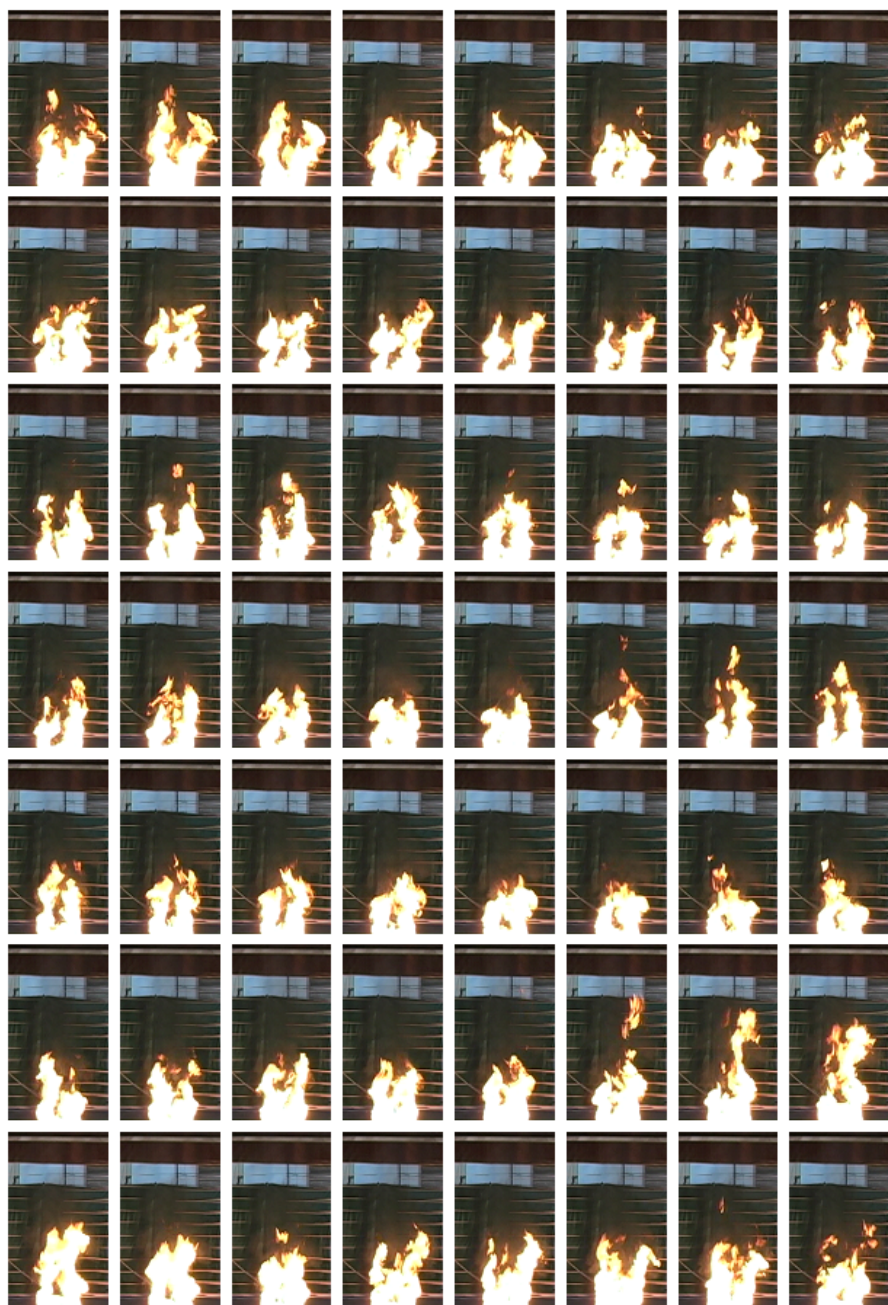


Figure 2.12: Example of sequential video frames sampled from a polyurethane foam fueled experiment. In this set of images which spans almost two seconds the continuous visual flame height fluctuates from 0.4 m to 0.9 m.

The calculations for the intensity field are based on a user defined computation grid. A grid sensitivity analysis was conducted with 5 mm, 10 mm, 20 mm, 40 mm and 80 mm square grids. Examples of grid cell resolution outputs from Streams for the natural gas fueled burner are shown in Fig. 2.13. The outputs shown are time averaged intensity fields generated with 5 resolutions listed above. In each output the x and y axis dimensions are in mm.

Since each pixel in the original images was equal to 5 mm, in the highest resolution case, the 5 mm analysis grid would match the best resolution of the original image. Four of the five cases resulted in similar results, only the 80 mm case generated significantly different results in flame height. As a result of the sensitivity analysis, a 10 mm grid was chosen as an optimum size for providing a sufficient level of resolution, enabling efficient processing of 30 s worth of video frames. At the 5 mm grid resolution, limitations within the processing system would not allow a full 30 s of video analysis. Therefore the intensity fields and the resulting plots and data generated for this study were developed with a 10 mm grid.

Another means of quantifying field data with Streams is the use of contour plots. Examples of the time averaged contour plots are shown in Figs. 2.14 and 2.15 for the natural gas, gasoline, and polyurethane fueled fires. Each contour line represents the percentage of time that the flame was at a given position. The region under examination, as shown as a black bounding rectangle, is 1400 mm high and 800 mm in width. The natural gas fire was sampled for 29 s, resulting in 870 images. The area bounded by the contour with the value 1 represents the area that the flame was visible 100 % of the time sampled. This can be considered the persistent flame region as defined by McCaffrey [54]. The remaining contours are in the intermittent flame region, with the 0.5 contour representing the mean flame height. Outside of the final contour, value 0.0, no visible flame was recorded; hence this contour marks the definitive start of the buoyant plume region.

Figure 2.15 shows two different contours for the polyurethane foam fueled experiment. The results from polyurethane fueled fire characterization experiments have an increased amount of variability due to the nature of the ignition source and the fuel itself. The polyurethane foam was readily

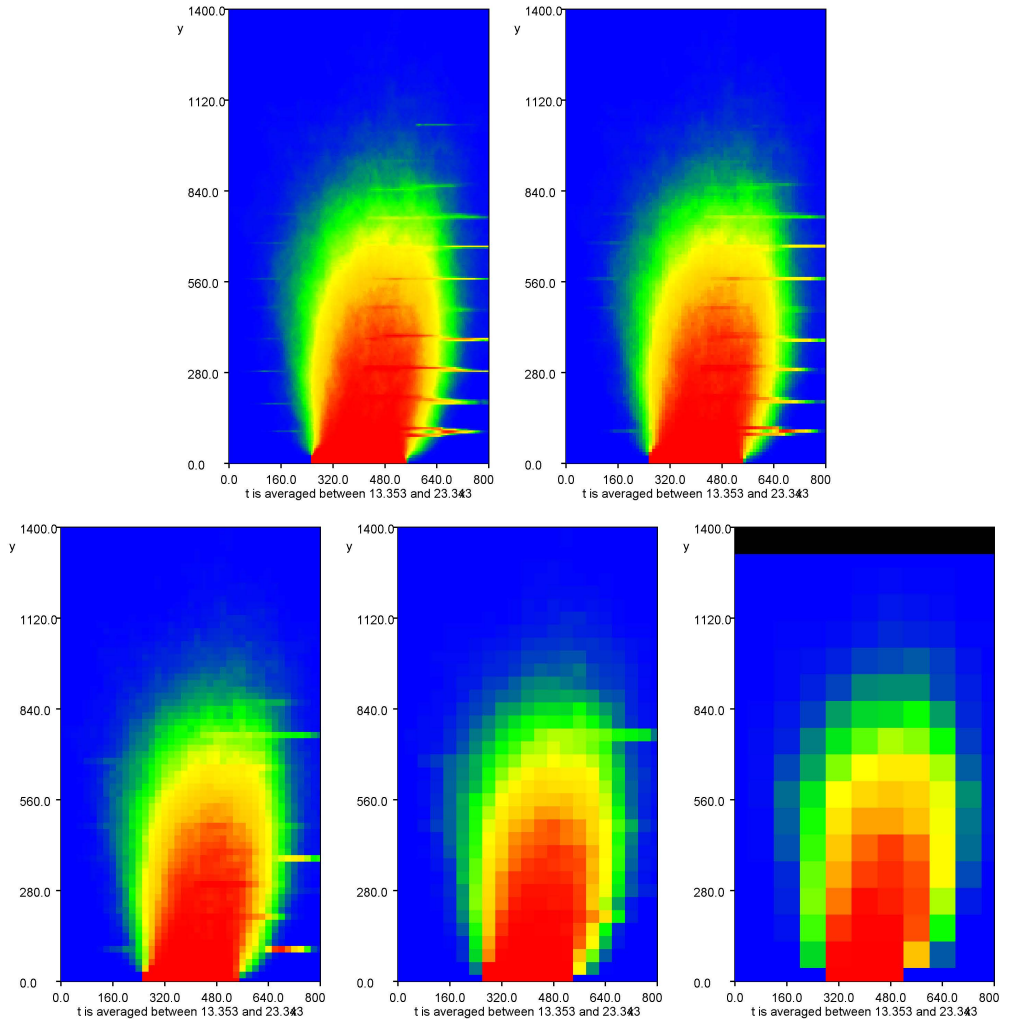


Figure 2.13: Comparison images of intensity fields derived from the video images of the natural gas fueled fire using Streams. The images, starting with the upper left, were generated with 5 mm, 10 mm, 20 mm, 40 mm and 80 mm resolutions.

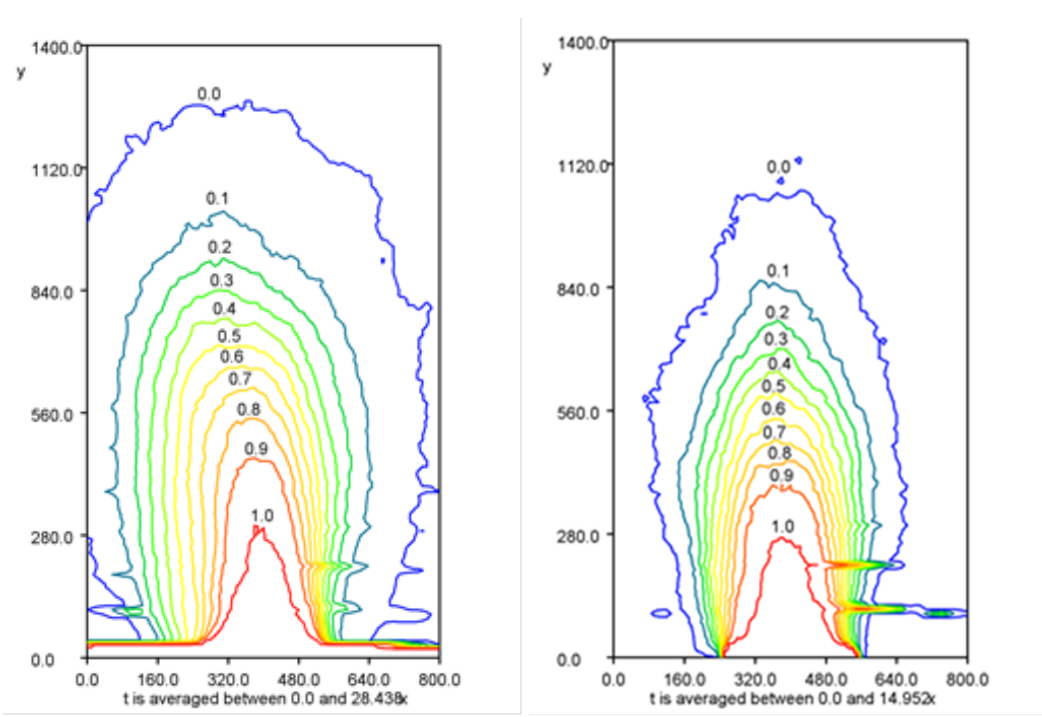


Figure 2.14: Plots showing the fraction of time that the flame was visible for the natural gas (left) and gasoline (right) fires.

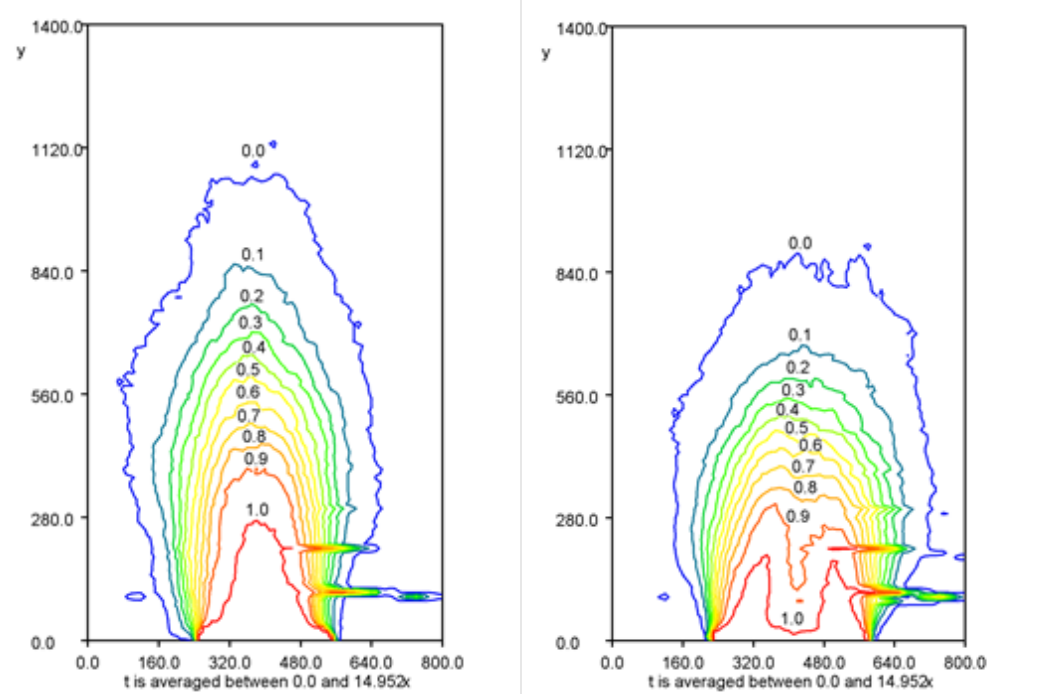


Figure 2.15: (Left) Plot showing the fraction of time that the flame was visible for the polyurethane foam fire. (Right) Polyurethane foam contour plot with bifurcated flames at time of peak heat release rate.

ignited with a small pilot flame similar to that used to ignite the natural gas and the gasoline. By comparison, a small flame ignited the gases flowing out the top of the natural gas burner and the flames from the natural gas cover entire burner surface within approximately one second. A similar ignition sequence occurs with the gasoline pan fires. The polyurethane foam has a more complicated flame spread sequence that resulted in significant changes to the peak heat release rate and the time to peak heat release. Once the polyurethane foam was ignited, it took approximately 60 s for the flame to spread across the top surface of the fuel. As the flames spread horizontally across the fuel surface, the fire also burns down into the fuel. In some cases the fire burned completely through the fuel in the center of the foam sample, resulting in a hollow flame at the time of the peak heat release rate. An example of a contour plot, exhibiting the hollow or bifurcated flames is shown at right in Fig. 2.15. Other methods of ignition for the polyurethane foam were considered in order to have a more uniform ignition of the top surface of the foam. Each method would have resulted in a larger release of energy from the ignition source or a starter fuel. Based on a few scoping experiments these methods did not improve the repeatability.

Based on the field data developed using Streams average flame heights for each fuel were determined. In Table 2.2, each of the values represents the average flame heights, given in mm with 95 % confidence limits based on a Type A statistical analysis of the data, for each of the source fuels shown as the percentage of time the flame was visible at that given height. For the natural gas fires, the averages are from ten 30 s segments, while the fire was monitored at approximately 80 kW. In some cases more than one 30 s segment was sampled per heat release rate experiment. Sixteen 30 s video segments, which included the peak heat release rate, were successfully analyzed from the seventeen gasoline heat release rate experiments. One of the videos was unusable for analysis due to reflected light which could not be edited out of the images. For same reason, the polyurethane foam flame height averages are the result from eight of the ten heat release rate experiments.

For both the natural gas and the gasoline experiments the 95 % confidence limits show less than 20 percent variation in visible flame height within the intermittent flame region. The percentage variation increases at the con-

Visible Fraction (%)	Visible Flame Heights (mm)		
	Natural Gas	Gasoline	Polyurethane Foam
10	980 ± 155 (16 %)	930 ± 130 (14 %)	650 ± 220 (34 %)
20	890 ± 125 (14 %)	850 ± 120 (14 %)	590 ± 190 (32 %)
30	820 ± 125 (15 %)	790 ± 110 (14 %)	540 ± 180 (33 %)
40	760 ± 105 (14 %)	740 ± 95 (13 %)	500 ± 165 (33 %)
50	705 ± 106 (15 %)	695 ± 95 (14 %)	470 ± 160 (34 %)
60	650 ± 100 (15 %)	655 ± 85 (13 %)	435 ± 135 (31 %)
70	590 ± 90 (15 %)	610 ± 90 (15 %)	400 ± 125 (31 %)
80	530 ± 85 (16 %)	555 ± 90 (16 %)	360 ± 110 (31 %)
90	440 ± 75 (17 %)	490 ± 95 (19 %)	315 ± 110 (35 %)
100	220 ± 84 (38 %)	350 ± 110 (32 %)	210 ± 125 (60 %)

Table 2.2: Average flame heights with 95 % confidence limits, for each of the source fuels shown as the percentage of time the flame was visible at that given height.

tinuous flame region, although the magnitudes of the height variations are similar to other sections of the intermittent flame region. The percentage variation is higher in the continuous flame region because the height of the continuous flame region is the smallest. The 95 % confidence limits for the polyurethane foam are about twice those of the natural gas and the gasoline.

2.3.6 Summary

The source fires have been characterized in terms of heat release rate, plume temperature, total heat flux, mass loss and flame height. This data has been collected for use in direct analysis of the burn patterns and as input into the engineering correlations and FDS models that are used later in this study.

Chapter III

Instrumented Non-combustible Wall Experiments

Once the characteristics of the fires had been measured, the next step was to measure the thermal impact that the fires had on a vertical target surface. In these experiments the target is a non-combustible wall. The non-combustible material was chosen to minimize any contribution from the wall to the fire. The fires were placed at predetermined, fixed positions away from the wall. In the remainder of the report the term burner will be considered synonymous with the pan for the liquid fuel or the block of solid fuel. Experiments were conducted with the closest edge of the burner located in the following positions from the wall: two burner widths (0.610 m), one burner width (0.305 m), one half burner width (0.150 m), and then touching the wall (0.0 m).

3.1 Experimental Arrangement

A free standing steel frame wall with a 12.7 mm thick, 2.44 m high by 1.22 m wide, calcium silicate board face was instrumented to measure the thermal exposure of the wall from the fire in terms of temperature and heat flux. Marinite Type I is the commercial name of the non-combustible board used in these experiments. It is normally used as a fire-resistant thermal insulation that also has structural strength. 90 % of the board is composed of calcium silicate and calcium meta-silicate. The remaining 10 % of the board is composed of a combination of organic fibers, fiber glass filament and crystalline silica (quartz) [55]. Material properties that impact heat transfer were selected from the manufacturer's literature and are presented in the table below [56].

Two vertical arrays of water cooled, Schmidt-Boelter total heat flux gauges,

Density (kg/m ³)	Thermal Conductivity		Specific Heat	
	Temperature (°C)	(W/mK)	Temperature (°C)	(kJ/kg °C)
737	24	0.13	93	0.28
	205	0.12	205	0.30
	316	0.11	316	0.32
	425	0.12	425	0.34
	538	0.12		

Table 3.1: Thermal properties for Marinite I, as reported by the manufacturer BNZ [56]

as previously described in the instrumentation section above, were installed at 20 cm intervals from 0.2 m to 1.2 m above the burner. One vertical array was centered on the burner and the other vertical array was centered on the right edge of the burner. The arrangement is shown in Fig. 3.1. Bare-bead, Chromel-Alumel (type K) thermocouples, with a 0.5 mm nominal diameter were installed next to the center of each heat flux sensors and continued, at 20 cm intervals, up to a height of 2.2 m above the surface of the burner. Photographs of the front and rear of the instrumented wall are shown in Figures 3.2 and 3.3. The thermocouples were installed in small holes from the back of the wall. The bead of the thermocouple was flush with the surface on the calcium silicate board and was in contact with the board, as shown in Figure 3.4. For the center array, a second thermocouple was installed on the backside of the calcium silicate board, approximately 10 mm below the TC positioned on the front surface of the wall. The photograph in Figure 3.5 shows a rear thermocouple with the bead in contact with the rear surface of the wall and the relative position to the thermocouple on the front surface of the wall. In a manner similar to the source fire characterization experiments, the instrumented wall experiments were conducted under the NIST Large Fire Research Laboratory's 3 m by 3 m oxygen depletion calorimeter.

3.2 Results

The results are presented for each of the four burner positions, (0.61 m, 0.31 m, 0.15 m and 0.0 m), and each of the three fuels in Appendix B. For the natural gas fueled experiments only two replicates were conducted at each

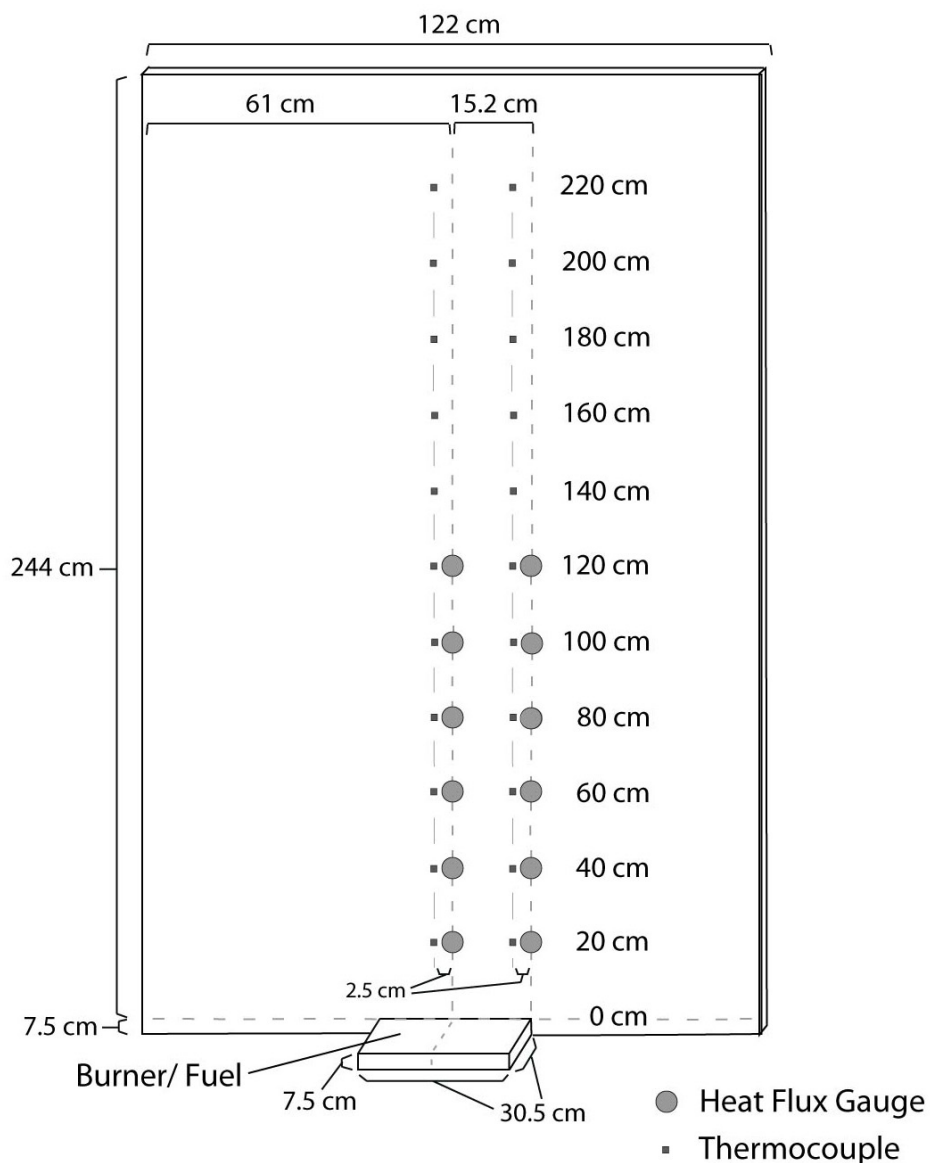


Figure 3.1: Diagram of the instrumented non-combustible wall. Two vertical arrays of total heat flux gauges and thermocouples were installed along the centerline of the burner and along the right edge of the burner.



Figure 3.2: Photograph of the front side of the instrumented non-combustible wall.



Figure 3.3: Photograph of the rear side of the instrumented non-combustible wall.

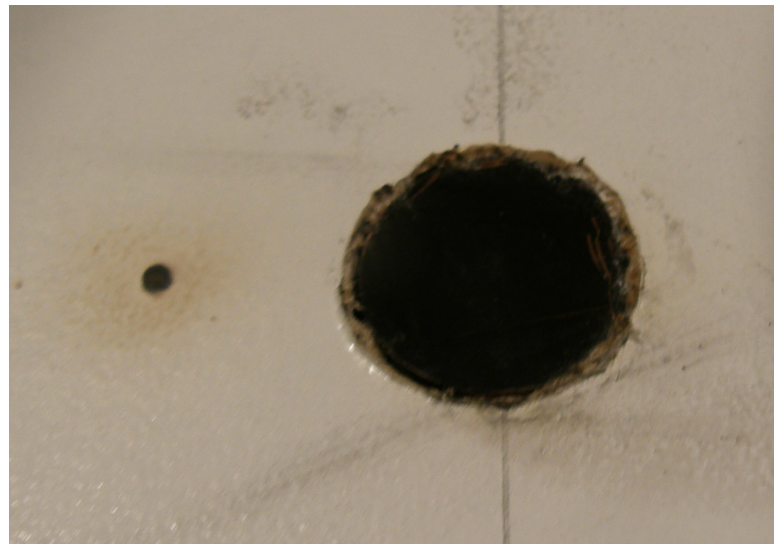


Figure 3.4: Photograph showing an example of the co-location of the heat flux gauges and the thermocouples on the front surface of the wall.

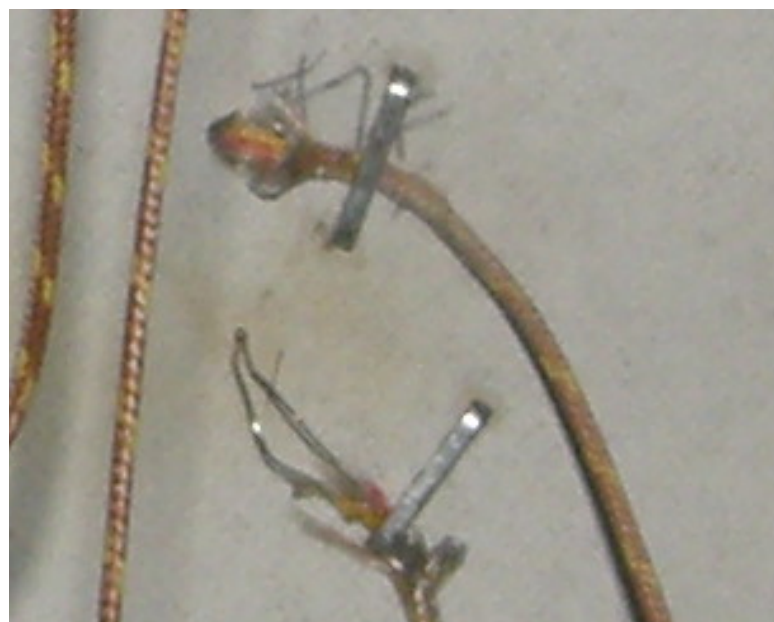


Figure 3.5: Photograph of an example of the co-location of the thermocouple on the rear surface of the wall relative to the thermocouple installed on the front surface of the wall.

position given the higher level of control and repeatability. For the gasoline and polyurethane fueled experiments, three replicates were conducted at each position. The position is measured as the distance between the edge of the burner closest to the wall and the wall. The results of the wall temperatures and heat fluxes are presented as averages of the replicate experiments. In the sections below, a full set of the averaged data from the natural gas fueled experiments will be presented to demonstrate the impact on distance from the wall on the temperatures in the plume as well as the conditions measured on the wall. Then composite graphs of the wall temperatures and heat flux measure on the wall versus distance will be shown for each fuel type.

Figures 3.6 through 3.9 show a complete set of data, averaged over two replicates, for the instrumented, non combustible wall natural gas burner experiments. Comparing the temperatures of the plume at the most distant point from the wall, 0.61 m and with the plume temperatures with the burner contacting the wall in Figure 3.6 shows an increase. However for the burner position, 0.15 m from the wall, a decrease in plume temperatures occurs after approximately 3 min after ignition. A review of the heat release rates and the test videos do not yield any clues as to the reason for this decrease which occurred in both experiments. In both experiments the heat release rate was steady and the video did not show any change in flame movement. Figures 3.7 and 3.8 show consistent trends of the thermocouple temperatures in the vertical arrays on the wall increasing as the burner was moved toward the wall. Figure 3.9 shows that the peak temperatures aligned with the vertical center of the burner on the backside of the gypsum wallboard peaked at approximately 100 °C.

Figures 3.10 and 3.11 provide the heat flux measurements for the two vertical arrays of gauges positioned along the centerline and the edge of the natural gas burner. The series of graphs show that the peak heat flux increases by as the burner is moved toward the wall. One exception is when the burner was moved from the 0.15 m position to the 0.0 m from the wall. In this comparison the peak heat flux values for the gauges located above the edge of the burner do not uniformly increase. In fact the peak heat flux actually decreased as the burner was moved from the 0.15 m position to the 0.0 m position. This decrease was due to the change in view angle between

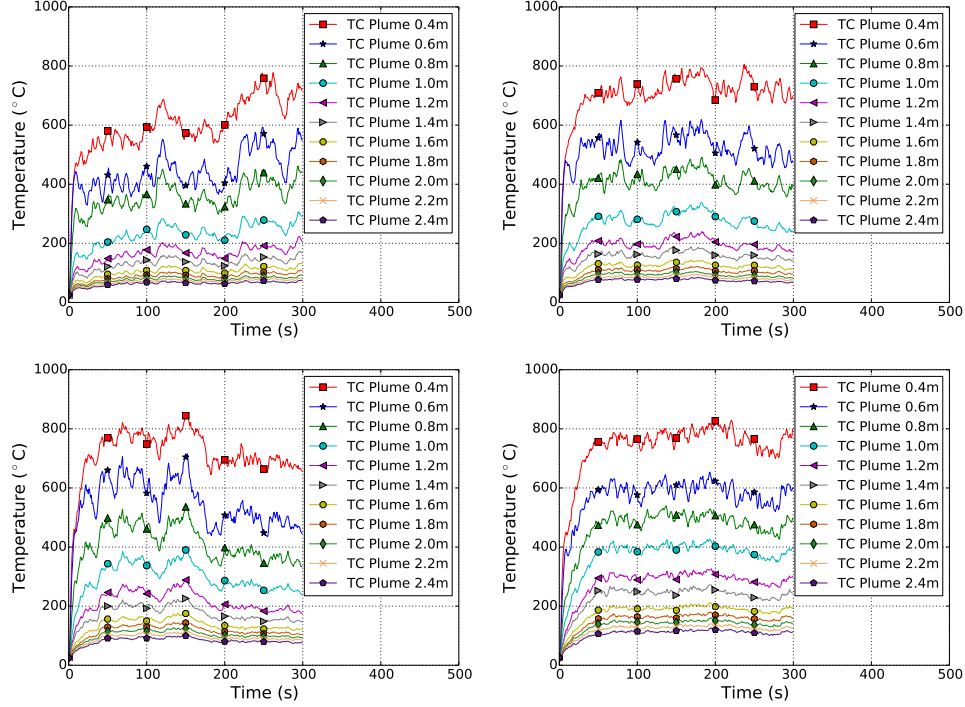


Figure 3.6: Plume temperatures along the centerline of the natural gas fueled burner. The temperatures are averages of two replicate experiments. Each graph displays data from a different distance between the edge of the burner and the instrumented wall. Beginning with the top left graph position and viewing left to right the distances from the wall are 0.61 m, 0.31 m, 0.15 m, and 0 m respectively.

the flame closest to the burner and the lower heat flux gauges at the edge of the burner.

In the following sections, the data is compiled so that averaged peak values, of a given measure, for each position from the wall will be presented on a single graph for a given fuel type.

3.2.1 Wall Temperatures

Figure 3.12 shows the temperatures of the array of thermocouples located along the vertical centerline of the burners for each of the three fuels. Reviewing the graph for each fuel demonstrates how the temperature at the wall decreased as the position of the burner was moved away from the wall. The

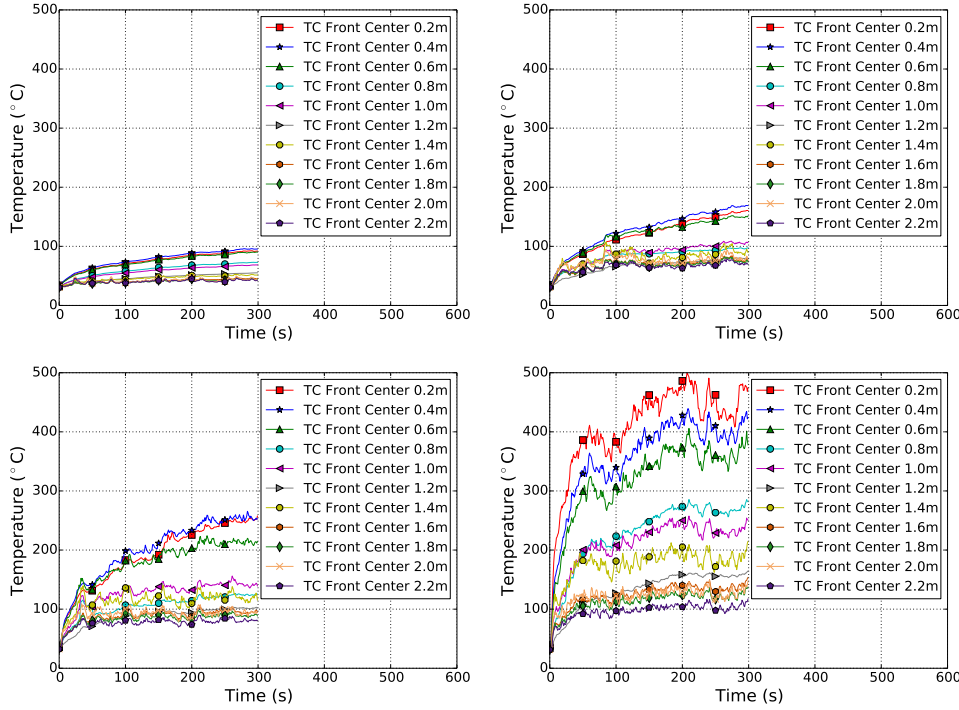


Figure 3.7: Wall Temperatures along the centerline of the natural gas fueled burner. The temperatures are averages of two replicate experiments. Each graph displays data from a different distance between the edge of the burner and the instrumented wall. Beginning with the top left graph position and viewing left to right the distances from the wall are 0.61 m, 0.31 m, 0.15 m, and 0 m respectively.

beads of the thermocouples were installed in the wall and were flush with the wall surface. In each graph, the average peak temperature of the replicate experiments, for each thermocouple position is shown. Moving from 0.2 m above the top surface of the burner up to 2.2 m above the top of the burner surface in increments of 0.2 m. As with the data analysis for the source fires, the peak averages were based on a 30 s period bounding the peak for the natural gas and gasoline fires. A 15 s interval bounding the peak was used for the polyurethane, in order to be more representative of the peak conditions.

Figure 3.13 presents the temperature of the vertical array of thermocouples positioned on the wall along the edge of the burner for each of the three fuels. The data is treated in the same manner as in Figure 3.12. For each

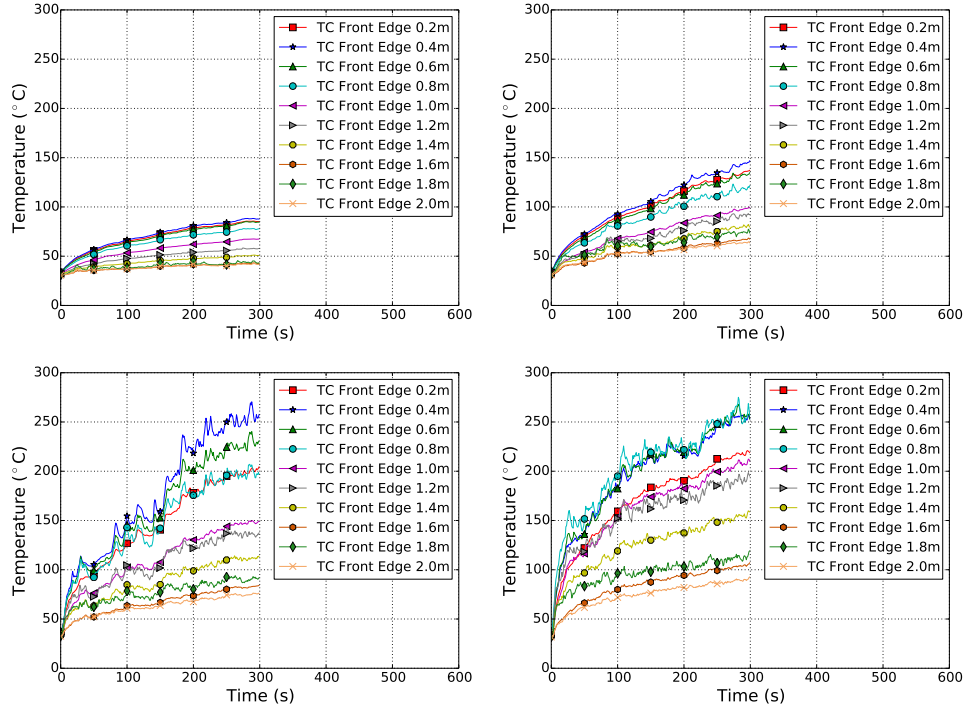


Figure 3.8: Wall Temperatures along the right edge of the natural gas fueled burner, when facing the wall. The temperatures are averages of two replicate experiments. Each graph displays data from a different distance between the edge of the burner and the instrumented wall. Beginning with the top left graph position and viewing left to right the distances from the wall are 0.61 m, 0.31 m, 0.15 m, and 0 m respectively.

fuel the average peak temperatures at the burner edge are significantly lower when the centerline temperatures when the burner is positioned against the wall. As the burners were moved away from the wall the temperatures at the centerline and the edge thermocouple arrays begin to converge.

Temperatures were also measured on the backside of the wall, along the vertical centerline of the burners, Figure 3.14. The temperature difference between the peak average temperatures on the front (fire side) of the wall at 0.2 m above the burner vs the corresponding temperatures on the backside of the wall have a difference of at least 400 °C. It is consistent with the temperature data shown in Figures 3.12 and 3.13, that as the burners were moved away from the wall the temperature differences are reduced.

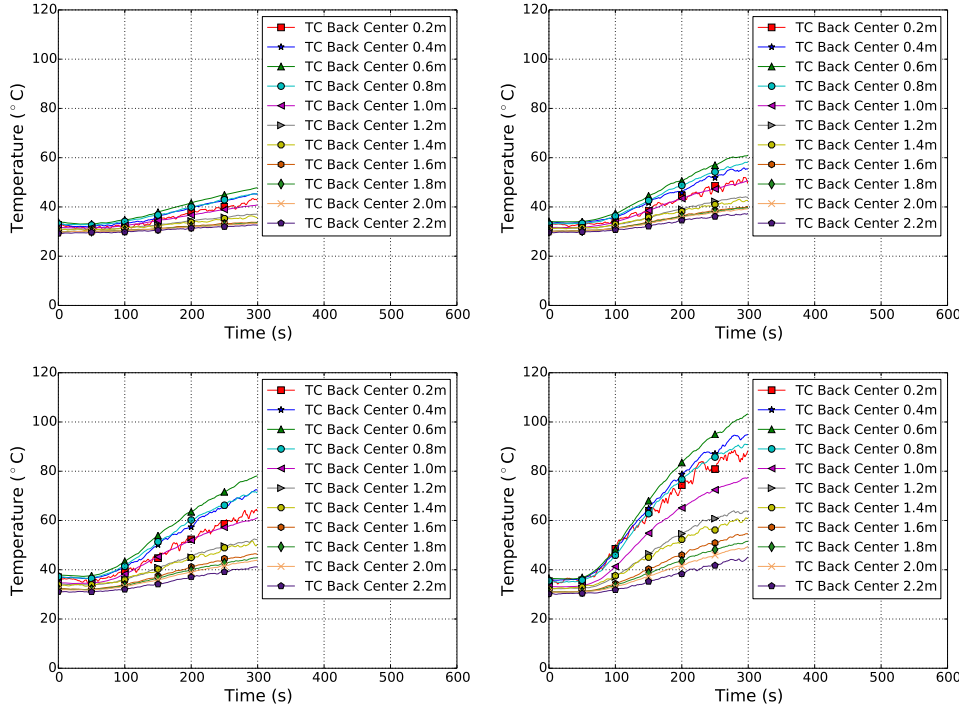


Figure 3.9: Backside wall Temperatures along the centerline of the natural gas fueled burner. The temperatures are averages of two replicate experiments. Each graph displays data from a different distance between the edge of the burner and the instrumented wall. Beginning with the top left graph position and viewing left to right the distances from the wall are 0.61 m, 0.31 m, 0.15 m, and 0 m respectively.

3.2.2 Heat Flux

Figures 3.15 and 3.16 show the results from the arrays of total heat flux gauges located along the vertical centerline and the edge of the burners for each fuel. The sensing surface of the gauges were installed flush with the wall surface and exposed to the fire. In each graph, the averaged peak heat flux for each of the replicate experiments and each position is shown. Moving from 0.2 m above the top surface of the burner up to 1.2 m above the top of the burner surface in increments of 0.2 m. Reviewing the graph for each fuel demonstrates how the heat flux at the wall decreased as the position of the burner was moved away from the wall. (Review video and tie in ST TC graph with edge peak NG at 0.15)

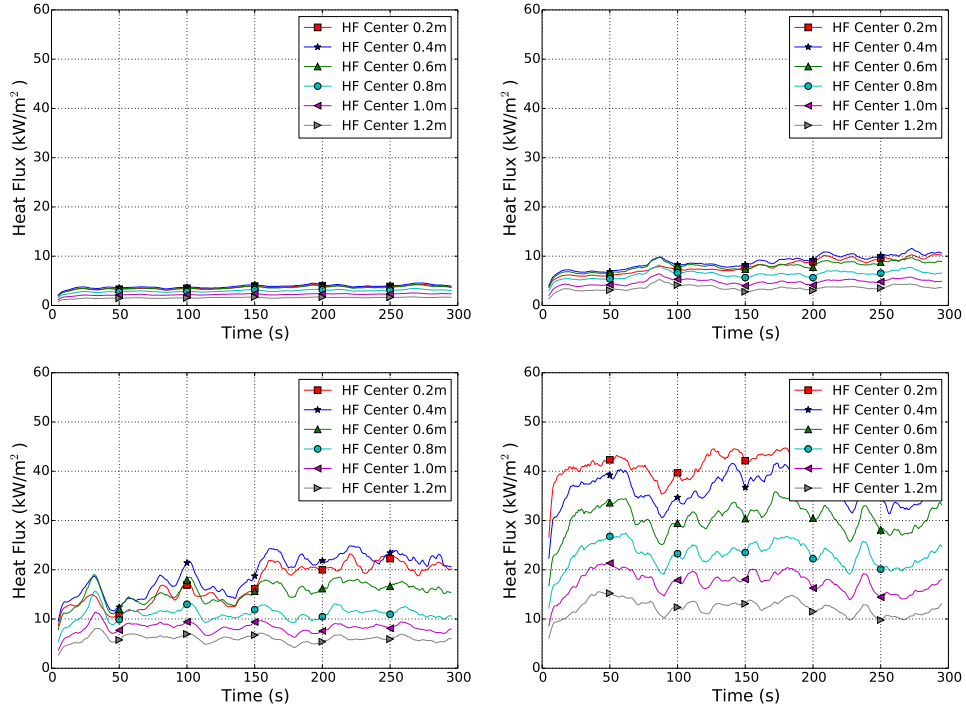


Figure 3.10: Heat flux at the wall along the centerline of the natural gas fueled burner. The heat fluxes are averages of two replicate experiments. Each graph displays data from a different distance between the edge of the burner and the instrumented wall. Beginning with the top left graph position and viewing left to right the distances from the wall are 0.61 m, 0.31 m, 0.15 m, and 0 m respectively.

3.3 Summary

These instrumented non-combustible wall experiments provide a data set for the fires conducted that can be compared against ignition data for gypsum wallboard from the literature to determine the potential for ignition of the paper surface of gypsum wallboard at a given distance from the wall with a given fuel. The Ignition Handbook by Babrauskas is the most comprehensive set of ignition data and related information ever written [38]. Table 19 in the Ignition Handbook includes calculated ignition temperatures from experimental data from two separate sources.

Quintiere and Harkleroad conducted a study with the Lateral Ignition and Flame Spread (LIFT) apparatus, which they developed [57, 58]. The

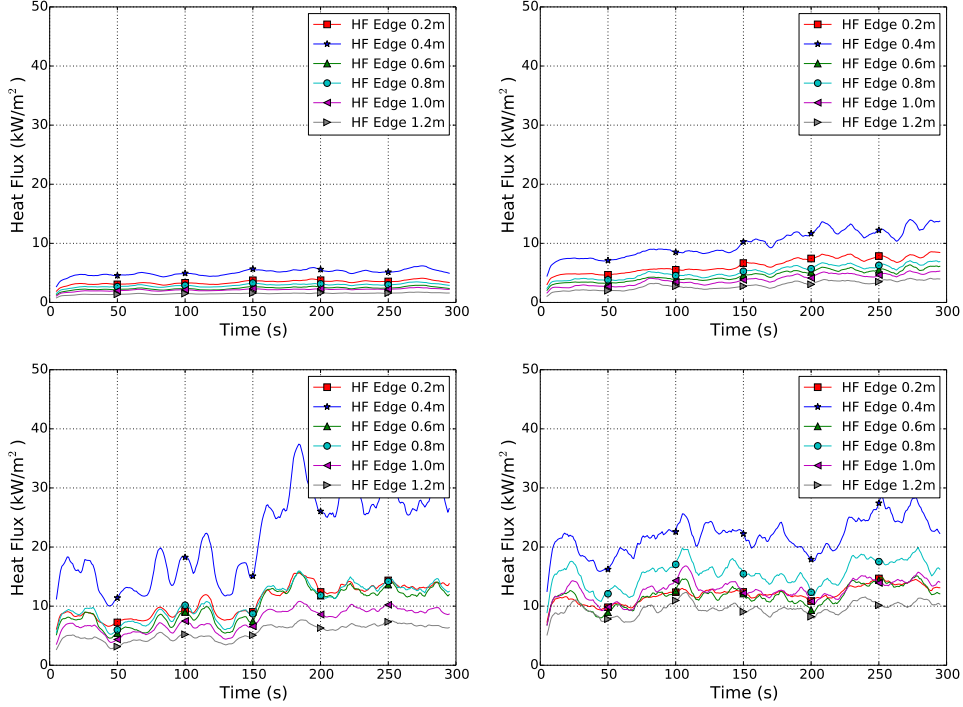


Figure 3.11: Heat flux at the wall along the edge of the natural gas fueled burner. The heat fluxes are averages of two replicate experiments. Each graph displays data from a different distance between the edge of the burner and the instrumented wall. Beginning with the top left graph position and viewing left to right the distances from the wall are 0.61 m, 0.31 m, 0.15 m, and 0 m respectively.

ignition temperature value calculated from the LIFT data for regular gypsum wallboard, 12.7 mm thick was 565 °C with a critical heat flux for ignition of 35 kW/m².

The second source, was a series of cone calorimeter experiments conducted by Dillon [33, 59]. The ignition temperature calculated from the cone calorimeter experiments for regular gypsum wallboard, 12.5 mm thick was 515 °C with a minimum heat flux required for ignition of 26 kW/m².

A review of the graphs of the peak average temperatures at the wall, burner centerline array, shows that all of the fuels had at least one thermocouple position with a peak of approximately 500 °C when the burner was against the wall. At 0.15 m away from the wall the peak average temperature

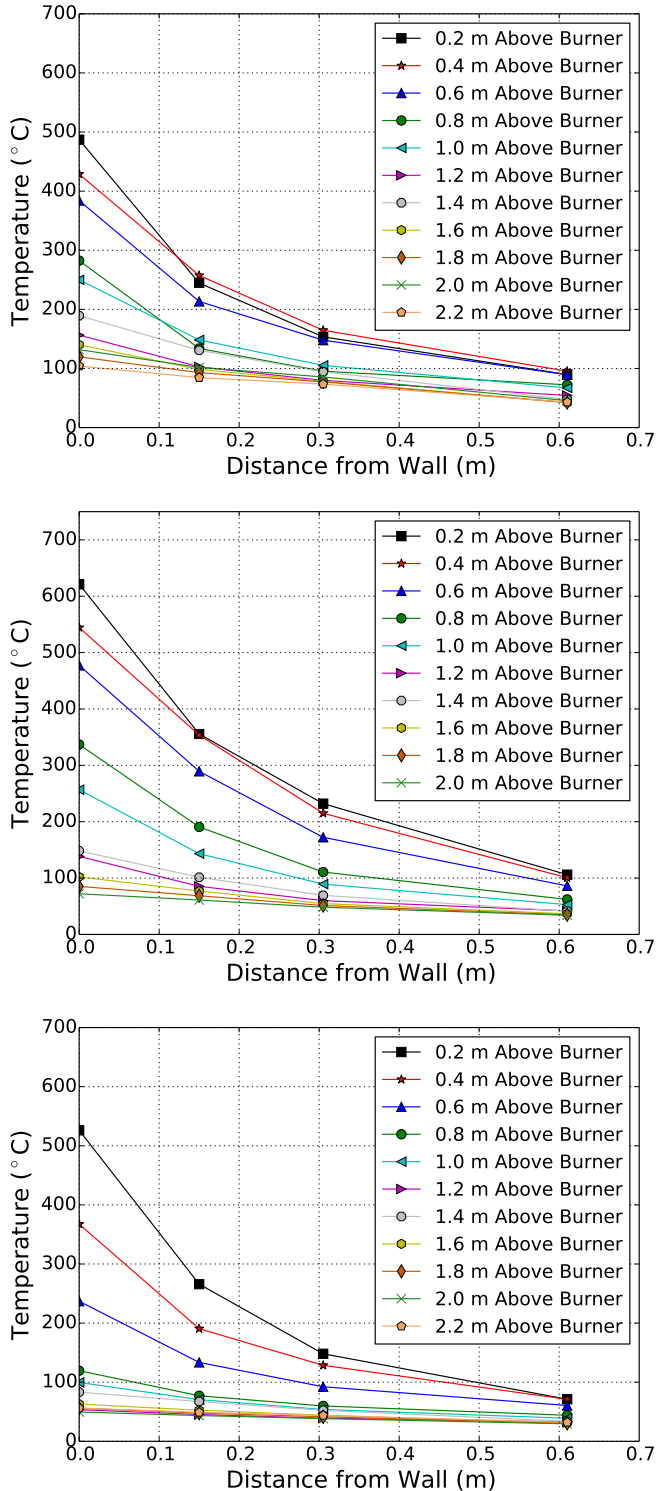


Figure 3.12: Composite graph of the wall temperatures along the centerline of the burners for each fuel. The peak temperatures are averages of replicate experiments for each instrument location at each position from the wall. Beginning with the top graph position and moving down the graph for natural gas, gasoline, and polyurethane foam are presented.

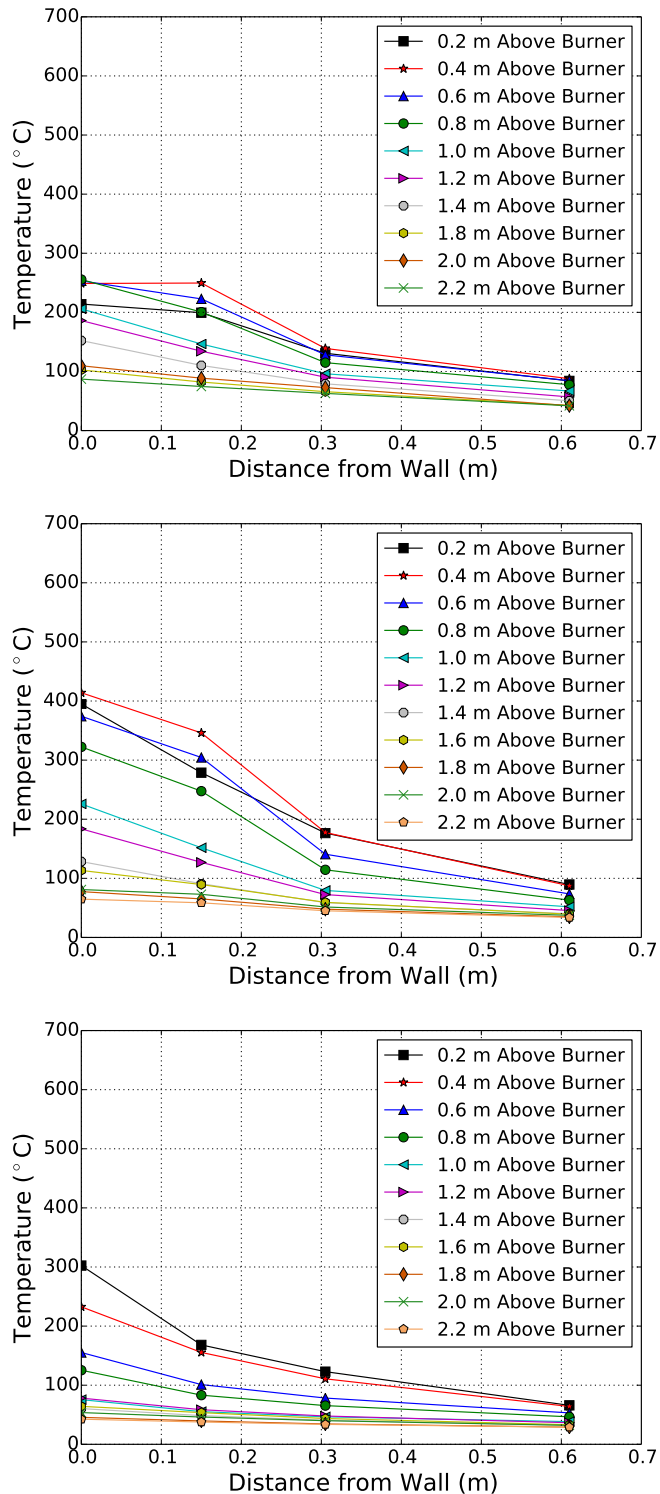


Figure 3.13: Composite graph of the wall temperatures along the edge of the burners for each fuel. The peak temperatures are averages of replicate experiments for each instrument location at each position from the wall. Beginning with the top graph position and moving down, the graphs for natural gas, gasoline, and polyurethane foam are presented.

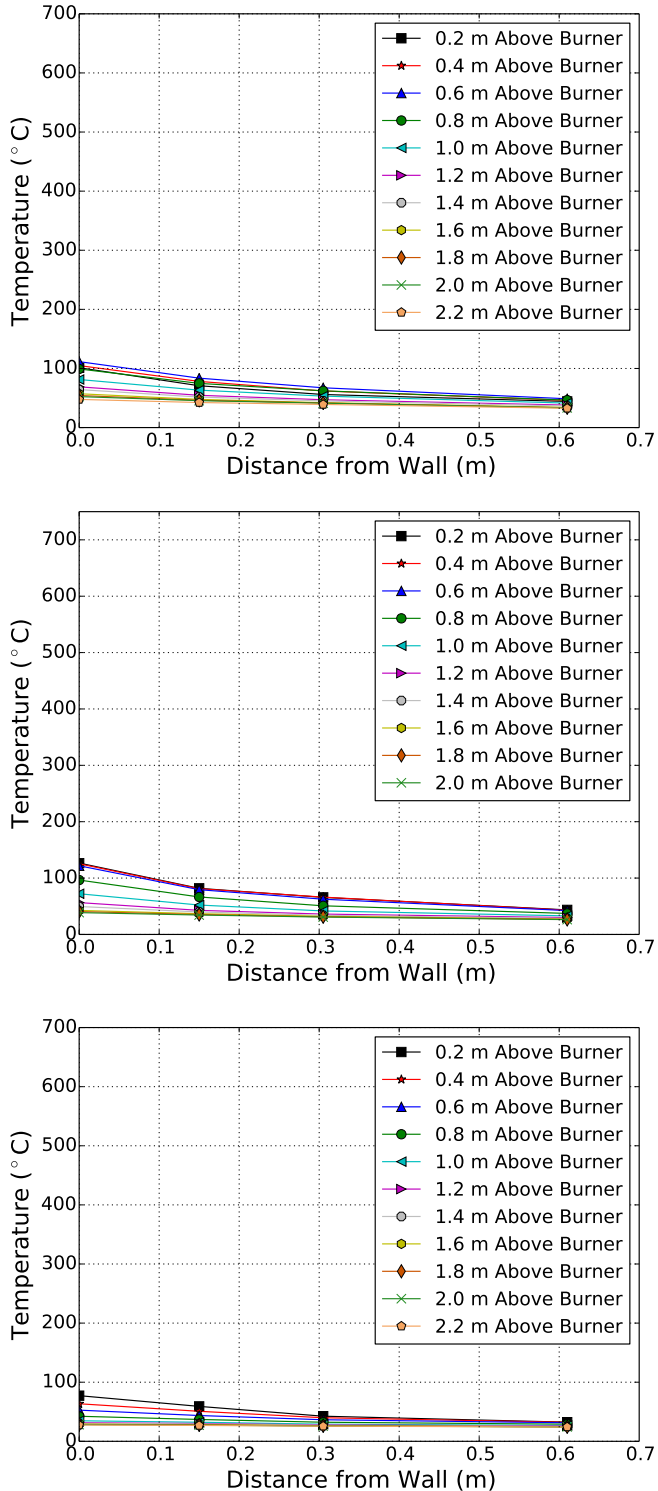


Figure 3.14: Composite graph of the backside wall temperatures along the vertical centerline of the burners for each fuel. The peak temperatures are averages of replicate experiments for each instrument location at each position from the wall. Beginning with the top graph position and moving down, the graphs for natural gas, gasoline, and polyurethane foam are presented.

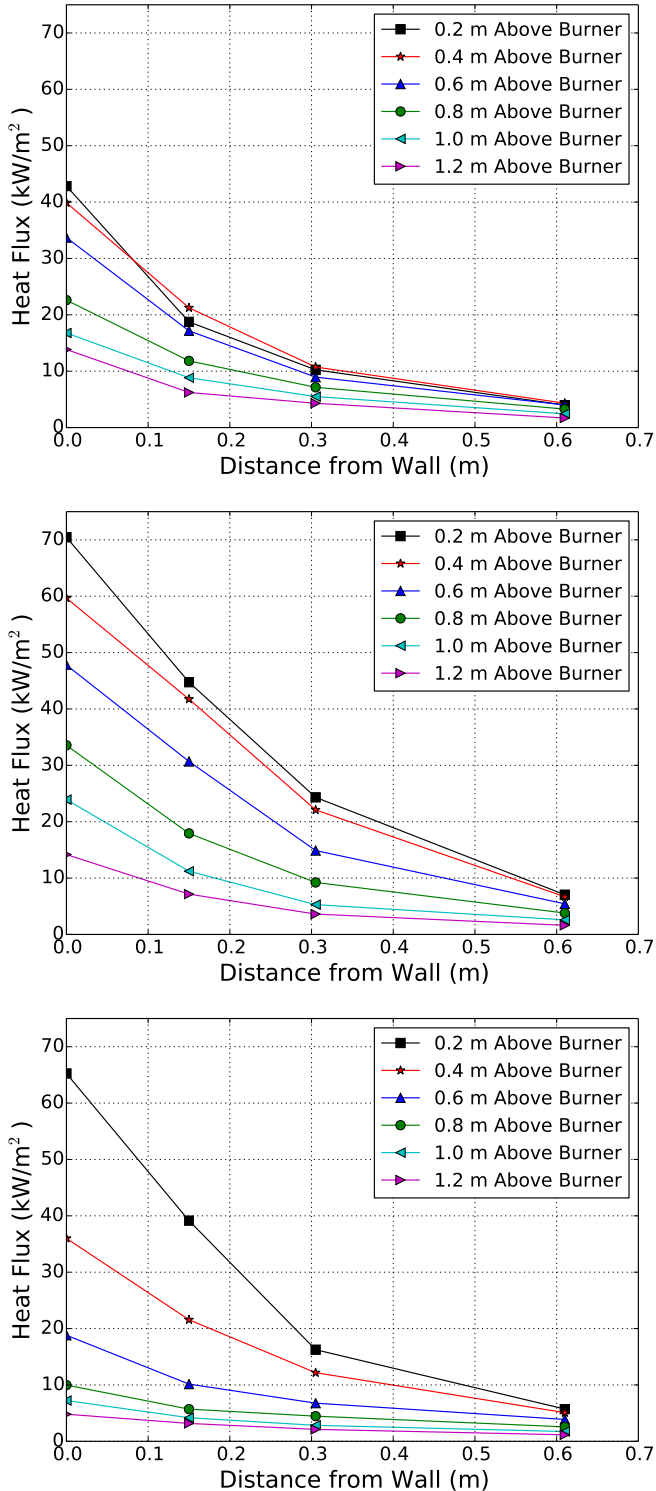


Figure 3.15: Wall heat fluxes along the centerline of the burners. The heat fluxes are averages of replicate experiments. Each graph displays data from a different distance between the edge of the burner and the instrumented wall. Beginning with the top graph position and moving down, the graphs for natural gas, gasoline, and polyurethane foam are presented.

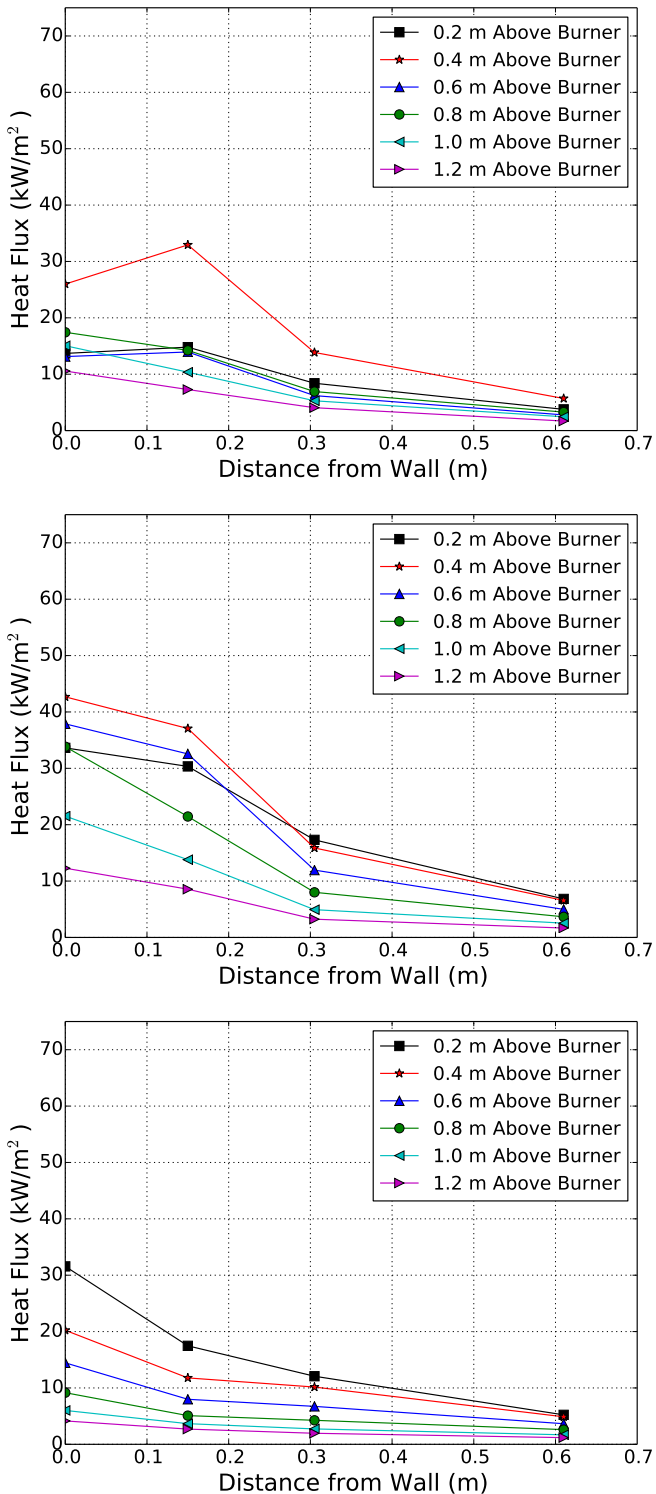


Figure 3.16: Wall heat fluxes along the edge of the burners. The heat fluxes are averages of replicate experiments. Each graph displays data from a different distance between the edge of the burner and the instrumented wall. Beginning with the top graph position and moving down, the graphs for natural gas, gasoline, and polyurethane foam are presented.

from this data set was provided by the gasoline fueled fire and it was approximately 350 °C. Based on temperature alone, the fires examined would only have the potential to ignite the paper surface of the gypsum wallboard when the burner was in contact with the wall. The peak average temperatures at the wall, burner edge array, would indicate that the paper may not ignite at the burner edge. The peak average temperature of approximately 400 °C was generated by the gasoline fueled fire when the burner was positioned against the wall.

Of course the temperatures of the thermocouples in the wall are a result of the energy transferred to the wall and the thermo-physical properties of the wall material. Assuming that the properties of calcium silicate board and the gypsum board are similar, the heat flux graphs were reviewed to see where the heat flux exceeded 35 kW/m². All of the fuels generated heat fluxes in excess of 35 kW/m² at the burner centerline array when the burners were against the wall. The gasoline and the polyurethane fueled burners also exposed the wall to heat fluxes higher than 35 kW/m² at 0.15 m from the wall. However only the burner against the wall positions provided a combination of heat flux and temperature that had the potential to ignite the paper on the gypsum wallboard based on the handbook data.

Chapter IV

Instrumented Gypsum Board Wall Experiments

4.1 Experimental Arrangement

This series of experiments combined the instrumentation used in the non-combustible wall experiments with gypsum wallboard, which has a combustible paper surface. These experiments were conducted in a similar manner as the non-combustible instrumented wall experiments, the only new variable is the painted, gypsum wallboard. These experiments enable us to examine our ignition/no ignition predictions from the previous experiments. A free standing, steel frame with a panel of gypsum wallboard attached to the surface was instrumented to measure the thermal exposure of the wall from the fire in terms of temperature and heat flux. The fires were initially placed at predetermined, fixed positions away from the wall. The burner was moved toward the wall until the burner was against the wall. If the results indicated that no burn pattern would result from a given combination of fuel and position, then that fuel and position combination were eliminated from the remainder of the experiments in the study.

The thermocouple arrangement for these experiments had one vertical array of thermocouples installed on the wall. The thermocouples were centered between the two vertical arrays of heat flux gauges as shown in Figure 4.1. As a means of ensuring contact between the gypsum wallboard and the thermocouple, the thermocouples were installed by pulling the positive and negative wires through holes drilled through the gypsum wallboard and positioning the bead of the thermocouple in a slit in the paper face made with a razor blade. A thermocouple installed in this manner shown in Figure 4.2.

Since these experiments were the culmination of the instrumented series of full scale tests, the use of gypsum wallboard was intended to provide some

insight into how much fire damage would result. These experiments proved to be challenging in terms of time and effort. Each panel of gypsum wallboard had to be carefully drilled for thermocouple and heat flux gauge placement. Since there was only one set of heat flux gauges this reduced the number of experiments that could be conducted on a given day. With other project demands, the number of instrumented wallboard experiments that could be conducted under the oxygen consumption calorimeter was reduced due to time constraints. The test matrix is shown in Table 4.2. There was also a concern that these experiments would have limited value due to potential interference from the water-cooled heat flux gauges and potential physical damage caused by drilling the holes for them.

4.2 Characterization of Gypsum WallBoard

According to the United States Geological Survey, most gypsum in the United States is used to make wallboards for homes and other structures. A typical home in the United States contains more than 7 metric tons of gypsum [60]. As defined by ASTM, gypsum wallboard is gypsum board designed for use on walls, ceilings, or partitions and that affords a surface suitable to receive decoration [61]. The ASTM standard further describes gypsum wallboard as having a noncombustible core, surfaced with paper bonded to the core. By weight, wallboard is composed of more than 85 % gypsum, less than 10 % cellulose, less than 3 % starch and approximately 1 % of both crystalline silica and fibrous glass [62]. Chemically gypsum can be described as calcium sulfate dihydrate, $(\text{CaSO}_4 \bullet 2\text{H}_2\text{O})$. By weight pure gypsum is approximately 79 % calcium sulfate and 21 % chemically bound water [63].

The gypsum wallboard used in these experiments is referred to as ‘regular’ as opposed to gypsum wallboard ‘Type C’ or ‘Type X’ which are used in fire rated assemblies. The gypsum wallboard used in these experiments was purchased from same manufacturer in an effort to have the most similar panels for use between the experiments. Each 1.22 m by 2.44 m by 12.7 mm thick panel weighed approximately 30.5 kg. The thermal properties of the gypsum wallboard panels are given in the Table 4.1. The first two rows of data were measured from samples of the gypsum wallboard used in these

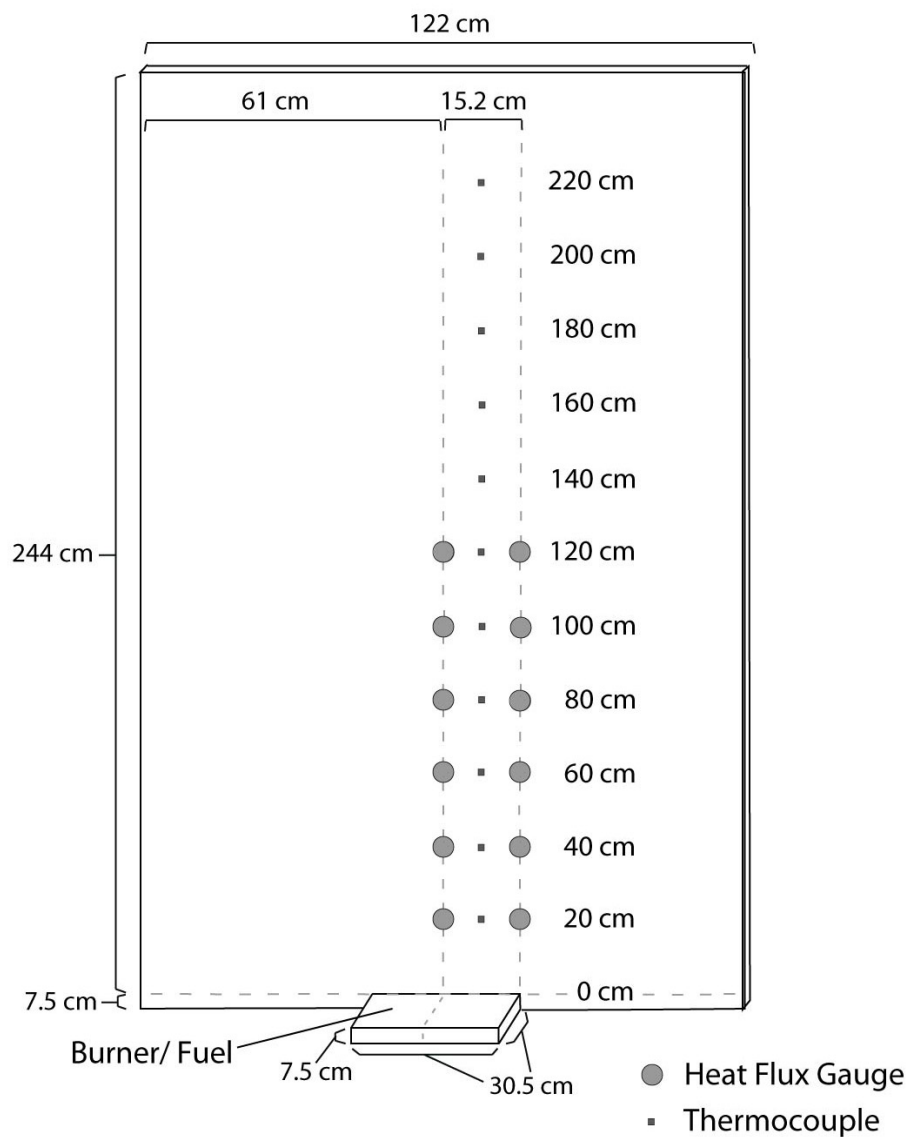


Figure 4.1: Diagram of the instrumented gypsum wallboard. Two vertical arrays of total heat flux gauges were installed along the centerline of the burner and along the right edge of the burner. A single vertical array of thermocouples was installed centered between the heat flux gauges.



Figure 4.2: Photograph of a nominal 0.5 mm thermocouple bead embedded in the gypsum wallboard.

Density (kg/m ³)	Thermal Conductivity		Specific Heat	
	Temperature (°C)	(W/mK)	Temperature (°C)	(kJ/kg °C)
807	24	0.14		1.09
	100	0.15		
790	20	0.18	20	0.90
	100	0.15	100	0.90
	200	0.13	200	0.80
	500	0.15	500	0.90

Table 4.1: Thermal properties for 12.7 mm gypsum wallboard

experiments. The bottom four rows of data are from cite{Gross:1985.

There have been a number of studies that have examined gypsum wallboard under elevated temperature conditions in terms of its thermal properties or in terms of its physical change as a result to exposure to heat. Schroeder conducted a study on the post-fire analysis of construction materials including gypsum. As gypsum is heated to temperatures above 80 °C it begins to change phase and degrade. Continued heating causes some of the chemically bound water to disassociate and the gypsum changes to a hemihydrate. This transformation occurs in the range of 98 °C to 130 °C. With additional heating the residue of the gypsum continues to transform and soften turning into anhydrite, commonly this process is known as calcination. Schroder exposed samples of gypsum to a range of heat fluxes and temperatures to determine the time for 80 °C (dihydrate phase), 200 °C (hemihydrate phase), and 500 °C (anhydrous phase) isotherms to penetrate to different depths in the gypsum. The crystal phase and the depth of penetration of the phase change was determined with the use of X ray diffraction add Schroder. NFPA 921 also discusses calcination and how the investigator can use the visual appearance or probing of the soft dyhydrated gypsum to map fire patterns.

After receipt of the gypsum wallboard panels, the panels were laid out on the floor of the NIST Large Fire Research Laboratory, finished paper side up and painted with a roller. The first coat was a latex primer, http://buyat.ppg.com/rep_pafpaintto. Once the primer dried a top coat of white latex paint was applied http://buyat.ppg.com/rep_pafp. After the panels dried, they were weighed. The average mass of paint on

Distance from wall (m)	Natural Gas Number of Tests	Gasoline Number of Tests	Polyurethane Foam Number of Tests
0.61	0	1	2
0.31	3	1	2
0.15	1	1	2
0.08	0	1	2
0.00	1	1	3

Table 4.2: Matrix of instrumented gypsum wallboard experiments

the finished surface of the gypsum wallboard was 0.33 kg. Then the paint thickness was estimated an ultrasonic coating thickness gauge [64]. Over the course of the experiments, random painted panels where checked with the ultra sonic device. The thickness of the paint varied from 0.05 mm to 0.13 mm. Some of the painted panels were then cut-up into samples for the bench-scale experiments.

4.3 Results

The complete set of results from the instrumented gypsum wallboard experiments are provided in Appendix C. Table 4.2 lists the experiments that were conducted for each fuel type. In this chapter, as in the previous chapter the averaged peak values for temperatures and heat fluxes will presented at varying distances from the wall. For the gasoline and polyurethane fires, an additional position, 0.08 m from the wall was added.

Figures 4.3,4.4 and 4.5 show the values for the natural gas burner experiments with the gypsum wallboard.

4.3.1 Wall Temperatures

The averaged peak temperatures of the wall mounted thermocouples for the three different fuels are shown in Figure 4.10.

4.3.2 Heat Flux

Figures 4.11 and 4.12 present the averaged peak values from the two heat flux gauge arrays. For the gasoline fire experiment at the 0.08 m position the

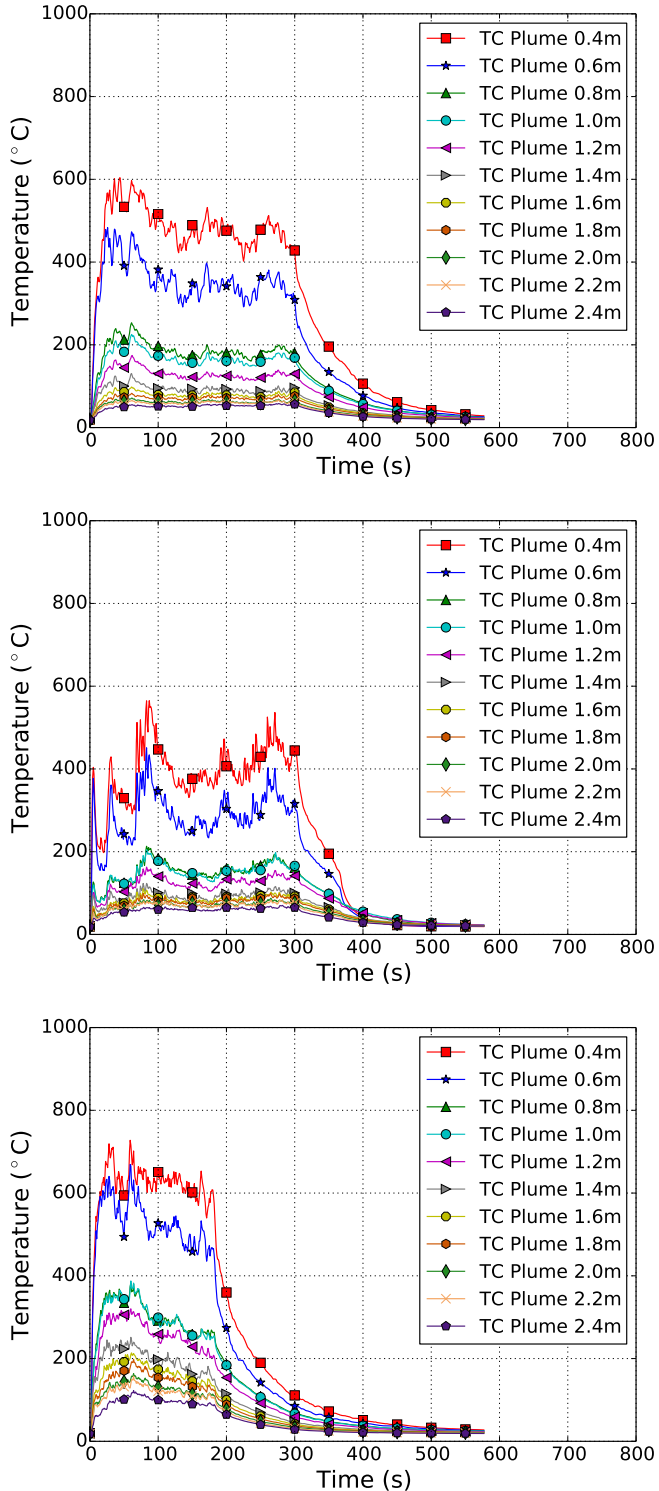


Figure 4.3: Plume temperatures along the centerline of the natural gas fueled burner. Each graph displays data from a different distance between the edge of the burner and the instrumented gypsum wallboard. Beginning with the top graph and moving down, the distances from the wall are 0.31 m, 0.15 m, and 0 m.

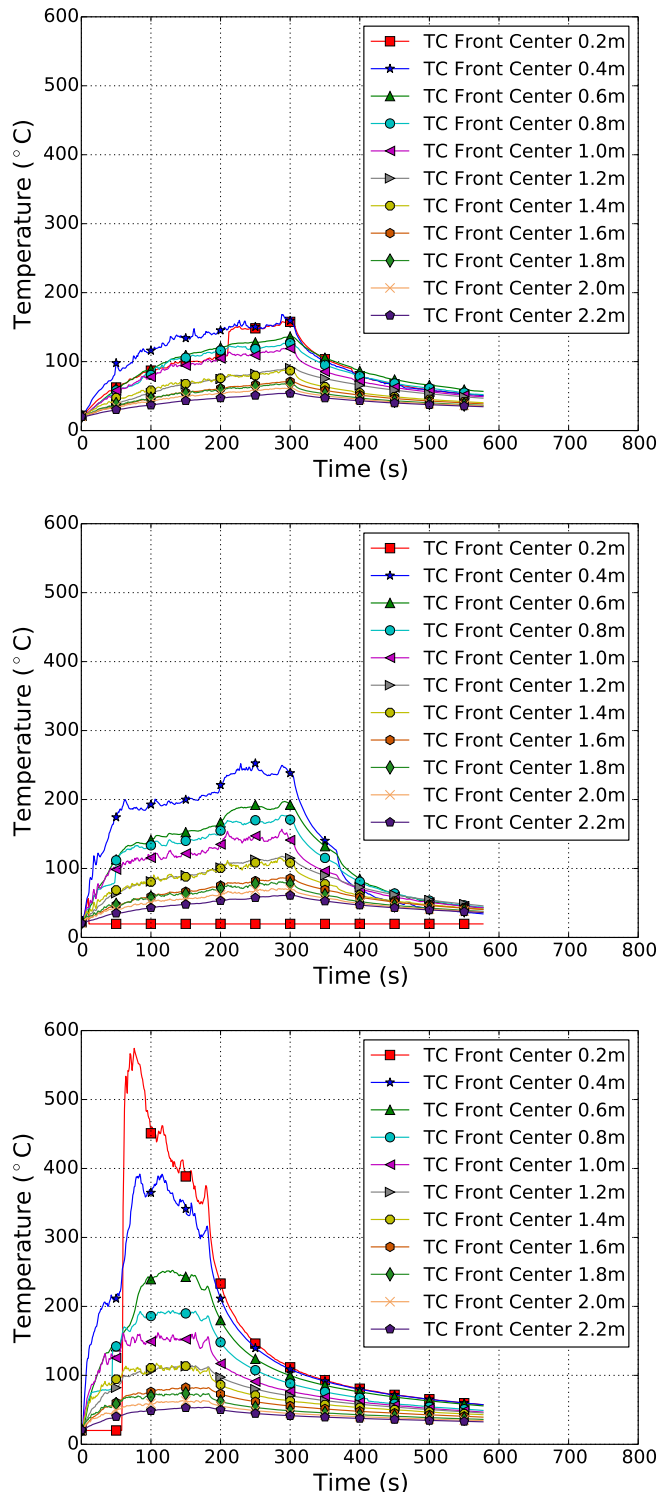


Figure 4.4: Front surface wall temperatures for the natural gas fueled burner. Each graph displays data from a different distance between the edge of the burner and the instrumented gypsum wallboard. Beginning with the top graph and moving down, the distances from the wall are 0.31 m, 0.15 m, and 0 m.

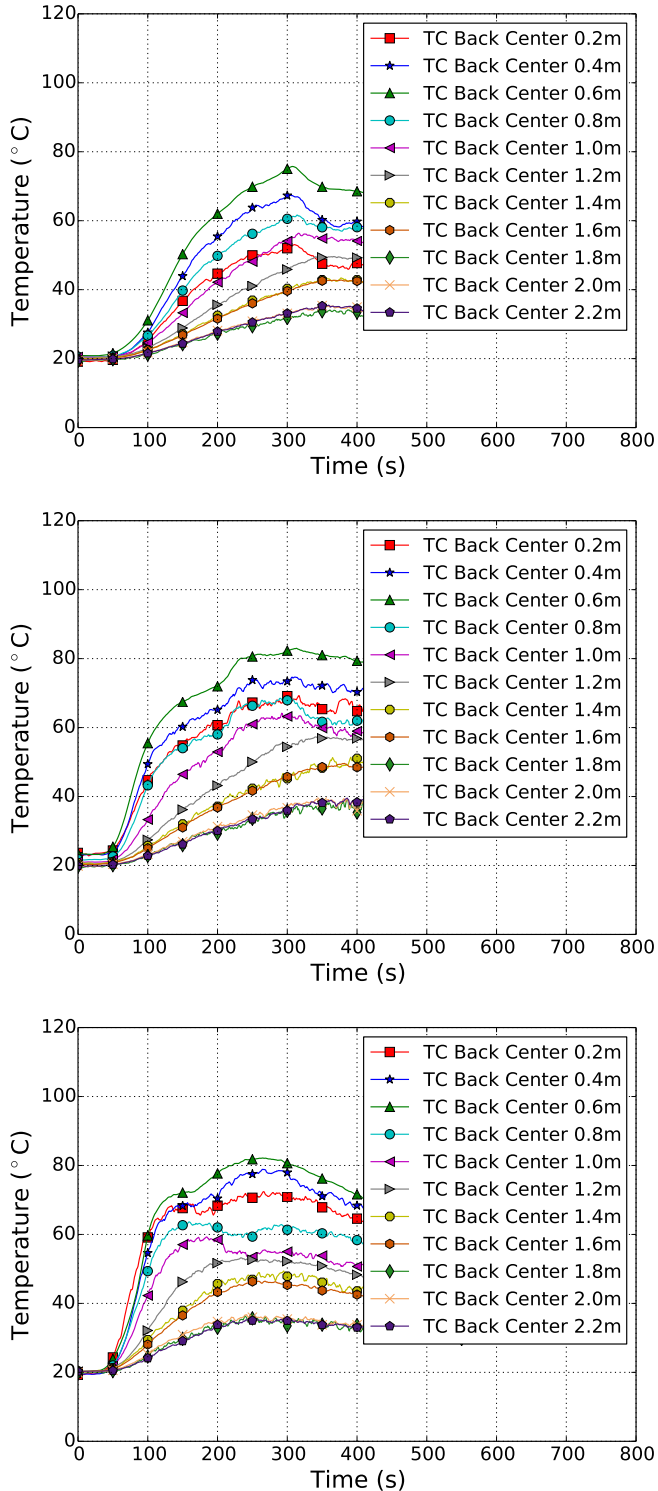


Figure 4.5: Backside wall temperatures along the centerline of the natural gas fueled burner. Each graph displays data from a different distance between the edge of the burner and the instrumented gypsum wallboard. Beginning with the top graph and moving down, the distances from the wall are 0.31 m, 0.15 m, and 0 m.

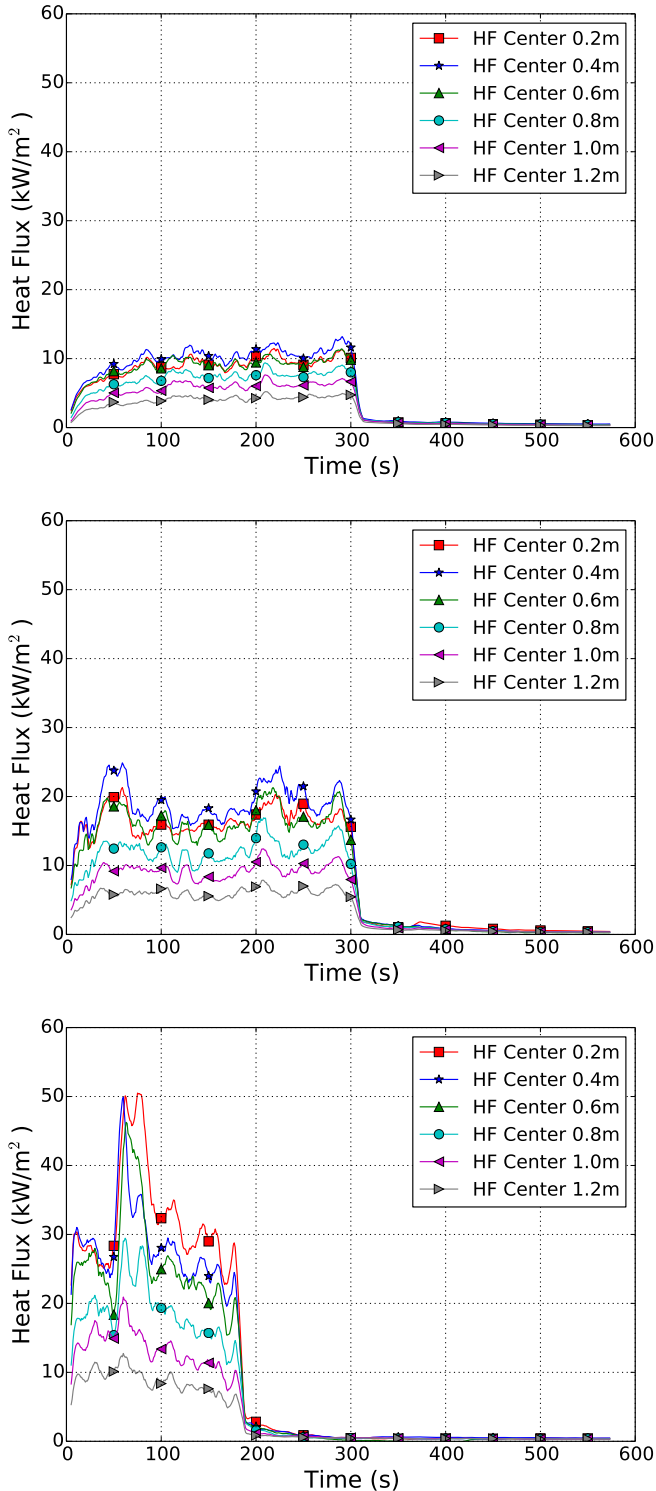


Figure 4.6: Wall heat flux along the vertical centerline of the natural gas fueled burner. Each graph displays data from a different distance between the edge of the burner and the instrumented gypsum wallboard. Beginning with the top graph and moving down, the distances from the wall are 0.31 m, 0.15 m, and 0 m.

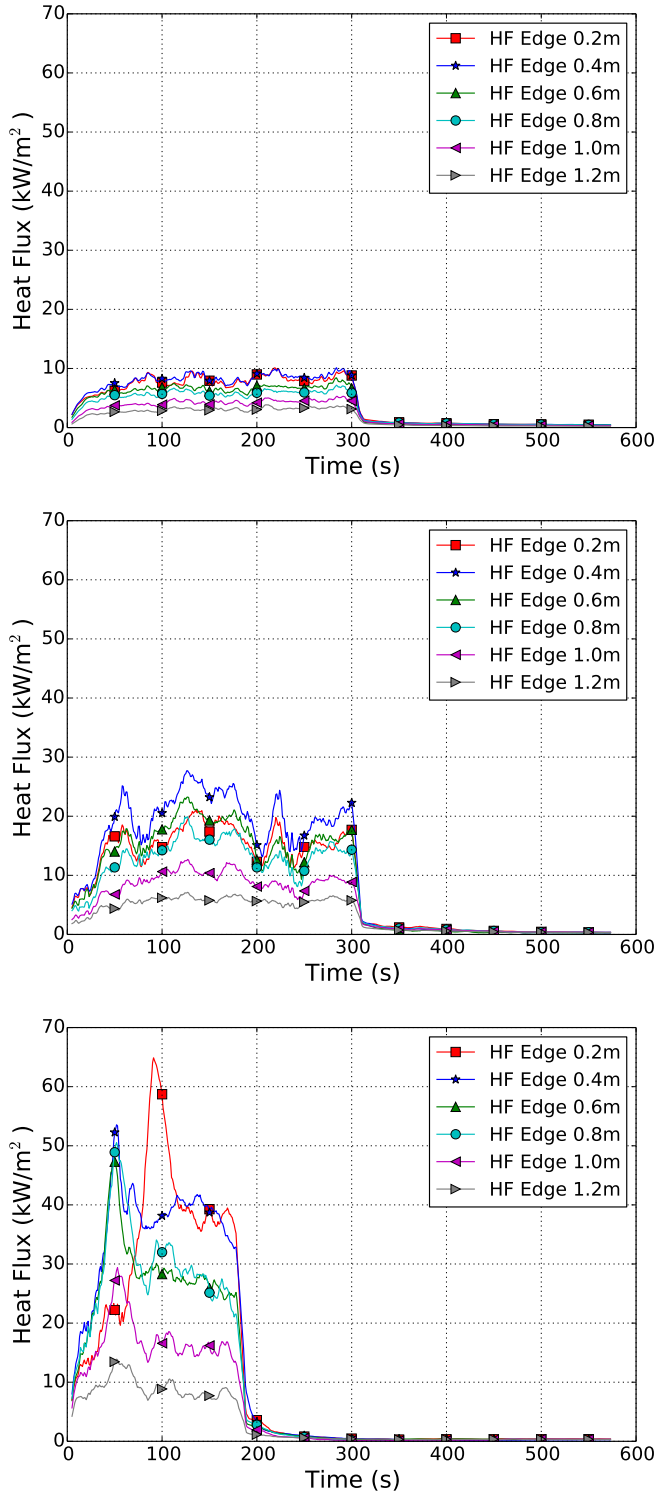


Figure 4.7: Wall heat flux along the edge of the natural gas fueled burner. Each graph displays data from a different distance between the edge of the burner and the instrumented gypsum wallboard. Beginning with the top graph and moving down, the distances from the wall are 0.31 m, 0.15 m, and 0 m.

wall temperatures and the heat flux values from the burner edge array had values that were higher than when those measured at the 0.0 m position. The peak heat release rates for the positions at 0.0 m, 0.08 m and 0.15 m were 120 kW, 110 kW, and 110 kW respectively. So it does not seem that a change in HRR was the source of the increase.

4.3.3 Fire Pattern

As defined in NFPA 921, a fire is the visible or measurable physical changes, or identifiable shapes, formed by a fire effect or group of fire effects [8]. In order to measure the dimensions of the fire pattern, such as height and width, a determination had to be made as to where the fire pattern stops. The boundary between the undamaged area and the area that has been damaged by the fire is known as the line of demarcation [8]. As presented in the introduction, DeHaan [13] categorizes the fire effects that form patterns as follows:

1. Surface deposits - no irreversible effect on surface
2. Surface thermal effects - physical change such a discoloration or melting
3. Charring - evidence of surface burning
4. Penetration - charring below the surface
5. Consumption - loss of surface material, charring throughout

Figure 4.13 is a photograph of the edge of a fire pattern generated by the natural gas burner. It will serve as visual definition of the line of demarcation to be used in this study to determine the limits of a fire pattern. Referring to DeHaan's classifications, there are no surface deposits such as light soot that could be brushed or blown off the gypsum wallboard. There is a thin band of surface thermal effects in the form of discoloration of the paint, this could be considered an outer bound of the pattern. To the left of the discoloration is clearly an larger area where charring (blackening of the paint/paper), penetration (lifting of the painted/paper residue), and consumption (areas where

the paint/paper residue is gone altogether). The last three classifications or criteria will be used in this study to define the edge of the fire pattern. Any area where the painted paper surface has been charred, penetrated such that it has lifted away from the gypsum core, or burned away will be considered part of the fire pattern and define the lines of demarcation for this study.

Soot and discoloration alone was not used in this study, since the gasoline and the polyurethane foam generate significant quantities of soot as shown in Figure 4.14. From the photograph the areas of penetration and consumption can be clearly delineated while the discolored and sooted areas tend to meld together. Further the focus of the measurements in this study are thermal, therefore the focus is on the burned, not burned line of demarcation.

Figure 4.15 provides a comparison between the area of discoloration of the paint with the natural gas burner positioned at 0.15 m away from the wall versus the area of consumed and penetrated paint/paper layer which exposed the gypsum underneath.

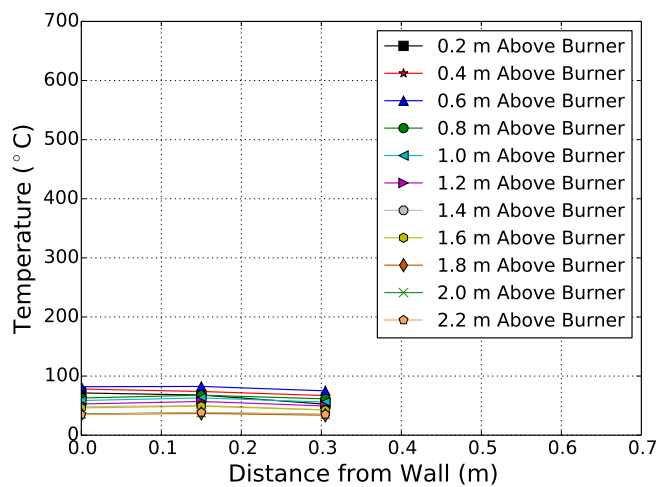


Figure 4.8: Averaged peak temperatures along the vertical centerline of the backside of the gypsum board wall for the natural gas burner fires

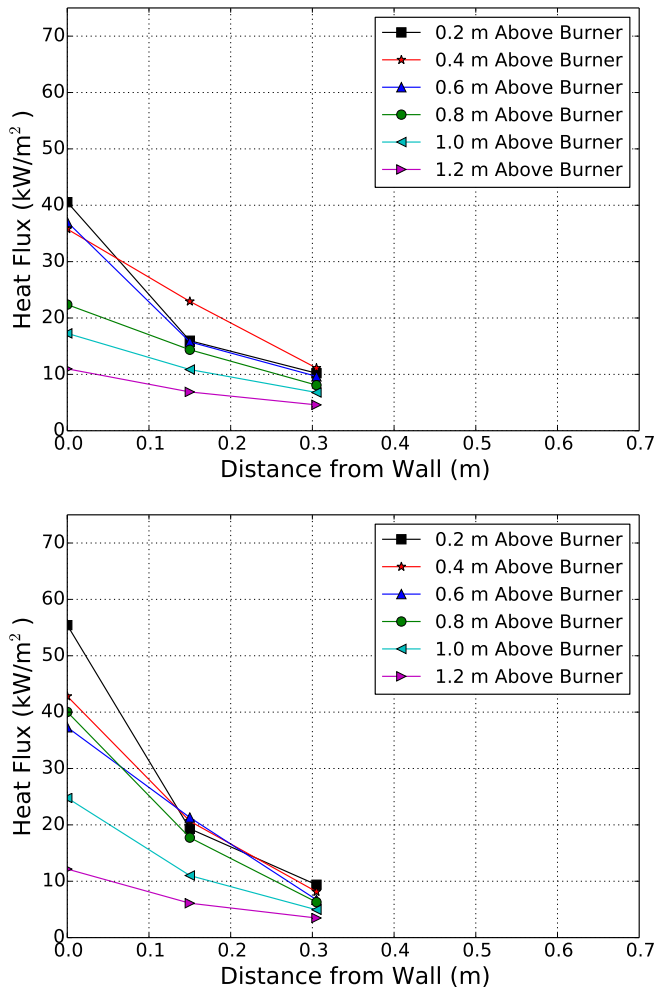


Figure 4.9: Averaged peak heat flux on the gypsum board wall along the vertical centerline and edge of the natural gas burner fires.

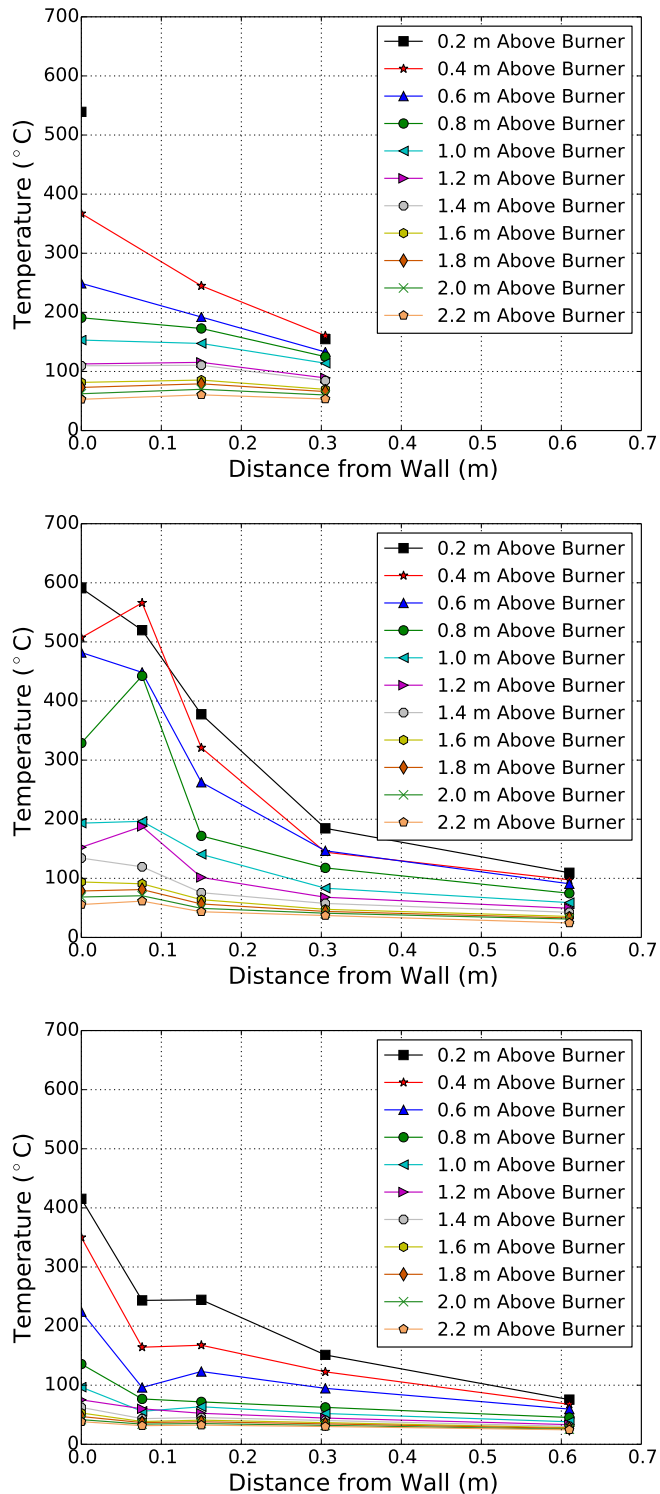


Figure 4.10: Averaged centerline temperatures, beginning with the top graph position and moving down, the graphs for natural gas, gasoline, and polyurethane foam fires are presented.

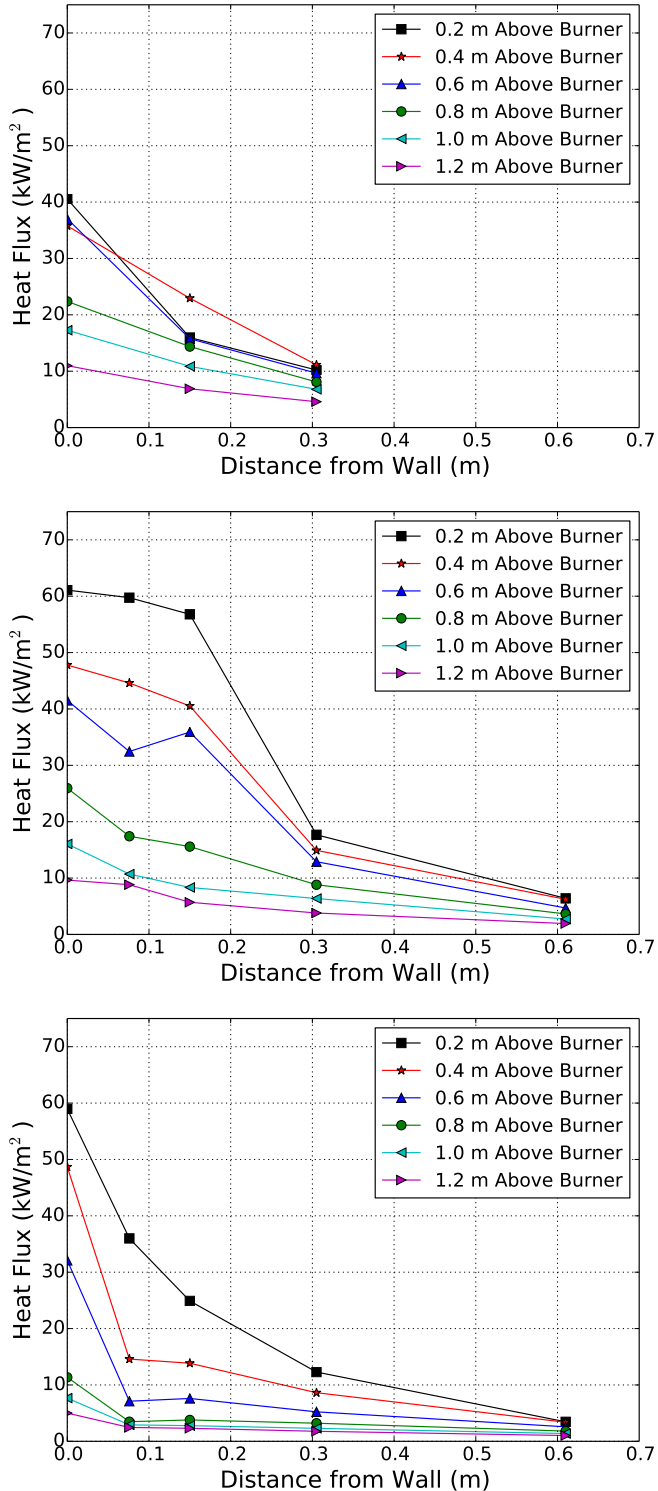


Figure 4.11: Averaged burner centerline heat flux, beginning with the top graph position and moving down, the graphs for natural gas, gasoline, and polyurethane foam fires are presented.

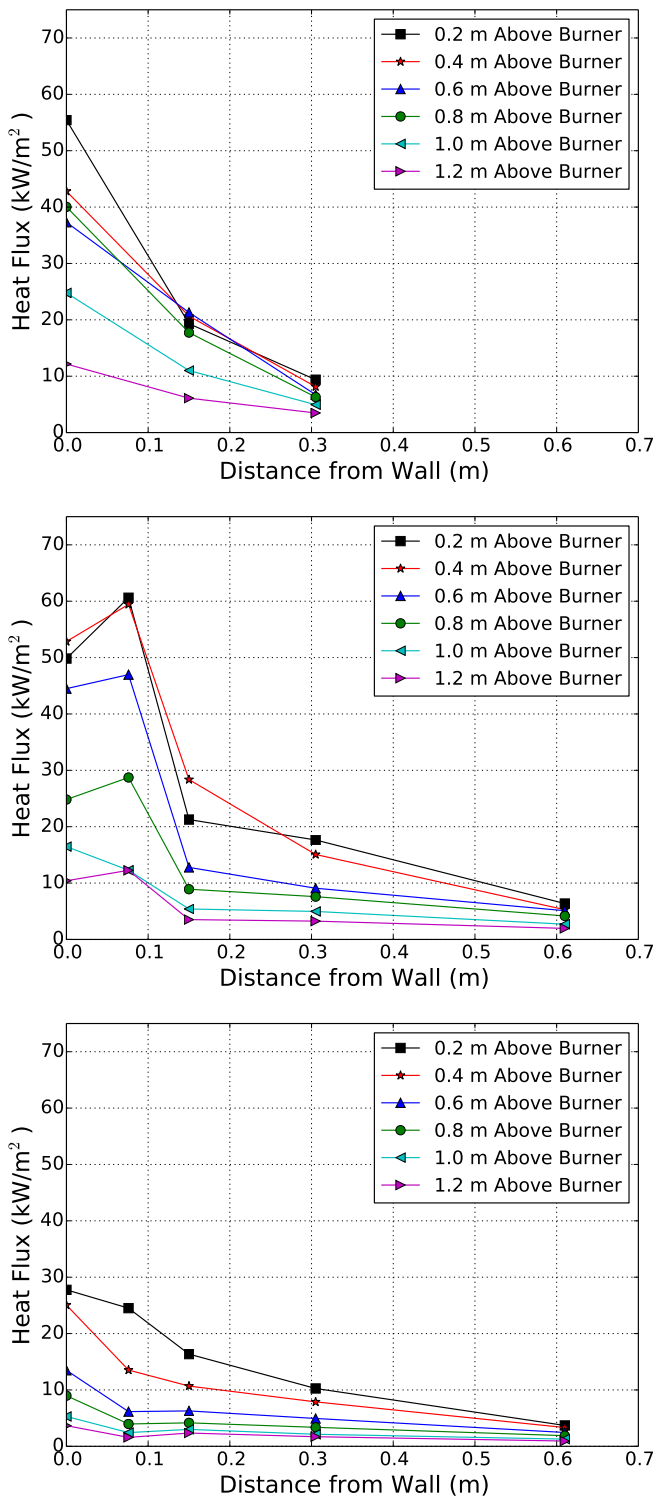


Figure 4.12: Averaged burner edge heat flux for the natural gas, gasoline, and foam fires, from the top down.



Figure 4.13: Photograph showing clear lines of demarcation from a fire pattern generated on painted gypsum wallboard by a natural gas fueled burner.



Figure 4.14: Photographs showing clear lines of demarcation from a fire pattern generated on painted gypsum wallboard by a gasoline fueled burner. Burned vs unburned area is clearly defined, whereas the difference between sooted and thermally discolored areas is not as clear.

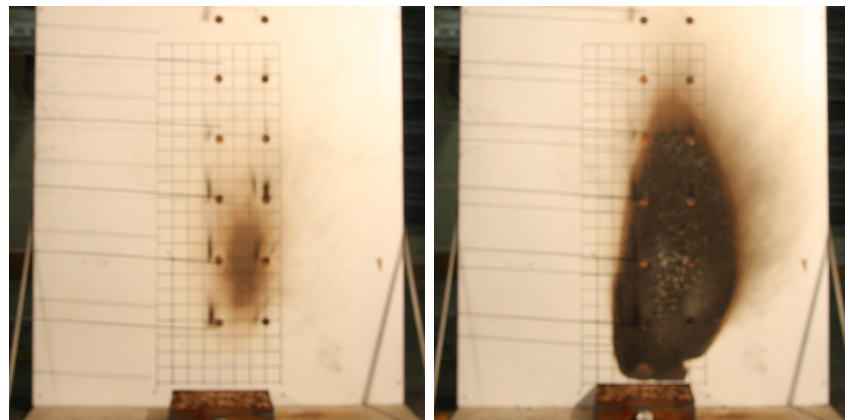


Figure 4.15: Photographs of the fire effects on the instrumented gypsum wallboard exposed to the natural gas burner fires. For the image on the left, the burner was positioned 0.15 m from the wall. For the image on the right, the burner was positioned 0.0 m from the wall.

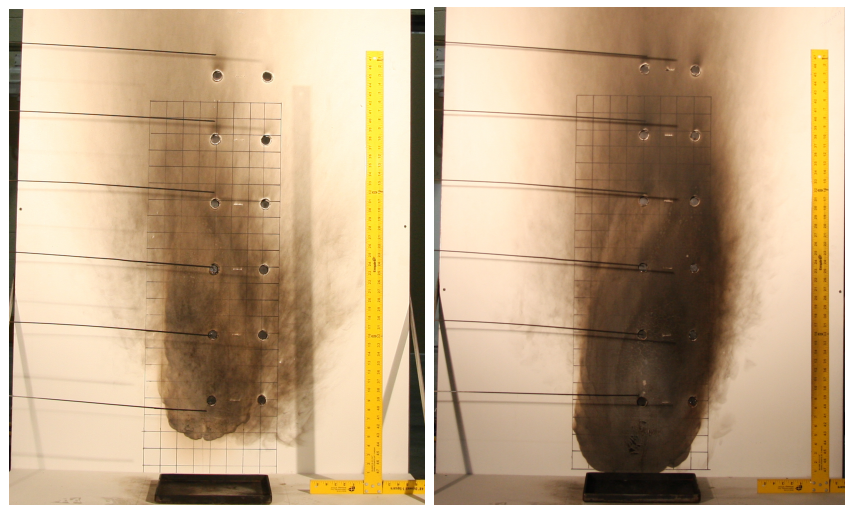


Figure 4.16: Photographs of the fire effects on the instrumented gypsum wallboard exposed to the gasoline burner fires. For the image on the left, the burner was positioned 0.15 m from the wall. For the image on the right, the burner was positioned 0.8 m from the wall.



Figure 4.17: Photographs of the fire effects on the instrumented gypsum wallboard exposed to the gasoline burner fires. For the image on the left, the burner was positioned 0.0 m from the wall. For the image on the right, the same panel after the soot was blown off, clean burn area is evident.

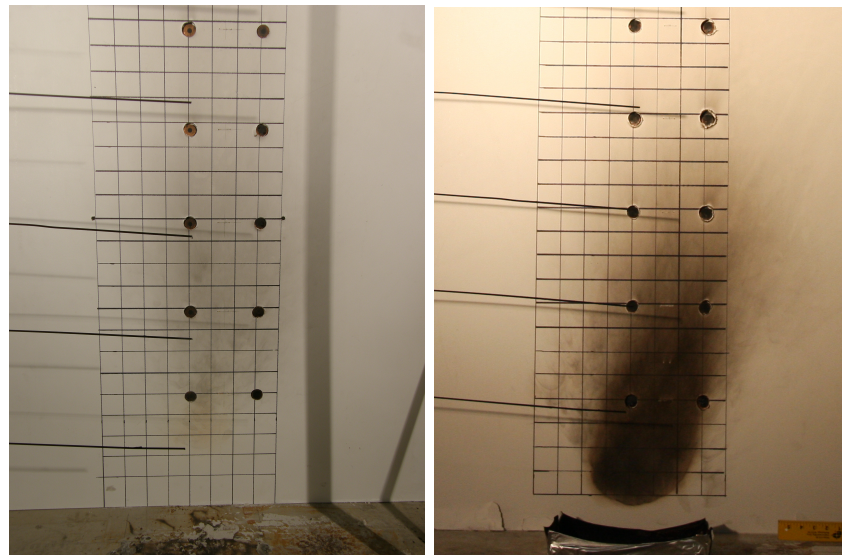


Figure 4.18: Photographs of the fire effects on the instrumented gypsum wallboard exposed to the polyurethane foam fires. For the image on the left, the burner was positioned 0.15 m from the wall. For the image on the right, the burner was positioned 0.08 m from the wall.

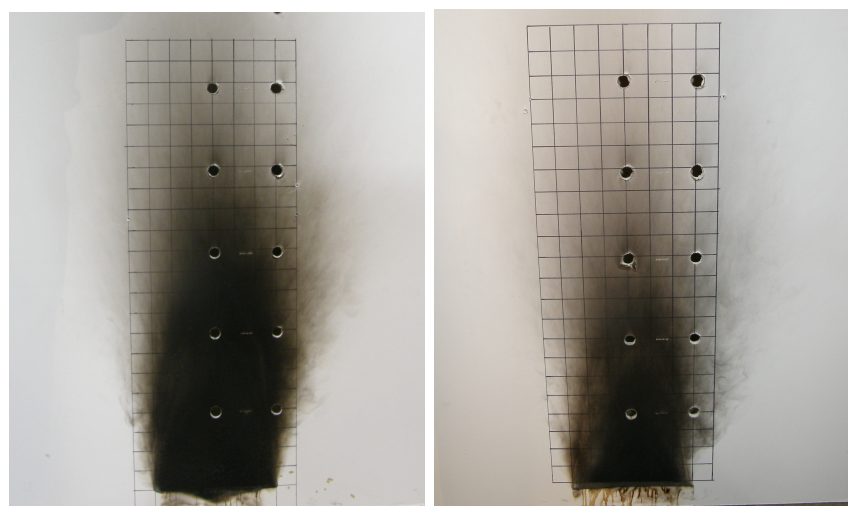


Figure 4.19: Photographs of the fire effects on the instrumented gypsum wall-board exposed to replicate polyurethane foam fires with the burner positioned 0.0 m from the wall.

Chapter V

Bench Scale Experiments

5.1 Cone Calorimeter Experiments

The cone calorimeter is one of the most commonly used bench-scale rate of heat release apparatus that uses the oxygen consumption method. It was developed at NIST in the 1980s [65]. The cone calorimeter has been adopted as ASTM E1354, Test Method for Heat and Visible Smoke Release Rates for Materials and Products Using an Oxygen Consumption Calorimeter [33]. The cone calorimeter consists of a heater, spark ignitor, sample holder, and load cell located underneath an exhaust hood. Typically, the sample is located in the open with free access of air to the combustion zone. The heater consists of a 5 kW electrical heating element inside an insulated stainless-steel conical shell. Samples can be tested in either a horizontal or vertical orientation. When tests are performed in the horizontal configuration, the specimen is positioned approximately 25 mm beneath the bottom plate of the cone heater. Flames and products of combustion pass through a circular opening at the top of the heater. The heater can expose samples to a maximum irradiance of approximately 100 kW/m^2 . Figure 5.1 is a schematic of the cone calorimeter.

For the ignition tests, an electric spark ignitor was positioned over the center of the horizontal samples to serve as a pilot. Combustion products and dilution air were extracted through the hood and exhaust duct by a high temperature fan. The flow rate can be adjusted between 0.01 and $0.03 \text{ m}^3/\text{s}$. The volumetric flow rate was kept constant during testing. The sample was mounted on a load cell to determine mass loss rate during a test, and smoke obscuration was measured using a laser light source. The gas flow rate in the exhaust duct was calculated from the pressure drop across and temper-

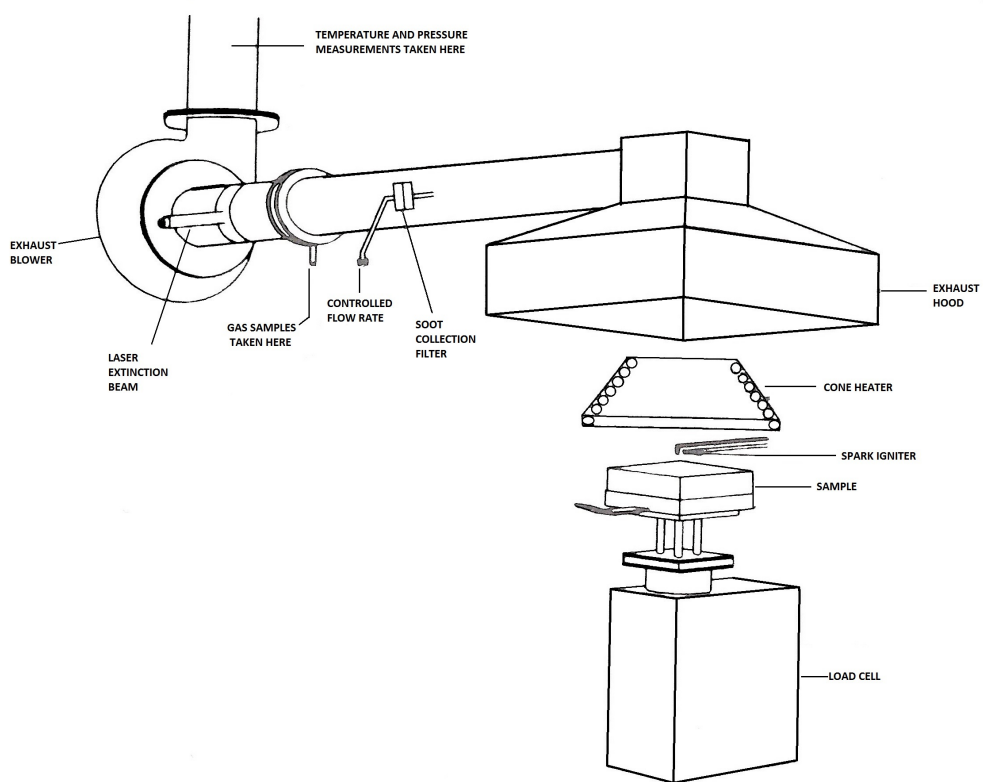


Figure 5.1: Sketch of the cone calorimeter

ature at an orifice plate in the duct. Finally, the concentrations of oxygen, carbon dioxide, carbon monoxide, were measured using appropriate instruments. Heat release rate was calculated from the gas concentration and mass flow measurements.

For this study samples were cut from painted gypsum wallboard panels. The samples were 100 mm square and 12.7 mm thick. The experiments were conducted with the samples in the horizontal position. The key measurements and observations made with the cone calorimeter were heat release rate per unit area of the samples and time to ignition. These experiments were conducted with heat fluxes of 25, 35, 50, 70 and 75 kW/m². Several other cone calorimeter experiments were conducted with a single type K thermocouple, installed in a slit in the painted paper on the gypsum wallboard samples. This was the same manner of thermocouple installation used in the instrumented gypsum board wall experiments. These experiments were conducted at heat fluxes of 30, 35, and 50 kW/m² to determine ignition time and surface temperature pairs.

5.2 Radiant Flooring Panel Experiments

The radiant flooring panel test method is known as ASTM E648, Standard Method of Test for Critical Radiant Flux of Floor-Covering Systems Using a Radiant Heat Energy Source [31]. The radiant flooring panel is used to measure the flame spread of a material while exposed to an incident radiant heat flux. The source of the heat flux is a pre-mixed air-gas-fueled radiant panel. The radiating surface measures 305 mm by 457 mm. The radiating surface is inclined at 30 ° above the horizontal. The test specimen is mounted horizontally beneath the radiant panel. The surface of the test sample exposed to the radiant panel is 1 m long and 0.2 m wide. Under standard operating conditions the radiant panel provides a heat flux distribution on the test specimen varying from 10 kW/m² at the measurement point, centered 100 mm from the edge of the sample closest to the panel to 1 kW/m² at the farthest measurement point 900 mm from the edge of the sample closest to the panel. A schematic of the radiant flooring panel apparatus is shown in Figure 5.2.

For these experiments a higher heat flux profile was required to propagate

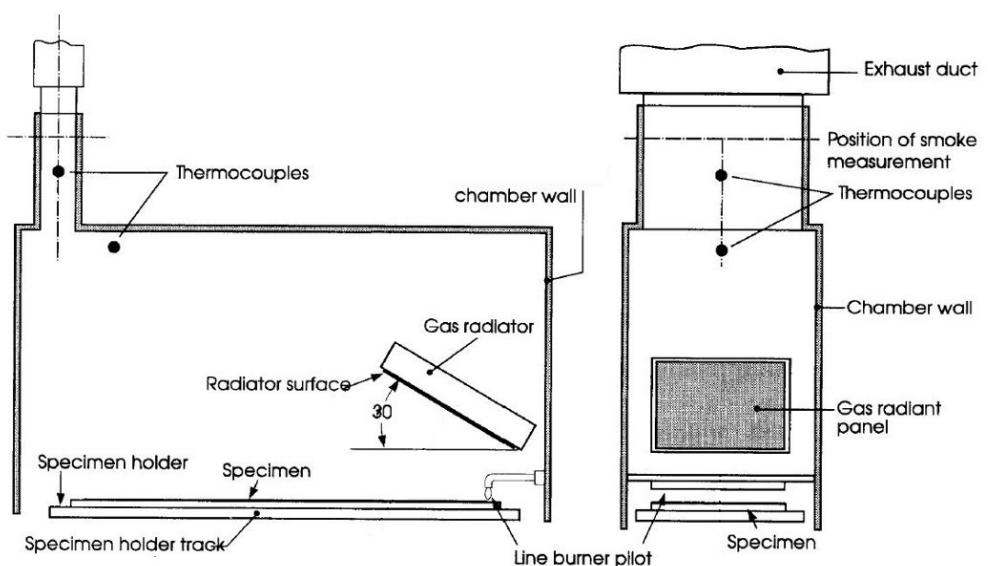


Figure 5.2: Schematic of the radiant flooring panel apparatus

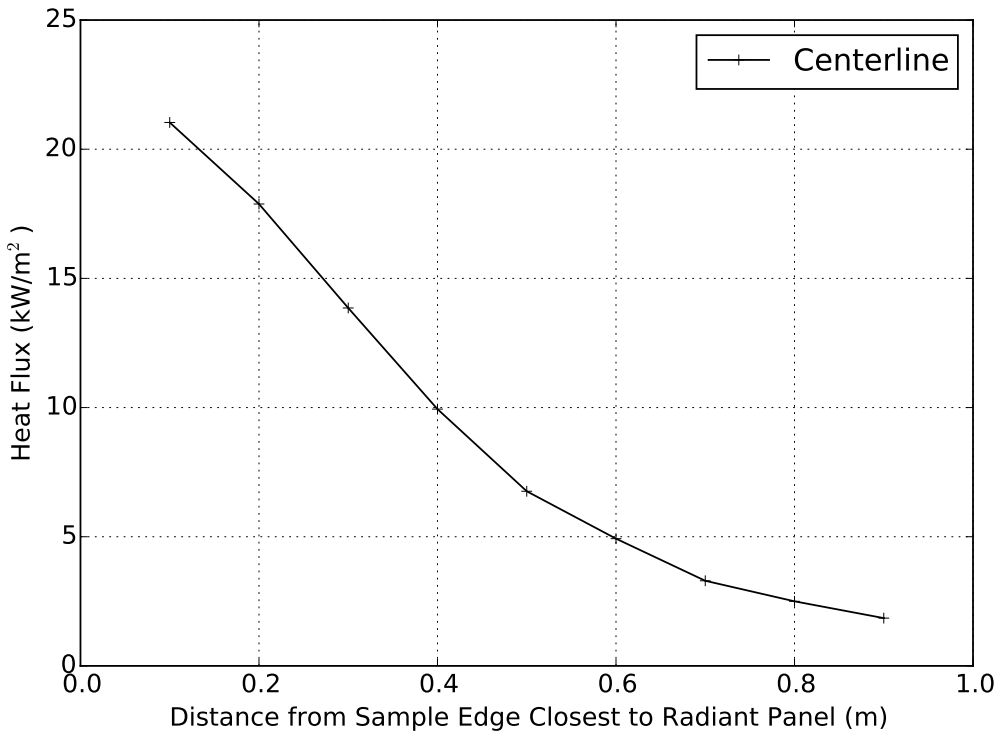


Figure 5.3: Incident heat flux profile along the centerline of the sample in the radiant flooring panel test apparatus

flame spread on the painted gypsum wallboard samples, so the air-gas flow supplying the radiant panel was increased to provide an incident flux ranging from approximately 21 kW/m^2 at the 100 mm position to 2 kW/m^2 at the 900 mm position. The incident heat flux curve used in these experiments is shown in Figure 5.3.

A diffusion, propane-fueled, pilot flame from a 254 mm long wide stainless steel burner tube, as specified in ASTM 648, was used to ignite the test sample near the edge of the sample closest to the panel [31]. The objective of these experiments was to determine the critical radiant flux for the painted gypsum wallboard samples. The critical radiant flux corresponds to the flux at the point of maximum flame propagation, or the point on the sample where the flame spread stopped. For this study the samples examined were cut from painted gypsum wallboard panels that were prepared from the supply of panels that were used in the compartment experiments.

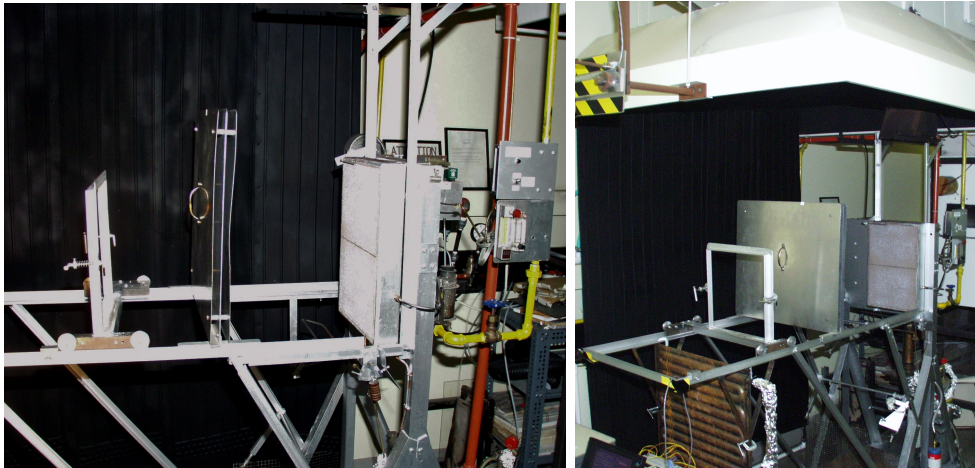


Figure 5.4: Photographs of the radiant panel experimental arrangement, on the left is a photograph which shows the radiant panel on the right, the aluminum heat shield in the center and the moveable sample mounting frame trolley for the gypsum wallboard sample on the left. The photograph on the right shows an isometric view of the test arrangement.

5.3 Radiant Panel Experiments

The vertical radiant panel used is documented in ASTM E162 and normally provides a measure of downward, opposed-flow flame spread [32]. The apparatus measures the surface flammability of materials using a pre-mixed air-gas-fired radiant panel that has a radiating surface 305 mm wide by 457 mm high.

For the purposes of this study a modified version of the test apparatus was used. The radiant panel and the controls for the radiant panel remained in place as documented in ASTM E162. However the sample mounting system was changed. A rail and trolley system was developed by Lawson and Twilley to expose fire fighter protective equipment to various heat fluxes by being able to move the test specimen to a predetermined position that correlated with a given heat flux [66]. This trolley was used to hold a sample of painted gypsum wallboard that was 362 mm square. The samples were vertical and parallel to the radiant panel. Figure 5.4 has photographs which show the radiant panel test arrangement.

Prior to conducting experiments with the gypsum wallboard samples,

heat flux gauge measurements taken at the center position of the sample were used to determine the positions on the trolley track for a specific radiant exposure. The positions were marked for 10, 12.5, 15, 17.5, 20, 22.5, and 25 kW/m². The area surrounding the center of the maintained the desired heat flux within at least 70 mm on either side of the center point and 100 mm above and below the center point. In other words, the area around the center point of the sample had heat flux measures similar, within the uncertainty of the device, to the center point measurement. Outside of the central area of the samples, the heat flux would decrease as the position approached the edge of the sample. The center point heat flux measures vs the distance from the radiating surface is provided in Figure 5.5

To conduct the experiments, the radiant panel was ignited and allowed to pre-heat for at least 60 minutes. The water cooled, Schmidt-Boelter total heat flux gauge was mounted in the center the sample holder, and the heat flux positions were confirmed. The heat flux gauge was then removed from the sample holder trolley. Just before the sample was mounted on the movable trolley, an aluminum heat shield was placed between the radiant panel and the sample holder trolley. Once the sample was mounted and the sample was moved to the appropriate distance from the radiant panel based on the heat flux desired for the experiment, the heat shield was removed. The removal of the heat shield would be recorded as the beginning of the exposure and therefore the beginning of the experiment. Each sample was exposed for 600 seconds. Each sample had a single bare-bead, Chromel-Alumel (type K) thermocouple, with a 0.5 mm nominal diameter bead in contact with the center point of each sample. During the experiments the samples were monitored for temperature and ignition. After the exposure time was completed the heat shield was once again placed between the sample and the radiant panel. The samples were cooled, removed and examined. The area of thermal damage to the painted paper surface of the gypsum board was compared with exposure heat flux. This was another means of potentially obtaining a measure of the critical heat flux.

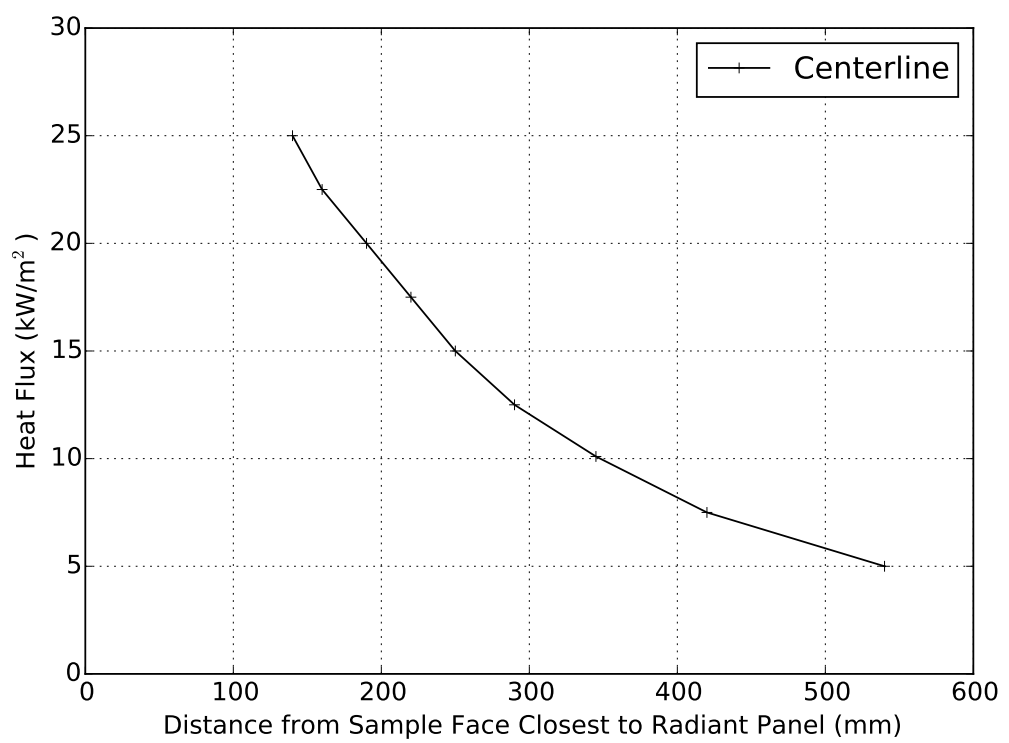


Figure 5.5: Incident heat flux profile based on the distance between the sample face and the radiant panel

Incident Heat Flux (kW/m ²)	Ignition	Time to Ignition (s)	Fire Effect
25	No	NA	Paint & paper charred & cracked
35	Yes	73	Paint & paper consumed
50	Yes	35	Paint & paper consumed
70	Yes	21	Paint & paper consumed
75	Yes	17	Paint & paper consumed

Table 5.1: Painted gypsum wallboard time to ignition results from the cone calorimeter

5.4 Results

The results from the three different bench scale experiments are presented and discussed in this section. All three test methods provided some insight into the ignition and the critical heat flux required for ignition or flame spread of the painted paper surface on the gypsum wall board. The cone calorimeter also provided values for heat release rate.

5.4.1 Ignition and Ignition Temperature

Three replicate time to ignition experiments were conducted with the cone calorimeter apparatus at each heat flux. The results of these experiments are shown in Table 5.1. The time to ignition values in the table are the average of the three times. Note that no ignition occurred at 25 kW/m². The exposure at 25 kW/m² resulted in charring and cracking of the painted paper surface of the gypsum wallboard sample. This began to occur, on average, at 270 s of exposure time. The samples were exposed to 25 kW/m² for 1800 s each and no ignition occurred. In the experiments with heat fluxes of 35 kW/m² or higher, ignition did occur and the painted paper surface of the gypsum board was consumed, leaving the gypsum board exposed. There were no surprises in the data with regard to the heat flux exposures. The time to ignition was reduced as the incident heat flux was increased.

Additional cone calorimeter experiments were conducted in the University of Canterbury Fire Laboratory. In these experiments the purpose was to obtain an estimate of the temperature of the painted paper surface at the

Incident Heat Flux (kW/m ²)	Ignition (Yes or No)	Time to Ignition (s)	Ignition Temperature (°C)
30	Yes	112	375
35	Yes	50	335
50	Yes	38	371

Table 5.2: Painted gypsum wallboard ignition temperature results from exposure in the cone calorimeter

time of ignition. Samples of painted gypsum wallboard were shipped from the NIST Fire Research Laboratory in Gaithersburg, MD., USA. In these experiments an additional incident heat flux level of 30 kg/m² was added to provide another test between the 25 and 35 kW/m² levels. The averaged ignition time and temperature pairs are shown in Table 5.2. The average time to ignition values between the two different calorimeters are within $\pm 50\%$ and $\pm 10\%$ at incident heat flux values of 35 and 50 kg/m², respectively. The average ignition temperatures from the nine experiments ranged from 335 to 375 °C.

In the radiant flooring panel experiments the gypsum wallboard was exposed to an incident heat flux that ranged from approximately 21 kW/m² to 2 kW/m² over the length of the sample. In addition to the heat flux from the radiant panel, there is a small flame front approximately 10 to 30 mm in height that serves as the pilot along the length of the sample and provides additional energy to the fuel immediately ahead of the flame. The impact is limited to a small distance ahead of the flame, estimated to be less than 5 mm, since the flame is drawn back to the leading edge of the sample (burned portion) by the draft of the radiant panel. This effect is shown in Figure 5.6. In Figure 5.6 several thermocouples can be seen. The exposed-bead, Chromel-Alumel (type K) thermocouples, with a 1.0 mm nominal diameter, were installed by pulling the positive and negative wires through holes drilled through the gypsum wallboard sample and positioning the bead of the thermocouple in a slit in the painted paper face made with a razor blade. This was the same installation method that was used in the instrumented gypsum board wall experiments and in the cone calorimeter samples to measure ignition temperature. The thermocouples were installed in the center of the

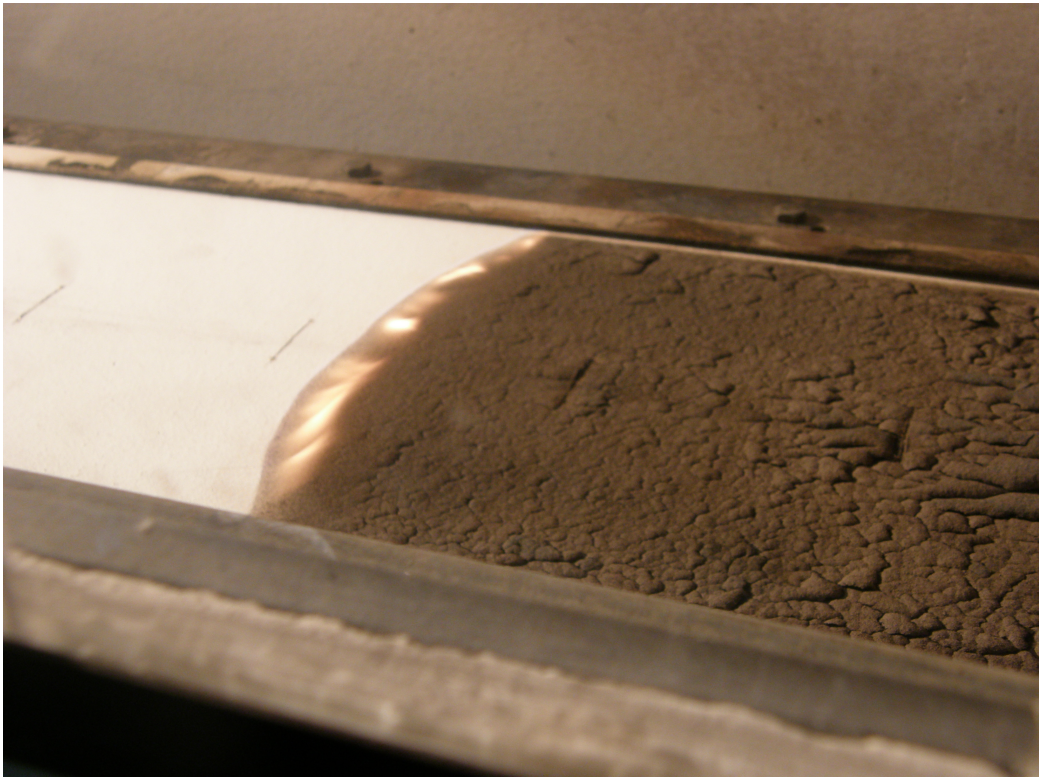


Figure 5.6: Photograph of the flame front burning on the gypsum wallboard sample in the flooring radiant panel. Thermocouples imbedded at 100 mm intervals in the surface of the painted paper can be seen in front of and behind the flame front. The flame is leaning back in the direction the radiant panel.

sample at 100 mm intervals beginning at 100 mm from the edge of the sample closest to the radiant panel. Three replicate experiments were conducted. The average time that the flame front reached the thermocouples and the temperature of the thermocouple just prior to the painted paper surface of the gypsum wallboard sample igniting is presented in Table 5.3.

With the flooring radiant panel test, the incident heat flux from the panel and the pre-heated gypsum wallboard sample enables flame spread for approximately 500 s. The temperatures prior to ignition ranged from an average of 315 °C for the 100 mm position to 242 °C for the 400 mm position. The average

Exposing the painted gypsum wallboard samples to the vertical radiant panel provided a wide range physical damage to samples as shown in

Postion (mm)	Incident Heat Flux (kW/m ²)	Ignition (Yes or No)	Time to Ignition (s)	Ignition Temperature (°C)
100	21	Yes	133	315
200	18	Yes	198	296
300	14	Yes	302	279
400	10	Yes	502	242
500	7	No	NA	NA

Table 5.3: Flooring radiant panel experiment flame spread results including time to ignition at 100 mm intervals and surface temperature just prior to ignition. The values are averages from three replicate experiments.

Figure 5.7. However based on visual observations there were no flaming ignitions. For one of the samples at 15 kW/m², small sections of the painted paper surface on the gypsum wall board would lift or partially separate from the gypsum core and would begin to glow. This process became more prevalent as the heat fluxes increased. The radiant exposure of 25 kW/m² caused the samples to collapse as they were being removed from the holder. Hence there were no photos of those samples. Figure 5.8 is a graph of the averaged time vs temperature curves for the three replicates at the 7 different heat flux levels. Notice that the samples exposed to 17.5 kW/m² and higher have a temperature increase to a peak temperature followed by a decrease. This trend may be indicative of the combustion of the paint and paper adding to the energy at the face of the sample. The temperatures at which the change in rate of temperature rise occur are between 300 and 400 °C.

5.4.2 Heat Release Rate per Unit Area

The cone calorimeter experiments generated heat release are per unit area values ranging from a low of approximately 160 kW/m² at an incident heat flux of 35 kW/m² to approximately 230 kW/m² at an incident heat flux of 75 kW/m². The average total heat released during each burn was 2.8 MJ/m².

5.4.3 Critical Heat Flux

Seven replicate experiments were conducted in the radiant flooring panel apparatus. The mean burn length was 432 mm with a 95% confidence limit of

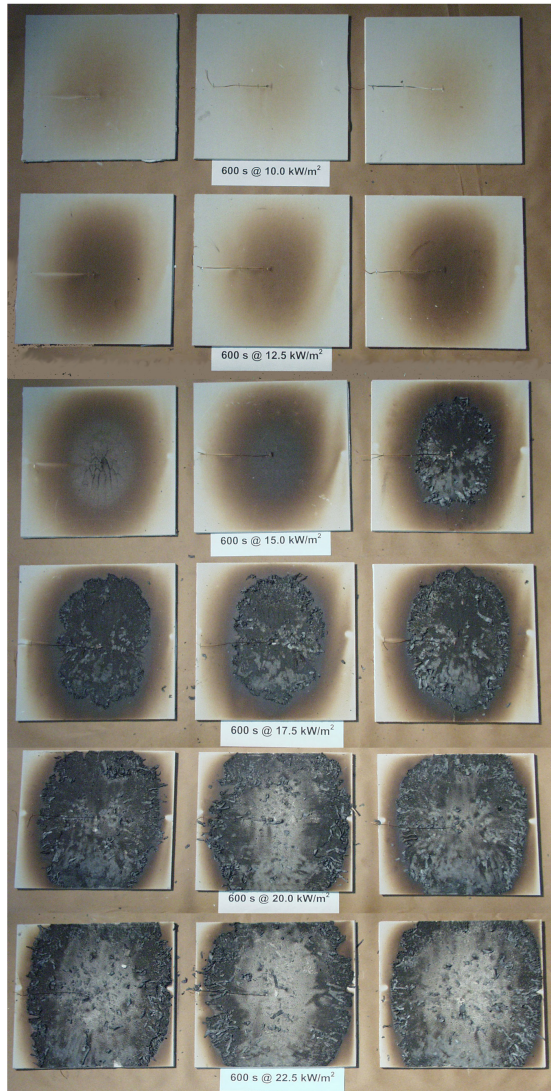


Figure 5.7: Photographs of the fire effects on the instrumented gypsum wall-board exposed to radiant heat from a natural gas fired panel. Each row of samples represents three replicate experiments at a given heat flux. Beginning with the top row and moving down the exposure heat fluxes were 10, 12.5, 15, 17.5, 20, and 22.5 kW/m^2 .

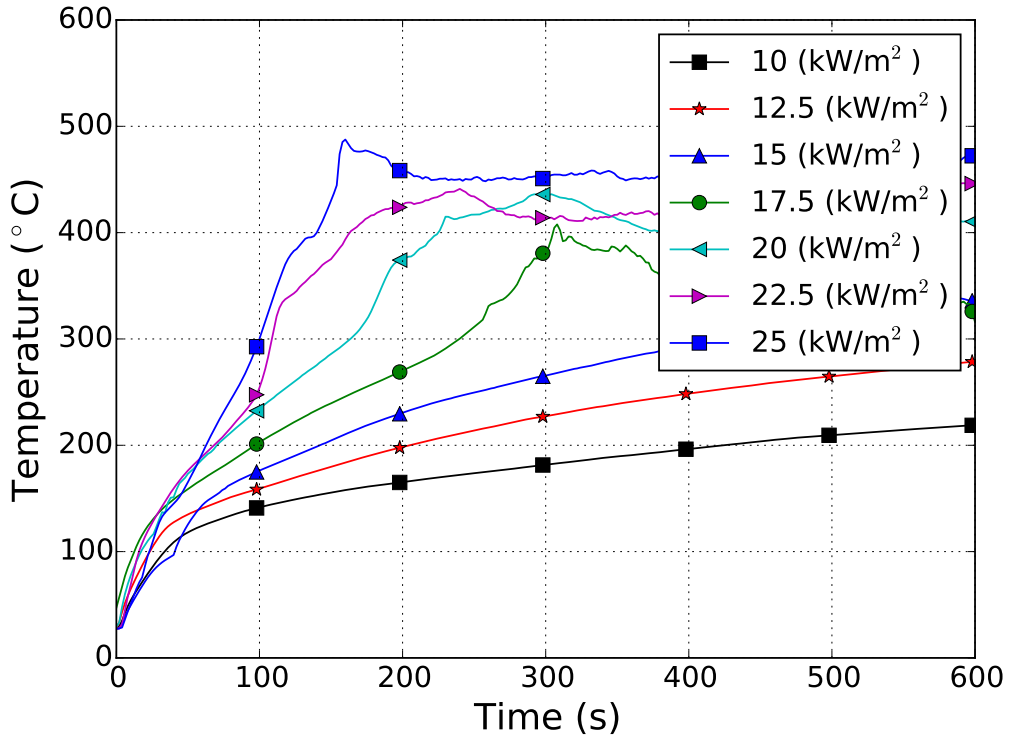


Figure 5.8: Time vs. temperature curves for the gypsum wallboard samples exposed to radiant heat from a natural gas fired panel at heat fluxes of 10, 12.5, 15, 17.5, 20, 22.5 and 25 kW/m^2 .

Incident Heat Flux (kW/m^2)	Heat Release Rate per Unit Area (kW/m^2)
35	163
50	179
70	255
75	231

Table 5.4: Painted gypsum wallboard heat release rate per unit area results from the cone calorimeter. Each value is based on an average of three tests.



Figure 5.9: Photographs of the radiant flooring panel experiments, on the left is a photograph aimed at the radiant panel showing the pilot flame on the sample as well as the flame front on the sample. The photograph on the right show the flame front on the sample just prior to flame out.

± 18 mm. Comparing this burn length range, 414 mm to 450 mm, to the incident heat flux curve provided a critical heat flux of approximately 8.9 kW/m^2 with a 95% confidence limit of $\pm 0.6 \text{ kW/m}^2$. Photographs showing a radiant flooring panel test underway and sample nearing the flameout position are provided in Figure 5.9.

While the vertical radiant panel did not provide ignition data or heat release rate values it did provide information on the fire effect development on the painted gypsum wallboard samples with respect to heat flux. Referring again to the five fire effect categories listed by DeHann [13] and examining the Figure 5.7 we see surface thermal effects of discoloration on the painted paper surface of the gypsum wallboard samples at both the 10 and 12.5 kW/m^2 incident heat flux exposures. The samples exposed to 15 kW/m^2 exhibit charring and given the thin nature of the painted paper surface penetration was evidenced on two of the three sample. The sample of the right also shows signs of the painted paper being consumed. The samples exposed to 17.5 kW/m^2 and above all show signs of significant levels of painted paper consumption. As the heat flux was increased, the area of damage also increased. Even though the incident heat flux values were lower than the characteristic value measured at the center of the sample, as the heat flux in the center increased

heat flux at the edges also increased above 15 kW/m^2 . Hence the damaged area increased outward toward the edges. It would appear in this test series, that 15 kW/m^2 is right on the threshold of painted paper penetration and consumption.

DeHaan [13] categorizes the fire effects that form patterns as follows:

1. Surface deposits - no irreversible effect on surface
2. Surface thermal effects - physical change such a discoloration or melting
3. Charring - evidence of surface burning
4. Penetration - charring below the surface
5. Consumption - loss of surface material, charring throughout

Each apparatus provided similar but different thermal exposure conditions and each test method has a specific parameter or parameters that they were designed to measure for. Currently there is no specific protocol for a fire model user to follow to develop input data. Nor is there a "standard" catalog of fire model inputs for a given material. As a result the literature is sourced for information and users may to conduct experiments, such as those above, in order to develop values or ranges of values which could be used in the calculations in Chapters 8 and 9 or to evaluate the validity of the calculations in those chapters.

Chapter VI

Fire Pattern Compartment Experiments

The fire pattern experiments were conducted in residential scale compartments built for the purpose of these experiments. The compartments were constructed on top of a portable wood floor platform. Each of the test compartments consisted of three 3.6 m long by 2.4 m high wood framed walls. The wood elements of the frame were composed of kiln-dried fir with a nominal cross section of 90 mm by 38 mm. A partial ceiling with a width of at least 1.2 m, measured from the back wall of the compartment was installed across the width of the compartment, this allowed for the plume to impact the ceiling and form a ceiling jet along the back wall, before the fire gases flowed up and out of the compartment and into the 6 m by 6 m hood in the NIST Large Fire Research Laboratory. The interior surface of the walls and ceiling was composed of 12.7 mm thick, regular core gypsum wallboard. As defined by ASTM, gypsum wallboard is designed for use on walls, ceilings, or partitions. It is composed of a non-combustible core, essentially gypsum, with paper bonded to the surface of the core. The back wall of the compartment consisted of three full gypsum board panels, each 1.2 m wide and 2.4 m high. The front wall of the compartment was open along the full width of the compartment to minimize the impact of entrained air being channeled through a doorway. These experiments were conducted without instrumentation in the walls for several reasons; to compare the non-instrumented gypsum wallboard fire pattern with the instrumented gypsum wallboard fire pattern results to determine if the instrumentation affected the pattern generation, to provide more realistic conditions, and to enable the conduct of additional replicate experiments given the limited laboratory availability. A photograph of the compartment fire experimental arrangement is shown in Figure 6.1. In the instrumented gypsum wallboard experiments, as the burners were moved away

from the position against the wall, the fire effects on the wall diminished significantly. Therefore most of the fire pattern compartment experiments were conducted with the burners against the wall or corner of the compartment or less than one burner length from the wall.

Prior to each burn, grid lines approximately 51 mm on center were drawn on the painted gypsum wallboard panel that would be exposed to the fire. After each burn, the fire patterns were photographed and analyzed for repeatability by looking at the portion of the grid that was burned. The fire damaged wallboard was subsequently removed, photographed again, and replaced with new sections of painted gypsum wallboard. Several types of fire pattern experiments were conducted in the compartments; to examine the impact of the wall construction on the resulting fire pattern; and to compare the fire patterns based on the burner centered on, or the rear wall, or in, or near a corner on the rear wall of the compartment.

6.1 Wall Position Experiments

The initial set of compartment experiments were conducted to examine if the type of wall construction would impact the development of the fire patterns. These experiments would determine how the walls for the remaining compartment fire pattern experiments would be constructed. Three cases were examined: 1) Open back, 12.7 mm thick, regular core, painted gypsum board on the front of a wood frame only, 2) Closed back, 12.7 mm thick, regular core, painted gypsum board on the front and back of a wood frame representative of an interior wall, and 3) Insulated, 12.7 mm thick, regular core, painted gypsum board on the front and back of a wood frame, with insulation in the voids of the wood frame representative of an exterior wall. The insulation was 90 mm thick fiber glass batting, a kraft paper facing, and an “R value” of 13. From the instrumented gypsum wallboard experiments, the peak temperatures on the backside of the wallboard occurred when the burners were positioned against the wall. The peak temperatures were similar for all of the fuels, approximately 80 °C, although the duration of the higher temperatures on the rear of the wallboard was longer for the natural gas and the gasoline fueled burners. Therefore the wall construction experi-

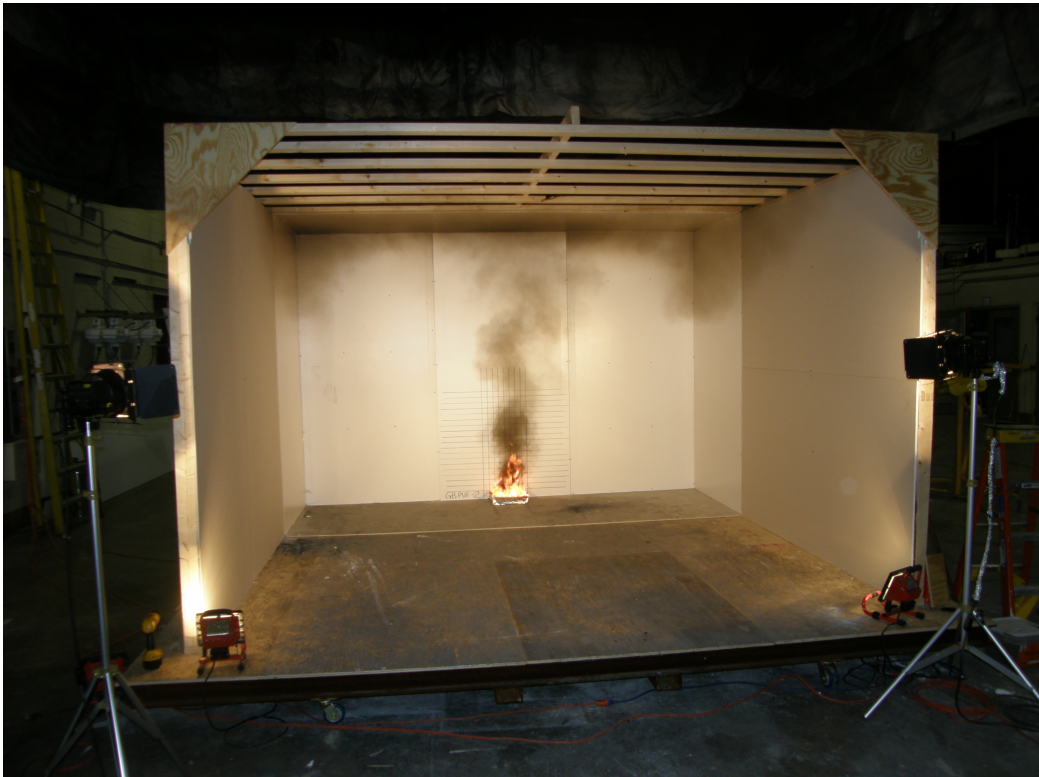


Figure 6.1: Photograph of the wall fire pattern experiments compartment arrangement. Experiment shown is being conducted with a polyurethane burner against the back wall.

ments were only conducted with the natural gas and gasoline fueled burners as the impact of insulating the back of the walls exposed to the fuels with the highest energy would produce the most significant differences, if any, to the fire patterns.

6.1.1 Experimental Arrangement

The burner was centered on the middle panel of the rear wall and was in contact with the wall. The wall behind the center panel of the rear wall was constructed either as open, closed, or insulated to meet the needs of the experiment. The burner was positioned against the face of the painted gypsum wallboard. As in the fire source characterization experiments the top of the fuel in each case was positioned 7.5 cm above the floor of the compartment.

The source fires remained the same in terms of fuels, amounts of fuels used, burner size and burn duration. The natural gas had a 300 s burn time which was approximately the upper bound for the total burn time for the 500 mL of gasoline. By using the same burners, these compartment fire pattern experiments can be correlated with the instrumented wall experimental results.

6.1.2 Results

Ten replicate experiments were conducted with each of the three wall construction types. The walls were exposed to both the natural gas and the gasoline burners. For these experiments the burner was in contact with the gypsum wallboard. A total of 60 experiments were conducted. The results will be presented by wall construction type. The order of presentation will be open, closed, and insulated wall construction.

For this analysis, the outline of the fire pattern, or the line of demarcation [8], was defined as the points where charring, penetration and consumption of the paper covering the gypsum wallboard stopped. The grids were used to assist with the determination of the fire pattern area and the sizing of the images. This defining edge was used to measure the dimensions of the fire pattern, such as height and width. Given the irregular shape of the patterns, the area of each pattern could not be calculated based solely on the maximum height and maximum width measurements. Therefore the areas of the grid cells within the fire pattern were added up to determine the area of the fire patterns. The analysis was carried out with a resolution of a quarter grid cell or approximately 0.003 m².

There were four measures that were taken to characterize each pattern: maximum height, maximum width, height at maximum width, and the area. Each dimensional value is presented with the 95 % confidence level (2σ) based on Type A statistical analysis of the fire pattern measurements.

There are also a number of qualitative terms from NFPA 921 that were used to describe features of the patterns. For example, "clean burn" to describe a lack of soot within a fire pattern area or "inverted cone" to describe the shape of the pattern [8].

Natural Gas

Figure 6.2 shows a comparison of the ten fire patterns generated by the natural gas burner on the wall with open back construction. The images within the figure are slightly different sized in an effect to make the images comparable. The average maximum height of the fire pattern generated by the natural gas burner on the open walls was $0.74 \text{ m} \pm 0.12 \%$. The average maximum width of the fire pattern from the same experiments was $0.24 \text{ m} \pm 0.06 \%$. The position from the top edge of the burner to the vertical position of the maximum width was $0.41 \text{ m} \pm 0.07 \%$. The area of the burn estimated by examining the damaged grid cells was $0.15 \text{ m}^2 \pm 0.05 \%$.

These fire patterns, as well as all of the other patterns in this study, are fire plume generated patterns. The bottom width of each patterns is similar to the width of the burner. Moving up from the burner, about 25 mm, the pattern width is reduced as a result of air entrainment into the plume. As the oxygen in the air mixes with the gaseous fuel and combusts, the plume and the pattern expands. As the flames move up the wall the width tends to increase until about half of the peak height of the pattern, then the pattern starts to reduce in width as the fuel is consumed and the volume of the flame is reduced. Based on observation alone, the visible flames extend well above the height of the resulting patterns. Even though the experiments were conducted under quiescent conditions, a noticeable bias to one side or the other can be seen in four of the ten experiments.

The fire pattern photographs from the ten closed wall construction experiments are shown in Figure 6.3. The patterns appear very similar in nature and size to the patterns that were generated on the open construction walls. The average maximum height of the fire patterns generated by the natural gas burner on the closed construction wall was the same as the patterns generated on the open construction wall, $0.74 \text{ m} \pm 0.06 \%$. The 95 % confidence limit is about half of the value from the open wall experiments. The average maximum width of the fire patterns was $0.24 \text{ m} \pm 0.02 \%$. Again similar to the previous experiments. The vertical position of the maximum width was $0.43 \text{ m} \pm 0.03 \%$. The area of the burn estimated by examining the damaged grid cells was $0.14 \text{ m}^2 \pm 0.01 \%$.

The basic shape of these patterns on the closed wall are very similar to the patterns on the open wall. Six of the ten patterns have a bump out or an unsymmetrical curve within 200 mm of the top of the burner. The cause of these bumps in the patterns could not be determined. Three of the patterns have a noticeable lean.

The last set of wall experiments with the natural gas burner was conducted with the insulated wall. The patterns from the ten replicate experiments are shown in Figure 6.4. The average maximum height of the fire patterns generated by the natural gas burner on the insulated walls was $0.71 \text{ m} \pm 0.10 \%$. The average maximum width of the fire patterns on the insulated walls were $0.23 \text{ m} \pm 0.04 \%$. The vertical position of the maximum width was $0.42 \text{ m} \pm 0.07 \%$. The area of the burn estimated by examining the damaged grid cells was $0.15 \text{ m}^2 \pm 0.02 \%$.

For all intents and purposes, the patterns generated on the three different types of wall construction were the same. The comparison of the numerical values can be seen in Table 6.1. Each of the sets of patterns have a few patterns with the bump on one side of the pattern within 200 mm of the burner, as discussed in the section on the closed wall construction.

Gasoline

Figure 6.5 shows a comparison of the ten fire patterns generated by the natural gas burner on the wall with open back construction. The images within the figure are slightly different sized in an effect to make the images comparable. The average maximum height of the fire pattern generated by the natural gas burner on the open walls was $0.74 \text{ m} \pm 0.12 \%$. The average maximum width of the fire pattern from the same experiments was $0.24 \text{ m} \pm 0.06 \%$. The position from the top edge of the burner to the vertical position of the maximum width was $0.41 \text{ m} \pm 0.07 \%$. The area of the burn estimated by examining the damaged grid cells was $0.15 \text{ m}^2 \pm 0.05 \%$.

These fire patterns, as well as all of the other patterns in this study, are fire plume generated patterns. The bottom width of each patterns is similar to the width of the burner. Moving up from the burner, about 25 mm, the pattern width is reduced as a result of air entrainment into the plume. As

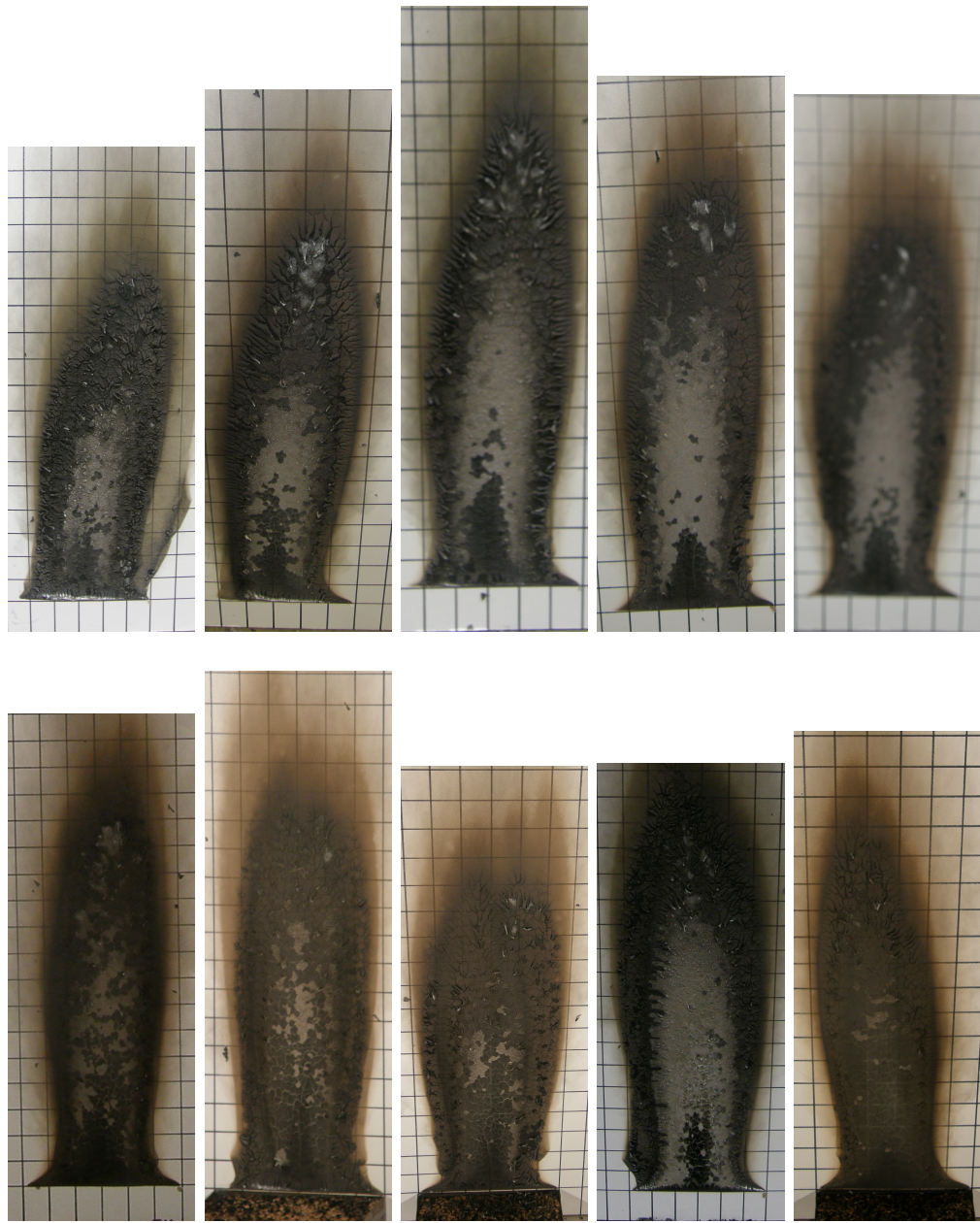


Figure 6.2: Photographs of the fire patterns from ten replicate natural gas burner against open wall construction.



Figure 6.3: Photographs of the fire patterns from ten replicate natural gas burner against closed wall construction.

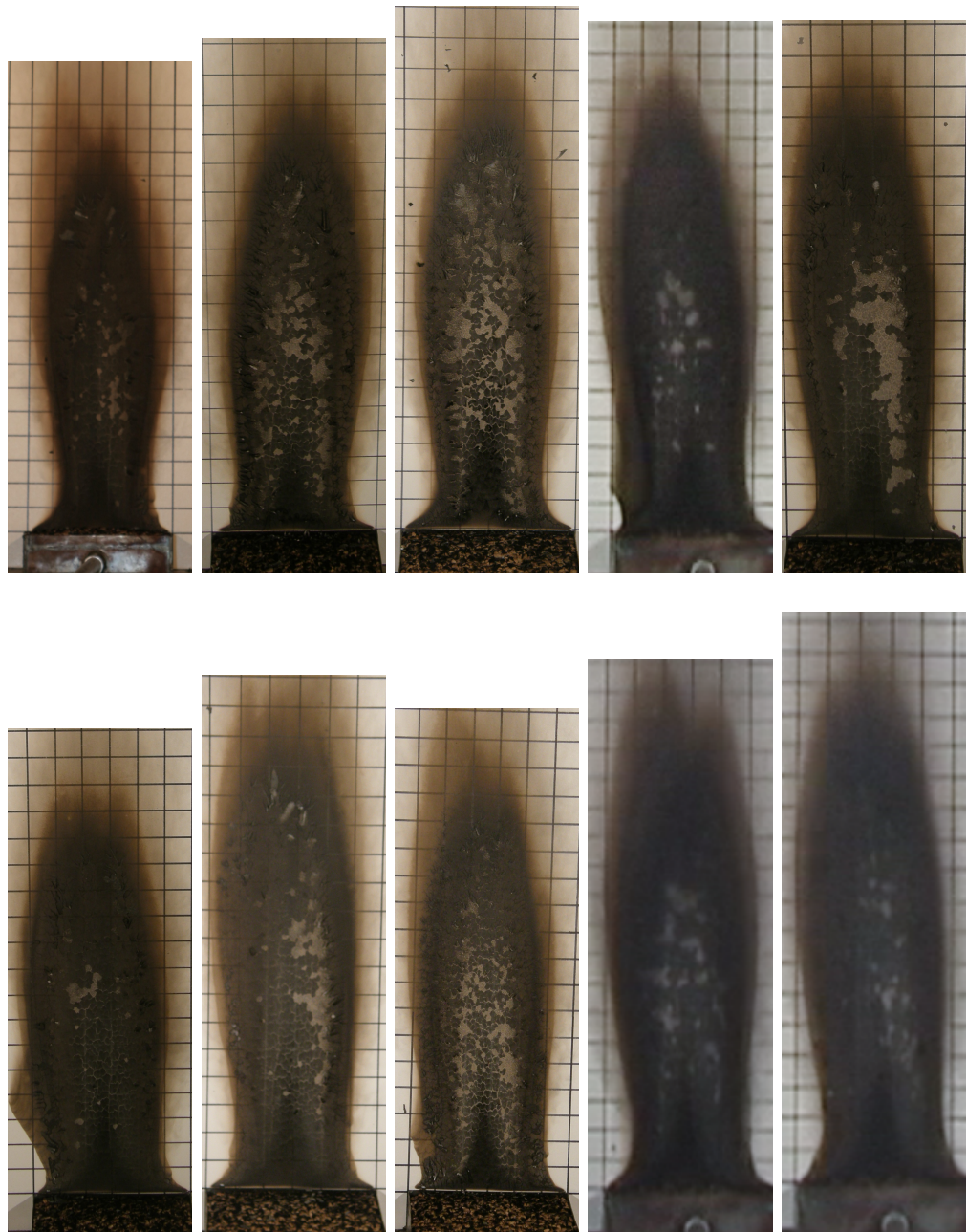


Figure 6.4: Photographs of the fire patterns from ten replicate natural gas burner against insulated wall construction.

the oxygen in the air mixes with the gaseous fuel and combusts, the plume and the pattern expands. As the flames move up the wall the width tends to increase until about half of the peak height of the pattern, then the pattern starts to reduce in width as the fuel is consumed and the volume of the flame is reduced. Based on observation alone, the visible flames extend well above the height of the resulting patterns. Even though the experiments were conducted under quiescent conditions, a noticeable bias to one side or the other can be seen in four of the ten experiments.

The fire pattern photographs from the ten closed wall construction experiments are shown in Figure 6.6. The patterns appear very similar in nature and size to the patterns that were generated on the open construction walls. The average maximum height of the fire patterns generated by the natural gas burner on the closed construction wall was the same as the patterns generated on the open construction wall, $0.74 \text{ m} \pm 0.06 \%$. The 95 % confidence limit is about half of the value from the open wall experiments. The average maximum width of the fire patterns was $0.24 \text{ m} \pm 0.02 \%$. Again similar to the previous experiments. The vertical position of the maximum width was $0.43 \text{ m} \pm 0.03 \%$. The area of the burn estimated by examining the damaged grid cells was $0.14 \text{ m}^2 \pm 0.01 \%$.

The basic shape of these patterns on the closed wall are very similar to the patterns on the open wall. Six of the ten patterns have a bump out or an unsymmetrical curve within 200 mm of the top of the burner. The cause of these bumps in the patterns could not be determined. Three of the patterns have a noticeable lean.

The last set of wall experiments with the natural gas burner was conducted with the insulated wall. The patterns from the ten replicate experiments are shown in Figure 6.7. The average maximum height of the fire patterns generated by the natural gas burner on the insulated walls was $0.71 \text{ m} \pm 0.10 \%$. The average maximum width of the fire patterns on the insulated walls were $0.23 \text{ m} \pm 0.04 \%$. The vertical position of the maximum width was $0.42 \text{ m} \pm 0.07 \%$. The area of the burn estimated by examining the damaged grid cells was $0.15 \text{ m}^2 \pm 0.02 \%$.

For all intents and purposes, the patterns generated on the three different types of wall construction were the same. The comparison of the numerical

values can be seen in Table 6.1. Each of the sets of patterns have a few patterns with the bump on one side of the pattern within 200 mm of the burner, as discussed in the section on the closed wall construction.

Polyurethane Foam

6.2 Corner Position Experiments

6.2.1 Experimental Arrangement

6.2.2 Results

Natural Gas

Gasoline

Polyurethane Foam

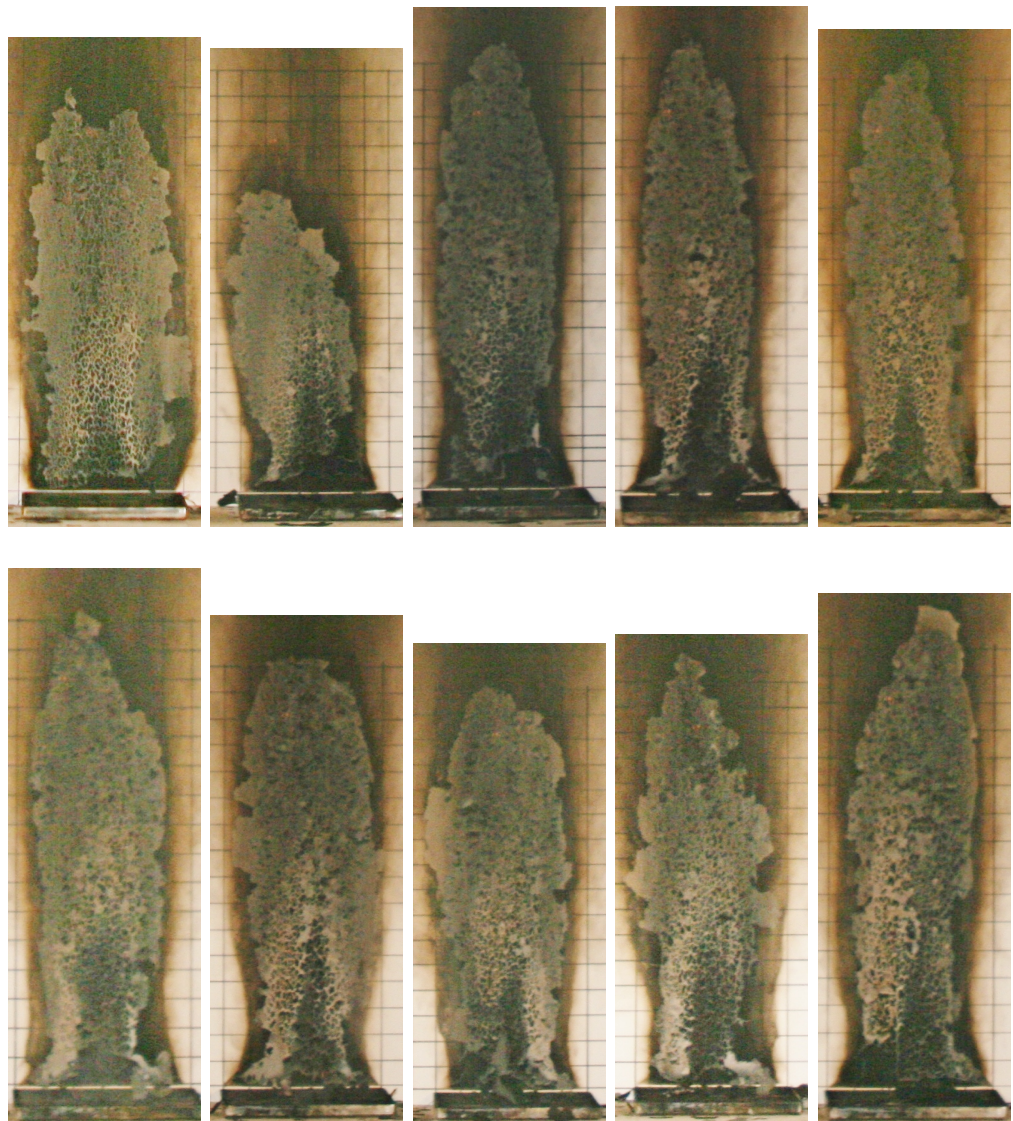


Figure 6.5: Photographs of the fire patterns from ten replicate gasoline burner against open wall construction.

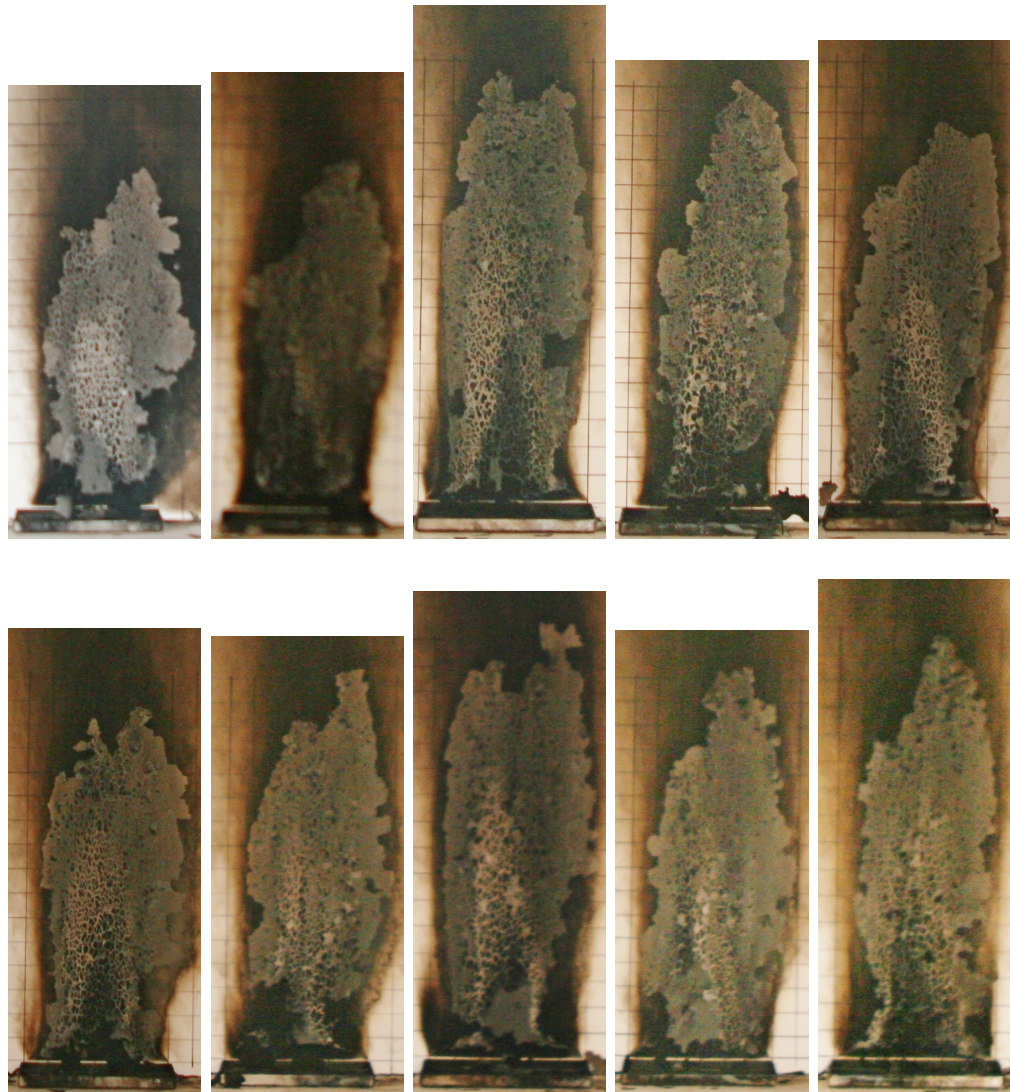


Figure 6.6: Photographs of the fire patterns from ten replicate gasoline burner against closed wall construction.

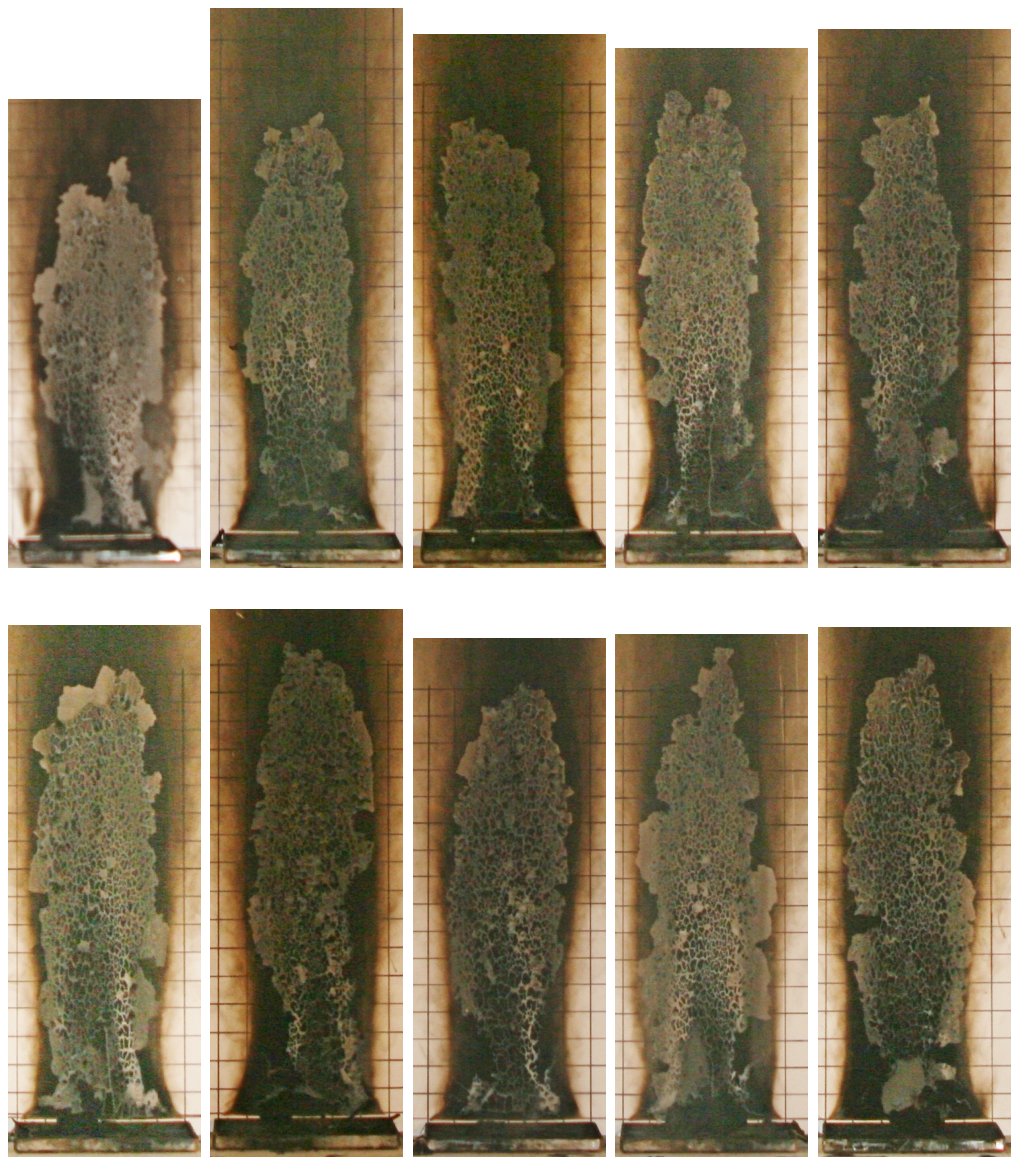


Figure 6.7: Photographs of the fire patterns from ten replicate gasoline burner against insulated wall construction.

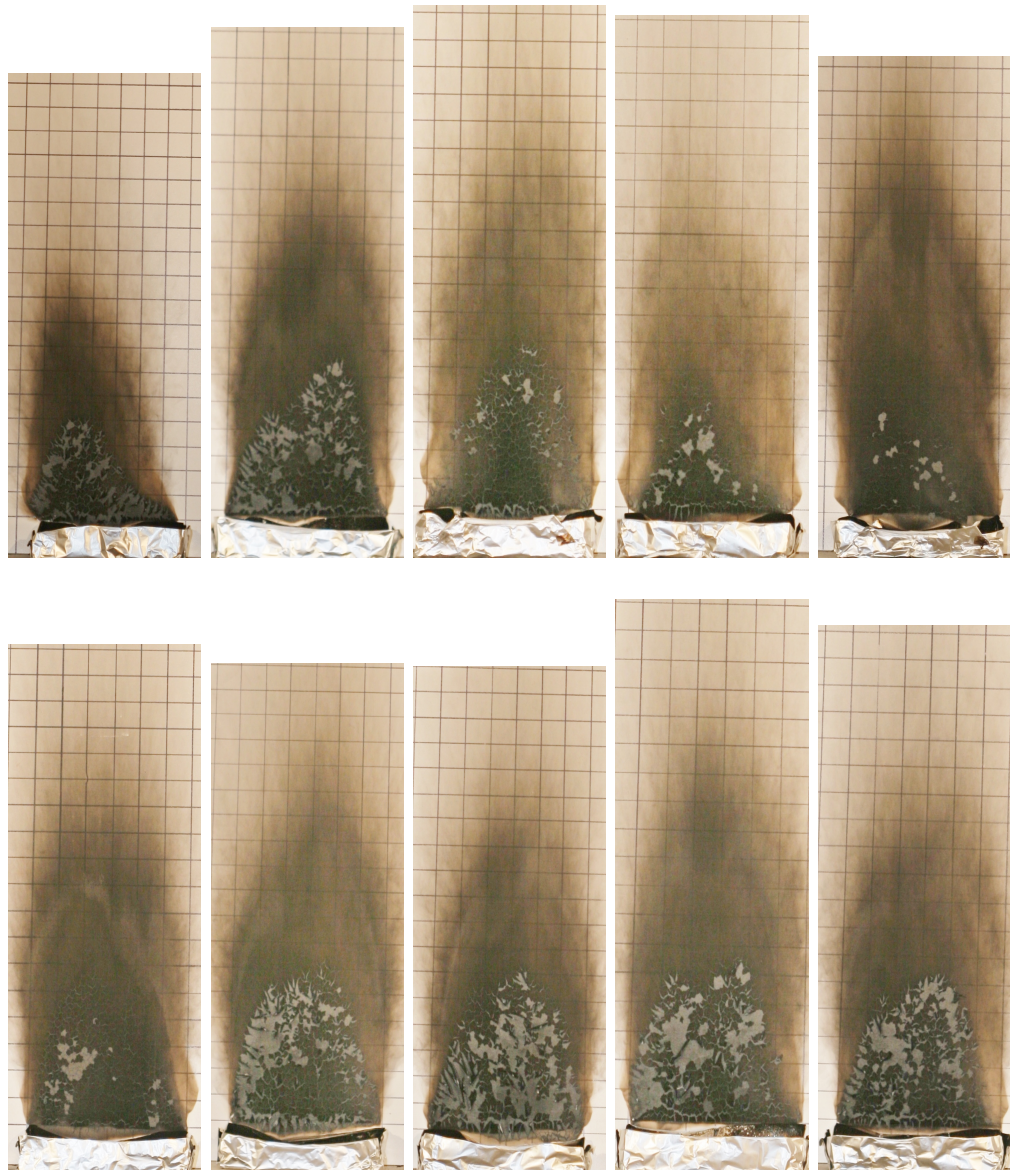


Figure 6.8: Photographs of the fire patterns from ten replicate polyurethane foam burner against open wall construction.

Fuel (# of tests)	Wall Type	Max. Height (m)	Max. Width (m)	Height at Max. Width (m)	Area (m ²)
Natural Gas (10)	Open	0.74 ± 0.12 (16 %)	0.24 ± 0.06 (25 %)	0.41 ± 0.07 (17 %)	0.15 ± 0.05 (33 %)
	Closed	0.74 ± 0.06 (8 %)	0.24 ± 0.02 (7 %)	0.43 ± 0.03 (7 %)	0.14 ± 0.01 (6 %)
	Insulated	0.71 ± 0.10 (14 %)	0.23 ± 0.04 (17 %)	0.42 ± 0.07 (17 %)	0.15 ± 0.02 (14 %)
Natural Gas (10)	Open	0.83 ± 0.15 (18 %)	0.28 ± 0.09 (32 %)	0.44 ± 0.14 (32 %)	0.17 ± 0.04 (24 %)
	Closed	0.80 ± 0.10 (13 %)	0.29 ± 0.04 (14 %)	0.44 ± 0.06 (14 %)	0.17 ± 0.04 (24 %)
	Insulated	0.82 ± 0.09 (11 %)	0.25 ± 0.08 (32 %)	0.40 ± 0.13 (32 %)	0.13 ± 0.04 (30 %)
Gasoline (10)	Open	0.83 ± 0.15 (18 %)	0.28 ± 0.09 (32 %)	0.44 ± 0.14 (32 %)	0.17 ± 0.04 (24 %)
	Closed	0.80 ± 0.10 (13 %)	0.29 ± 0.04 (14 %)	0.44 ± 0.06 (14 %)	0.17 ± 0.04 (24 %)
	Insulated	0.82 ± 0.09 (11 %)	0.25 ± 0.08 (32 %)	0.40 ± 0.13 (32 %)	0.13 ± 0.04 (30 %)

Table 6.1: Comparison of fire pattern dimensions as a function of wall construction type. Values presented with 95 % confidence limits.

Chapter VII

Summary of Experimental Results

Needed?

Chapter VIII

Comparison of Algebraic Fire Characterizations with Fire Pattern Results

8.1 Evidence of a Fire Pattern

Ratio from heat flux from source fire data vytó second item ignite

$$\dot{q}'' = (\dot{Q}\chi_r)/(4\pi R^2) \quad (8.1)$$

where \dot{q}'' is the heat flux per unit area kW/m^2 , \dot{Q} is the heat release rate (kW), χ_r is the radiative fraction, and R = distance from the point source to the target (m).

Source fire plume temp and shape factor from vertical cylinder

$$\dot{q}'' = \epsilon\sigma F_{12}T^4 \quad (8.2)$$

where ϵ is the emissivity, σ is the StefanBoltzmann Constant ($5.67 \times 10^8 \text{ W/m}^2 \text{ K}^4$) and F_{12} is the radiative shape factor.

8.2 Flame Height Correlation

discuss the premise McCaffery

$$Z_c = 0.08\dot{Q}^{2/5} \quad (8.3)$$

where Z_c is the continuous flame height (m)

$$Z_i = 0.20\dot{Q}^{2/5} \quad (8.4)$$

where Z_i is the intermittent flame height (m)

Heskestad widely used NRC CFITrainer texts

8.2.1 Correlation Descriptions

Heskestad, developed an empirical method for calculating the mean visible flame height for fuels which do not have substantial in-depth combustion. Appropriate fuels would “include liquid pool fires and other horizontal surface fires” add cites. Given that the fuel configurations are square, a conversion of the fuel surface area to the effective diameter is required in order to use Heskestad’s flame height equation directly. Setting the area of the fuel surface, 0.093 m^2 , equal to $\pi D^2/4$ and then solving for D yields an effective diameter of 0.344 m . Calculating the flame heights with the average peak heat release rates measured from the three fuels yields 1.0 m and 0.73 m for natural gas, gasoline, and polyurethane foam respectively. Taking the uncertainty of the measurements used to determine the heat release rate ($\pm 11 \%$) into account generates a range of values. The range of calculated values are compared with the mean flame height and range for flame heights based on photographic analysis for each of the fuels in Table z.

$$H_f = 0.235 \dot{Q}^{\frac{2}{5}} - 1.02D \quad (8.5)$$

where H_f is the flame height (m), \dot{Q} is the heat release rate (kW), and D is the burner diameter (m).

8.3 Comparison of Results

Chapter IX

Comparison of Field Model Simulations with Experimental Results

9.1 Fire Dynamics Simulator and Smokeview

Fire Dynamics Simulator [67] is a computational fluid dynamics (CFD) model developed and maintained by NIST that solves a form of the Navier-Stokes equations appropriate for low-speed, thermally driven flow with an emphasis on smoke and heat transport from fires. Within a CFD model, the computational domain is divided into small three-dimensional rectangular control volumes or computational cells. The CFD model computes the density, velocity, temperature, pressure, and gas concentrations in each cell. Based on the laws of conservation of mass, momentum, and energy, the model tracks the generation and movement of fire gases. One of the most important aspects of FDS is that it is mathematically verified [68] and validated against fire test data [69] to ensure that it is accurate and provides the expected results, given appropriate input data. A complete description of the FDS model is provided in the FDS Technical Reference Guide [70].

Smokeview is a software tool designed to visualize simulation results from FDS [71]. Smoke-view visualizes smoke and other attributes of the fire simulation by showing tracer particle flow and two dimensional (2D) or three dimensional (3D) shaded contours of gas flow data, including temperature and flow vectors showing flow direction and magnitude. Smokeview has the ability to visualize fire and smoke by displaying a series of partially transparent planes where the transparencies in each plane (at each grid node) are determined from soot densities computed by FDS. Smokeview can also visualize data at particular snapshots in time using 2D or 3D contours of data that show temperature, flow direction, and flow magnitude. Smokeview also

has a feature that can represent a fire pattern on a surface based on user supplied threshold criteria.

9.1.1 Simulation of Fires

An FDS model was developed to simulate the instrumented wall experiments with the natural gas burner. Three different computational cell resolutions were examined to determine which resolution provided the best match to both the data from the instruments as well as the data from the fire patterns generated in the wall experiments. The three computational grid sizes used were : 80 mm, 40 mm, and 20 mm.

9.1.2 Input Data

Input data was collected from the experimental results presented in Chapters II and V, and from literature sources in order to simulate the instrumented wall experiments using FDS.

Geometry the domain of the model was cubic with 2.4 m on a side. The resulting number computational cells for each case ranged from 27,000 for the 80 mm case to 1,728,000 for the 20 mm cases. An isometric view of the model outlined by the domain is shown in Figure . The face of the wall is located 1.35 m from the front of the domain. The wall was modelled with material properties for gypsum board. Thermal conductivity = 0.28 Specific Heat = 1.00 Density = 582

Instruments FDS has devices, which are used to simulate thermocouples and total heat flux gauges. This devices were positioned in locations similar to the locations used in the physical experiments, in the plume region and on the wall. A radiative heat flux gauge was also modelled to provide data at the 0.95 m from the centerline of the burner and 1.0 m above the top of the burner. In addition, FDS features devices that can not be implemented such as a device, which can be used to examine the heat release rate per unit length. In this case, this device was used to determine flame height based on that measure. Fire The burner was modeled as an obstruction, with the same physical size as the burner. It was modelled with a steady state heat release rate of 888.89 kW/sq m. The chosen fuel reaction was ‘methane since

the majority (check percentage) of the natural gas used in the laboratory experiments was methane.

9.2 Comparison of FDS with Source Fire Results

Compare Natural Gas at 0.61 m from instrumented wall and at 0.0 m from instrumented wall - problem bounds.

9.2.1 Grid Size Analysis

9.2.2 Plume Temperatures

9.2.3 Heat Flux

9.2.4 Flame Height

9.3 Comparison of FDS with Fire Pattern Results

Chapter X

Discussion

Impact of Instrumentation on Walls?

Impact of Wall Construction

Chapter XI

Future Research Needs

Chapter XII

Conclusions

References

- [1] Liora Kolska Horwitz James Brinkd Sharon Holt Marion Bamford Francesco Berna, Paul Goldberga and Michael Chazan. Microstratigraphic evidence of in situ fire in the Acheulean strata of Wonderwerk Cave, Northern Cape province, South Africa. In Donald K. Grayson, editor, *Proceedings of the National Academy of Sciences of the United States of America*.
- [2] C. Mock, M. Peck, M. Peden, and E. Krug. A WHO Plan for Burn Prevention and Care. Fact sheet number 365, World Health Organization (WHO).
- [3] The Geneva Association Staff. Fire and Climate Risk. (29):18.
- [4] U.S. Fire Administration, Federal Emergency Management Agency. *America Burning Revisited, National Workshop*, Tyson's Corner, Virginia, November 1997.
- [5] M.J. Karter. Fire Loss in the United States During 2013. Report FLX10-01, National Fire Protection Association.
- [6] The Five E's of Prevention A New Approach.
http://www.usfa.fema.gov/downloads/pdf/coffee-break/fm/fm_2013_13.pdf.
- [7] R. Campbell. Intentional Fires. Report, National Fire Protection Association.
- [8] National Fire Protection Association. *NFPA 921, Guide for Fire and Explosion Investigations*.
- [9] Crime in the United States. <http://www.fbi.gov/about-us/cjis/ucr/crime-in-the-u.s/2010/crime-in-the-u.s.-2010/property-crime/arsonmain>.

- [10] D. J. Icove and T.K. Hargrove. Project arson: Uncovering the true arson rate in the united states. In *International Symposium on Fire Investigation Science and Technology*. National Association of Fire Investigators, September 2014.
- [11] J Almirall and K Furton. *Analysis and Interpretation of Fire Scene Evidence*. CRC Press.
- [12] Niamh Nic David. *Fire Investigation*. CRC Press.
- [13] J.D. DeHaan and D.J. Icove. *Kirks Fire Investigation*. Pearson Prentice Hall, seventh edition.
- [14] Icove, DeHaan, and Haynes. *Forensic Fire Scene Reconstruction*. Pearson Education, Inc.
- [15] J.J. Lentini. *Scientific Protocols for Fire Investigation*. Taylor & Francis.
- [16] Randall Noon. *Engineering Analysis of Fires and Explosions*. CRC Press.
- [17] J Shanley. USFA Fire Burn Pattern Tests. Report, United States Fire Administration.
- [18] A.D. Putorti. Full Scale Room Burn Pattern Study. NIJ Report 601-97, National Institute of Justice.
- [19] J. Sutula. Practical Applications of The Fire Dynamics Simulator in Fire Protection Engineering Consulting. 15:27–31.
- [20] K.J. Overholt. Verification and Validation of Commonly Used Empirical Correlations for Fire Scenarios. NIST Special Publication 1169, National Institute of Standards and Technology.
- [21] S.M. Olenick and D.J. Carpenter. An Updated International Survey of Computer Models for Fire and Smoke. 13.

- [22] ASTM International. *ASTM E1355-12, Standard Guide for Evaluating the Predictive Capability of Deterministic Fire Models*.
- [23] K. McGrattan, S. Hostikka, R. McDermott, J. Floyd, C. Weinschenk, and K. Overholt. Fire Dynamics Simulator Technical Reference Guide. Special Publication 1018, National Institute of Standards and Technology.
- [24] Recommendations of The Research Advisory Council on Post-fire Analysis. Report, February 2002.
- [25] Christopher B. Wood Nicholas A. Dembsey Gregory E. Gorbett, Brian J. Meacham. Use of Damage in Fire Investigation: a review of fire patterns analysis, research, and future direction. *Fire Science Reviews*, 2015. in press.
- [26] S. Carmen. Burn pattern development in post-flashover fires. In *International Symposium on Fire Investigations*. Investigations Institute, 2008.
- [27] A. Tinsley and Gorbett. Fire investigation origin determination survey. *Fire and Arson Investigator: Journal of the International Association of Arson Investigators*, 63:24–40, 2013.
- [28] C.L. Beyler. Analysis of the Fire Investigation Methods and Procedures Used in the Criminal Arson Cases Against Ernest Ray Willis and Cameron Todd Willingham. report, Hughes Associates, Inc.
- [29] National Research Council of the National Academies.
- [30] Roger Nokes. Streams. Report, University of Canterbury, Dept. of Civil and Natural Resources Engineering.
- [31] ASTM International. *ASTM E648, Standard Test Method for Critical Radiant Flux of Floor-Covering Systems using a Radiant Heat Energy Source*.

- [32] ASTM International. *ASTM E162, Standard Test Method for Surface Flammability of Materials Using a Radiant Heat Energy Source*.
- [33] ASTM International. *ASTM E1354, Standard Test Method for Heat and Visible Smoke Release Rates for Materials and Products Using an Oxygen Consumption Calorimeter*.
- [34] C.L. Beyler. Fire Plumes and Ceiling Jets. 11:53–75.
- [35] G. Hesketh. *Handbook of Fire Protection Engineering*. National Fire Protection Association, fourth edition.
- [36] G. Forney. Smokeview, A Tool for Visualizing Fire Dynamics Simulation Data. Special Publication 1017-1, National Institute of Standards and Technology.
- [37] K.D. Rohr. The U.S. Home Product Report, Forms and Types of Materials First Ignited in Fires: Flammable or Combustible Liquids. Report, National Fire Protection Association.
- [38] Vytenis Babrauskas. *Ignition Handbook*. Fire Science Publishers.
- [39] Carl Chasteen. Prevelence of the use of gasoline in arson fires.
- [40] Polyurethane Foam Association. Flexible Polyurethane Foam: Industry at a Glance. http://www.pfa.org/Library/IAG_no_logo.pdf.
- [41] In Touch, Information on Flexible Polyurethane Foam. http://www.pfa.org/intouch/pdf/IntouchV11_1.read.pdf. Vol. 2, No. 3.
- [42] Marty Ahrens. Home Fires That Began with Upholstered Furniture. Report, National Fire Protection Agency (NFPA).
- [43] B. Evarts. Home Fires That Began With Mattresses and Bedding. Report, National Fire Protection Association (NFPA).

- [44] ASTM International. *ASTM E2067, Standard Practice for Full-Scale Oxygen Consumption Calorimetry Fire Tests.*
- [45] R.A. Bryant, T.J. Ohlemiller, E.L. Johnsson, A.H. Hamins, B.S. Grove, W.F. Guthrie, A. Maranghides, and G.W. Mulholland. The NIST 3 MW Quantitative Heat Release Rate Facility: Description and Procedures. NISTIR 7052, National Institute of Standards and Technology.
- [46] Omega Engineering, Inc. *The Temperature Handbook.*
- [47] L.G. Blevins. Behavior of Bare and Aspirated Thermocouples in Compartment Fires. In National Institute of Standards and Technology, editors, *Proceedings of the 33rd National Heat Transfer Conference, HTD99-280.*
- [48] W M Pitts, R D Braun, R D Peacock, H E Mitler, E L Johnsson, P A Reneke, and L G Blevins. Temperature Uncertainties for Bare-Bead and Aspirated Thermocouple. In National Institute of Standards and Technology, editors, *Thermal Measurements: The Foundation of Fire Standards.*
- [49] Medtherm Corporation. *Series 64 Heat Flux Transducers.* Bulletin 118.
- [50] W.M. Pitts, A.V. Murthy, J.L. de Ris, J.R. Filtz, K. Nygard, D. Smith, and I. Wetterlund. Round robin study of total flux gauge calibration at fire laboratories. 41:459–475.
- [51] Mettler-Toledo, Worthington, Ohio. *National Type Evaluation Program, Certificate Number 00-075A1,* 2002.
- [52] B.N. Taylor and C.E. Kuyatt. Guidelines for Evaluating and Expressing the Uncertainty of NIST Measurement Results. NIST Technical Note 1297, National Institute of Standards and Technology.
- [53] K. Goble. *Height of Flames Projecting from Compartment Openings.* Master's thesis.

- [54] B.J. McCaffrey. Purely Buoyant Diffusion Flames: Some Experimental Results. NBSIR 79-1910, National Bureau of Standards (currently NIST).
- [55] BNZ. *Marinite*, rev 02 edition.
- [56] BNZ Materials Inc. *Marinite I: Refractory Products, Fire-Resistant Thermal, Structural Insulation*, BNZ R-3261-W edition.
- [57] ASTM International. *ASTM E1321, Standard Test Method for Determining Material Ignition and Flame Spread Properties*.
- [58] James Quintiere, Margaret Harkleroad, and Yuki Hasemi. Wall Flames and Implications for Upward Flame Spread. Report, National Institute of Standards and Technology.
- [59] S.E. Dillon, W.H. Kim, and J.G. Quintiere. Determination of Properties and the Prediction of the Energy Release Rate of Materials in the ISO 9705 Room-corner Test. Report, National Institute of Standards and Technology, Building and Fire Research Laboratory.
- [60] USGS. Gypsum statistics and information.
<http://minerals.usgs.gov/minerals/pubs/commodity/gypsum/>, 2015.
- [61] ASTM International. *ASTM C1396, Standard Specification for Gypsum Board*.
- [62] Gypsum Association. *Gypsum Board Typical, Mechanical and Physical Properties*.
- [63] J. Randall Lawson. An Evaluation of Fire Properties of Generic Gypsum Board Products. NBS IR 77-1265, National Bureau of Standards (now NIST).
- [64] DeFelsko Corporation. *PosiTector 200, Instruction Manual V. 2.0, Ultrasonic Coating Thickness Gage*.

- [65] V. Babrauskas. Development of the Cone Calorimeter: A Bench Scale Heat Release Rate Apparatus Based on Oxygen Consumption. *Journal of Fire and Materials*, 8:81–95, 1984.
- [66] J R Lawson and W H Twilley. Development of an apparatus for measuring the thermal performance of fire fighters' protective clothing. report NISTIR 6400, National Institute of Standards and Technology.
- [67] K. McGrattan, S. Hostikka, R. McDermott, J. Floyd, C. Weinschenk, and K. Overholt. *Fire Dynamics Simulator, User's Guide*. National Institute of Standards and Technology, Gaithersburg, Maryland, USA, and VTT Technical Research Centre of Finland, Espoo, Finland, sixth edition, September 2013.
- [68] K. McGrattan, S. Hostikka, R. McDermott, J. Floyd, C. Weinschenk, and K. Overholt. *Fire Dynamics Simulator, Technical Reference Guide, Volume 2: Verification*. National Institute of Standards and Technology, Gaithersburg, Maryland, USA, and VTT Technical Research Centre of Finland, Espoo, Finland, sixth edition, September 2013.
- [69] K. McGrattan, S. Hostikka, R. McDermott, J. Floyd, C. Weinschenk, and K. Overholt. *Fire Dynamics Simulator, Technical Reference Guide, Volume 3: Validation*. National Institute of Standards and Technology, Gaithersburg, Maryland, USA, and VTT Technical Research Centre of Finland, Espoo, Finland, sixth edition, September 2013.
- [70] K. McGrattan, S. Hostikka, R. McDermott, J. Floyd, C. Weinschenk, and K. Overholt. *Fire Dynamics Simulator, Technical Reference Guide*. National Institute of Standards and Technology, Gaithersburg, Maryland, USA, and VTT Technical Research Centre of Finland, Espoo, Finland, sixth edition, September 2013. Vol. 1: Mathematical Model; Vol. 2: Verification Guide; Vol. 3: Validation Guide; Vol. 4: Configuration Management Plan.
- [71] G.P. Forney. *Smokeview (Version 6), A Tool for Visualizing Fire Dynamics Simulation Data, Volume I: User's Guide*.